九州大学学術情報リポジトリ
Kyushu University Institutional Repository

Specific Ion Effects on Counterion Distribution in Surfactant Adsorbed Films Studied through Surface Tensiometry and Total Reflection XAFS

今井, 洋輔

https://doi.org/10.15017/1441031

出版情報：九州大学, 2013, 博士（理学）, 課程博士
バージョン：
権利関係：全文ファイル公表済

KYUSHU UNIVERSITY

Specific Ion Effects on Counterion Distribution in Surfactant Adsorbed Films Studied through Surface Tensiometry and Total Reflection XAFS

Yosuke Imai

March 2014

Abstract

In this thesis, “the specific ion effect on interfacial and colloidal phenomena” was investigated by examining the counterion distribution in the surfactant adsorbed films with the aid of X-ray absorption fine structure under total reflection condition (TR-XAFS) followed by solvation structure analysis as well as by evaluating thermodynamic physicochemical variables through surface tensiometry followed by the analysis based on our original thermodynamic formulation. In Chapter 1, the scientific background for this study was summarized. In Chapter 2, the materials and experimental apparatus used for this study were summarized.

In Chapter 3, the relation between the counterion distribution and the surface charge density was investigated for the single surfactant systems of dodecyltrimethylammonium bromide (DTAB), hexadecyltrimethylammonium bromide (HTAB), DTAB with added NaBr and 1-decyl-3-methylimidazolium bromide (DeMIMBr). In the TR-XAFS technique, the spectra evaluated through the extended X-ray absorption fine structure (EXAFS) analysis were expressed as linear combinations of two specific spectra corresponding to fully hydrated bromide ions (free-Br) and partially dehydrated bromide ions bound to the hydrophilic groups of surfactant ions (bound-Br) in the adsorbed film, and the ratio of bound-Br was determined to evaluate the counterion distribution. The values of the bound ratio of bromide ions of HTAB and DTAB with added NaBr were rather close to that of DTAB at a fixed surface density of surfactant ions which indicated that the difference in chain length and adding electrolyte are not so much influential on counterion distribution, whereas the bound ratio of DeMIMBr was evidently smaller than that of DTAB due to

the effective packing of imidazolium rings at surface which provided the conceivable situation that the adsorbed molecules were definitely not homogeneously dispersed but a part of them were molecularly dispersed around the domains (islands or clusters) with the bound Br ions.

In Chapter 4, the distribution and miscibility of counterions in the electrical double layers of adsorbed films containing binary counterions was investigated by relating the bound ratio to the surface composition of counterions and the excess Gibbs energy. It was suggested that in the DTAB-DTAC system the mixing of Cl^- ions had practically no influences to the distribution of Br^- ions in the adsorbed film and ideal mixing was observed because the nature of counterions were similar to each other. In the HMIMBr-HMIMBF_4 system the hydrogen bonding between BF_4^- ion and imidazolium cation was essential, which caused a kind of segregation of the counterion distribution. In the DTAB-DTABF_4 systems, on the other hand, preferential binding of counterions due to lower adsorption energy of BF_4^- and a remarkable difference in size between them yielded the preferable counterion mixing in the electrical double layer.

In Chapter 5, the effect of valence and size of counterions on the miscibility and distribution of binary counterions was clarified by employing the DTAB-DTA_2SO_4 system and adopting the same methodology as shown in Chapter 4 with newly derived thermodynamic equations. The evaluated composition of counterions in the adsorbed film revealed that the space among larger SO_4^2 is effectively occupied by smaller Br^- ions. The determined ratio of bound-Br revealed that the vicinity of hydrophilic heads of surfactant ions is occupied by monovalent Br^- ions preferentially even to divalent SO_4^{2-} ions. The obtained negative excess Gibbs energy in the adsorbed film was reasonably explained from the enthalpy and entropy contributions respectively arising

from the preferential binding of Br^- ions having smaller hydration free energy and adsorption energy and the sharing the confined space by SO_4^{2-} and Br^- ions having different size. From the results of Chapter 4 and 5, the three essential factors that cause the specific ion effect, the size and hydration of counterions and the hydrogen bonding with surfactant ions and counterions was suggested.

In Chapter 6, the effect of the arrangement of hydrophilic head groups in the adsorbed films on counterion distribution was investigated with employing the HTAB-DTAB mixed system. From the obtained smaller value of the ratio of bound-Br than that for DTAB, it was suggested that the staggered arrangement of surfactant ions enhances the inhomogeneous distribution of ion species similarly to DeMIMBr system demonstrated in Chapter 3. From these results, it was suggested that both the density and arrangement of surface charge due to surfactant ions could influence counterion distribution in the electrical double layer. At the last of this chapter, the perspective of the study on the specific counterion effect using TR-XAFS technique was presented.

Contents

Chapter 1 General Introduction ..……1

Chapter 2 Experimental …….8

2-1 Materials ...…..8

2-2 Surface tension measurement ...…10

2-3 Total-reflection XAFS measurement ……12

2-4 References ……14

Chapter 3 Counterion Distribution in Single Surfactant Systems Investigated by Total Reflection XAFS ...…16

3-1 Introduction ……16

3-2 Determination of the ratio of bound-Br through EXAFS analysis …….18

3-3 Counterion distribution in the DTAB, HTAB, DTAB-NaBr and DeMIMBr systems ……26

3-4 References ……29

Chapter 4 Miscibility and Distribution of Binary Counterions in Surfactant Adsorbed Films …...…31

4-1 Introduction ..…….31

4-2 Determination of surface compositions of counterions through Jump value analysis …….34

4-3 Miscibility and distribution of binary counterions in the DTAB-DTAC,

DTAB-$DTABF_4$ and HMIMBr-$HMIMBF_4$ systems ..……39

4-4 References ..……45

Chapter 5 Valence and Size Effects on Miscibility and Distribution of Binary Counterions in Surfactant Adsorbed Films ...……48

5-1 Introduction ……..…48

5-2 Surface tension data and thermodynamic equations for the DTAB-DTA_2SO_4 system .……49

5-3 Effect of counterions on adsorption of surfactant ions ..……54

5-4 Miscibility of counterions ..……56

5-5 TR-XAFS spectra of the DTAB-DTA_2SO_4 system for evaluating the surface composition and ratio of bound-Br ...……63

5-6 Relation between distribution and miscibility of counterions ..……63

5-7 References ..……77

Chapter 6 The Effect of the Arrangement of Hydrophilic Head Groups in the Adsorbed Films on Counterion Distribution ..……80

6-1 Introduction ..……80

6-2 Counterion distribution in the HTAB-DTAB mixed system ..……82

6-3 References ..……90

Chapter 7 Summary ...……91

Acknowledgments ...……93

Chapter 1 General Introduction

Since the discovery of the Hofmeister series in 1888 [1], "Specific ion effect on interfacial and colloidal phenomena" has been one of the most important issues in the relevant scientific fields [2-4]. From an experimental point of view, it has been studied by observing salt effects on lipid membranes [5, 6], biological macromolecules [7, 8], bubbles [9, 10], surfactant aqueous solutions [11, 12], foam films [13, 14] and other colloidal systems. In addition, the adsorption of electrolytes (often negative adsorption) and the effects of counterion on adsorbed films of ionic amphiphiles at air/water interface are also the related issues and the distribution of inorganic ions at air/water interface has been often interpreted using theoretical models [15-22] in terms of size, polarizability, hydration and other properties of ions that have not been accounted by the classical simple Poisson-Boltzmann (PB) theory [23]. For clarifying the specific ion effect, Kalinin and Radke introduced an idea that the binding of counterion to head group of surfactant ion was accompanied with partial dehydration and then the radius of counterions was different from each other between their bare and hydrated states in the double layer [15]. Warszynski et al. considered the possibility of the penetration of counterion into the Stern layer and the arrangement that head group of surfactant ion and counterion were at the same level [16]. Ninham and Yaminsky claimed that the dispersion force between ion and interface should be included [17], and Ivanov et al. advanced their idea that made it possible to calculate the specific adsorption energy of counterions without using adjustable parameters [18]. Levin et al. considered that small ions could not approach the interface due to their firm hydration shell, meanwhile large and polarizable ions could move across the interface due to

cavitation energy [19]. Kjellander et al. insisted the importance of ion-ion correlation being describable with two-body correlation function [20]. These theories have given us a more realistic description for the specific counterion effect in the electrical double layer.

In addition to these experimental and theoretical studies, our group has clarified that the chemical structure of hydrophilic head groups also greatly influences counterion distribution. In the adsorbed film of 1-hexyl-3-methylimidazolium tetrafluoroborate ($HMIMBF_4$), for example, $HMIM^+$ and BF_4^- ions occupy the same level of the surface due to ion pairing generated by the strong hydrogen bonding between $HMIM^+$ and BF_4^- [24, 25] similarly to the surface of pure $HMIMBF_4$ liquid confirmed by several techniques [26-30]. This is different from the general observation for conventional alkyltrimethylammonium ions, and suggests that not only the nature of counterion itself but also the interaction between counterion and surfactant ion should be considered for examining the ion specific effect.

The counterion distribution in the interface has been evaluated on the basis of the physicochemical variables obtained from such as surface tension, surface potential and X-ray reflectivity measurements followed by theoretical fitting with the models of electrical double layer in which the different number of planes are introduced to define the two bulk phases and the Stern and diffuse layers [15-23, 31]. Besides these methodologies, a rather new and newly-devised approach of X-ray absorption fine structure under total reflection condition (TR-XAFS) has been employed to evaluate the counterion distribution, in which any model of electrical double layer itself is not required. TR-XAFS method applied to ions at solution surfaces is much more difficult than the transmission XAFS method conventionally applied to bulk phases, because

TR-XAFS requires a specially designed experimental setup and skillful manipulation. However we have succeeded in collecting TR-XAFS spectra and evaluating the counterion distribution from the extended X-ray absorption fine structure (EXAFS) analysis in terms of the ratio of the fully hydrated bromide ions distributed in the diffuse double layer (free-Br) to those bound to the hydrophilic heads of surfactant ions (bound-Br) [24, 32, 33], which means that counterion distribution is explored from the difference of the hydration state of counterions.

In this thesis, the specific ion effect is investigated by examining the counterion distribution in the surfactant adsorbed films with the aid of the bound ratio evaluated from TR-XAFS measurement as well as by evaluating thermodynamic physicochemical variables through surface tensiometry followed by the analysis based on our original thermodynamic formulation. The thesis is constructed as follows.

In Chapter 2, the materials and experimental apparatus are summarized.

In Chapter 3, the results for the single surfactant systems are summarized. First are shown the method and processes in order to obtain the ratio of bound-Br from the extended X-ray absorption fine structure (EXAFS) analysis. Then the ratio of bound-Br is plotted against the surface density of surfactant ions estimated from the surface tensiometry for the single systems of dodecyltrimethylammonium bromide (DTAB) [34], hexadecyltrimethylammonium bromide (HTAB), DTAB with added NaBr salt [35] and 1-decyl-3-methylimidazolium bromide (DeMIMBr) [32]. The conterion distribution is discussed from the viewpoints of effects of the chain length, the added electrolyte and the hydrophilic headgroup on it.

In Chapter 4, the results for binary surfactant systems with the common surfactant ions but with different counterions are summarized. First the phase diagram of

adsorption (PDA) and the excess Gibbs energy (EGE) from the thermodynamic analysis of the surface tesiometry are illustrated for examining the miscibility of counterions for DTAB-DTAC, DTAB-$DTABF_4$ and HMIMBr-$HMIMBF_4$ mixed systems [33]. Then the bound ratio is examined in relation to the PDA and EGE and the specific ion effects is explored from the viewpoints of the miscibility and the preferential binding of counterions to hydrophilic head groups.

In Chapter 5, the effect of valence and size of counterions on miscibility and distribution of binary counterions is clarified by employing DTAB-DTA_2SO_4 system and adopting the same methodology as shown in Chapter 4. First the thermodynamic equations applicable to DTAB-DTA_2SO_4 system are derived, and the PDA and the EGE vs. surface composition diagram are constructed for examining the miscibility of counterions. Then the relation between the miscibility and distribution of counterions is examined by reference to the results of the other binary mixed systems demonstrated in Chapter 4.

In Chapter 6, the preliminary results for counterion distribution in HTAB-DTAB mixed system is shown. From our previous thermodynamic study, it was suggested that DTAB molecules could use effectively the space among the hydrocarbon chains among the hydrocarbon chains of HTAB molecules and their polar head groups took a staggered arrangement at the surface [36]. Then, relating the ratio of bound-Br to surface density of surfactant ions, the effect of surface charge due to head group on counterion distribution is explored. At the last of this chapter the perspective of the study on specific ion effect is also presented.

References

1. Hofmeister, F. *Arch Exp Pathol Pharmakol* **1888**, 24, 247.
2. Kunz, W. *Specific ion effects*; World Scientific Publishing Co.: Singapore, 2011.
3. Issues 1 and 2 of *Curr. Opin. Colloid Interface Sci*. **2004**, 9, 1-198.
4. Jungwirth, P.; Winter, B. *Annu. Rev. Phys. Chem*. **2008**, 59, 343.
5. Leikin, S.; Parsegian, V. A.; Rau, D. C.; Rand, R. P. *Annu. Rev. Phys. Chem.* **1993**, 44, 369.
6. Ryhanen, S. J.; Saily, V. M. J.; Kinnunen, P. K. *J. Phys. Condens. Matter* **2006**, 18, 1139.
7. Nostro, P. L.; Fratoni, L.; Ninham, B. W.; Baglioni, P. *Biomacromolecules* **2002**, 3, 1217.
8. Nostro, P. L.; Nostro, A. L.; Ninham, B. W.; Pesavento, G. ; Fratoni, L.; Baglioni, P. *Curr. Opin. Colloid Interface Sci.* **2004**, 9, 97.
9. Safouane, M.; Langevin, D. *Chem. Phys. Chem.* **2009**, 10, 222.
10. Henry, C. L.; Dalton, C. N.; Scruton, L.; Craig, V. S. J. *J. Phys. Chem. C* **2007**, 111, 1015.
11. Para, G.; Jarek, E.; Warszynski, P. *Colloids and Surfaces A* **2005**, 261, 65.
12. Anacker, E.W.; Ghose, H. M. *J. Am. Chem. Soc*. **1968**, 90, 3161.
13. Ivanov, I. B.; Slavchov, R. I.; Basheva, E. S.; Sidzhakova, D.; Karakashev S. *Adv. in Colloid and Interface Sci.* **2011**, 168, 93.
14. Schelero, N.; Hedicke, G.; Linse, P.; Klitzing, R. V. *J. Phys. Chem. B* **2010**, 114, 15523.
15. Kalinin, V. V.; Radke, C. J. *Colloids and Surfaces A* **1996**, 114, 337.
16. Warszynski, P.; Barzyk, W.; Lunkenheimer, K.; Fruhner, H. *J. Phys. Chem. B* **1998**,

102, 10948.

17. Ninham, B. W.; Yaminsky, V. *Langmuir* **1997**, 13, 2097.
18. Ivanov , I. B.; Marinova, K. G.; Danov, K. D.; Dimitrova, D.; Ananthapadmanabhan, K. P.; Lips, A. *Adv. in Colloid and Interface Sci*. **2007**, 134, 105.
19. Levin, Y.; Santos, A. P.; Diehl, A. *Phys. Rev. Lett*. **2009**, 103, 257802.
20. Kjellander, R.; Marcelja, S. *J. Chem. Phys*. **1985**, 82, 2122.
21. Manciu, M.; Ruckenstein, E. *Adv. in Colloid and Interface Sci*. **2003**, 105, 63.
22. Leroy, P.; Lassin, A.; Azaroual, M.; Andre, L. *Geochimica et Cosmochimica Acta* **2010**, 74, 5427.
23. Davies, J. T.; Rideal, E. K. *Interfacial Phenomena*; Academic Press: New York, 1963.
24. Shimamoto, K.; Onohara, A.; Takumi, H.; Watanabe, I.; Tanida, H.; Matsubara, H.; Takiue, T.; Aratono, M. *Langmuir* **2009**, 25, 9954.
25. Matsubara, H.; Onohara, A.; Imai, Y.; Shimamoto, K.; Takiue, T.; Aratono, M. *Colloids and Surfaces A* **2010**, 370, 113.
26. Jeon, Y.; Sung, J.; Bu, W.; Vaknin, D.; Ouchi, Y.; Kim, D. *J. Phys. Chem. C* **2008**, 112, 19649.
27. Law, G.; Watson, P. R.; Carmichael, A. J.; Seddon, K. R. *Phys. Chem. Chem. Phys.* **2001**, 3, 2879.
28. Lockett, V.; Sedev, R.; Bassell, C.; Ralston, J. *Phys. Chem. Chem. Phys.* **2008**, 10, 1330.
29. Bowers, J.; Vergara-Gutierrez, M. C.; Webster, J. R. P. *Langmuir* **2004**, 20, 309.
30. Dong, K.; Zhang, S.; Wang, D.; Yao, X. *J. Phys. Chem. A* **2006**, 110, 9775.
31. Luo, G.; Malkova, S.; Yoon, J.; Schultz, D. G.; Lin, B.; Meron, M.; Benjamin, I.;

Vanysek, P.; Schlossman, M. L. *Science* **2006**, 311, 216.

32. Aratono, M.; Shimamoto, K.; Onohara, A.; Murakami, D.; Tanida, H.; Watanabe, I.; Ozeki, T.; Matsubara, H.; Takiue, T. *Anal. Sci.* **2008**, 24, 1279.
33. Imai, Y.; Shimamoto, K.; Takiue, T.; Matsubara, H.; Aratono, M. *Colloid Polym. Sci*. **2010**, 288, 1005.
34. Takiue, T.; Kawagoe, Y.; Muroi, S.; Murakami, R.; Ikeda, N.; Aratono, M.; Tanida, H.; Sakane, H.; Harada, M.; Watanabe, I. *Langmuir* **2003**, 19, 10803.
35. Kashimoto, K.; Takata, Y.; Matsuda, T.; Ikeda, N.; Matsubara, H.; Takiue, T.; Aratono, M.; Tanida, H.; Watanabe, I. *Langmuir* **2006**, 22, 8403.
36. Kashimoto, K.; Matsubara, H.; Takahara, H.; Nakano, T.; Takiue, T.; Aratono, M. *Colloid. Polym. Sci.* **2004**, 283, 329.

Chapter 2 Experimental

2-1. Materials

Dodecyltrimethylammonium bromide (DTAB) purchased from Wako Pure Chemical Industries (99%) was purified by recrystallizing it five times from the mixture of acetone and ethanol (5:1 volume ratio). Dodecyltrimethylammonium chloride (DTAC) was synthesized and purified according to the method described in previous paper [1].

Dodecyltrimethylammonium tetrafluoroborate ($DTABF_4$) was synthesized by exchanging Br^- ions of DTAB by adding equimolar amount of sodium tetrafluoroborate ($NaBF_4$) in the aqueous DTAB solution and then recrystallized twice from water. $NaBF_4$ was purchased from Kanto Kagaku Co., Ltd. (98%) and recrystallized from water and then baked at 170 ℃ for 7h under reduced pressure [2].

Bis-dodecyltrimethylammonium sulfate (DTA_2SO_4) was synthesized and purified in reference to the method described elsewhere [3] with some modifications. DTA_2SO_4 was obtained by exchanging Br^- ions of DTAB by adding a half molar amount of Ag_2SO_4 to the ethanol solution of DTAB. Ag_2SO_4 (99.5%) was purchased from Wako Pure Chemical Industries and used as received. The solution was ultra-sonicated for 9 hrs, and then AgBr precipitate was removed by filtration using a syringe filter with 0.2 μm pores. Evaporating the filtrates yielded a white humid crude product, and further drying it under vacuum at 90 ℃ yielded a white solid salt. This solid was recrystallized two times from the mixture of acetone and methanol (4:1 volume ratio) followed by drying under vacuum at 90 ℃ at each recrystallization process, and finally we obtained the purified white crystal of DTA_2SO_4. The

anhydrous crystal could not be obtained even after the drying under vacuum for one day. The small amount of water in the crystal (about 1 wt%) was estimated by Karl-Fischer moisture meter, which was taken into account in the calculation of the molality of the sample aqueous solution.

Hexadecyltrimethylammonium bromide (HTAB) was purchased from Nakarai Chemical Industry (99%) and recrystallized three times from a mixture of ethanol and acetone. Sodium bromide (NaBr) purchased from Aldrich Chemical Co. Inc. (99.99%) was used without further purification.

1-hexyl-3-methylimidazolium tetrafluoroborate ($HMIMBF_4$) and 1-hexyl-3-methylimidazolium bromide (HMIMBr) were purchased from Wako Pure Chemical Industries, Ltd. and from Kanto Kagaku Co., Ltd., respectively. Organic impurities were removed by extracting them 10 times using hexane for $HMIMBF_4$ and ethyl acetate for HMIMBr, and then dried under reduced pressure [4]. 1-decyl-3-methylimidazolium bromide (DeMIMBr) was synthesized by mixing 1-bromodecane (Aldrich, 99%), which had been purified by distillation at 370 K under reduced pressure of 3 mmHg, and 1-methylimidazole (Aldrich 99%) in anhydrous toluene at the temperature of an ice-water bath. The crude product was recrystallized three times from toluene and ethylacetate [5].

The purity of these surfactants was confirmed by elemental analysis, ^1H NMR and observing no minimum on the surface tension vs. molality curve around the critical micelle concentration (cmc).

2-2. Surface tension measurement

Surface tension γ of the aqueous solution was measured by drop volume and pendant drop techniques. In drop volume technique, the apparatus developed by Aratono et al. [6] was used and the schematic of that is shown in Fig. 2-1(a). The drop of sample solution was hung on the tip of capillary of a glass syringe in a saturated atmosphere of sample solution. The value of surface tension γ was evaluated in the following procedure. First the drop was developed to about 95 % of its final volume. After reaching the adsorption equilibrium, the plunger was gradually pushed by using micrometer until the drop was detached [7], and the volume of a detached drop V was evaluated by multiplying the internal diameter of syringe and the distance of plunger progress. Then, the γ value was calculated from the force balance between the gravity and surface tension on the drop just before the drop falling by the following equation [8, 9].

$$\gamma = \frac{V\Delta\rho g}{r}F \qquad (2-1)$$

where V is the volume of a detached drop, g the local acceleration of gravity, r the radius of the tip of capillary, $\Delta\rho$ the density difference between air and aqueous solution and F the empirical correction factor mainly involving the effect of the remaining of some amount of solution on capillary after detaching the drop. F was calculated from the following equation,

$$F = 0.1482 + 0.27896\left(r/V^{1/3}\right) - 0.166\left(r/V^{1/3}\right)^2. \qquad (2-2)$$

In the pendant drop technique, the apparatus shown elsewhere [10] was used and the schematic of that is shown in Fig. 2-1(b). The surface tension was evaluated through the procedure developed by Sakamoto et al. [10]. First the image of the drop

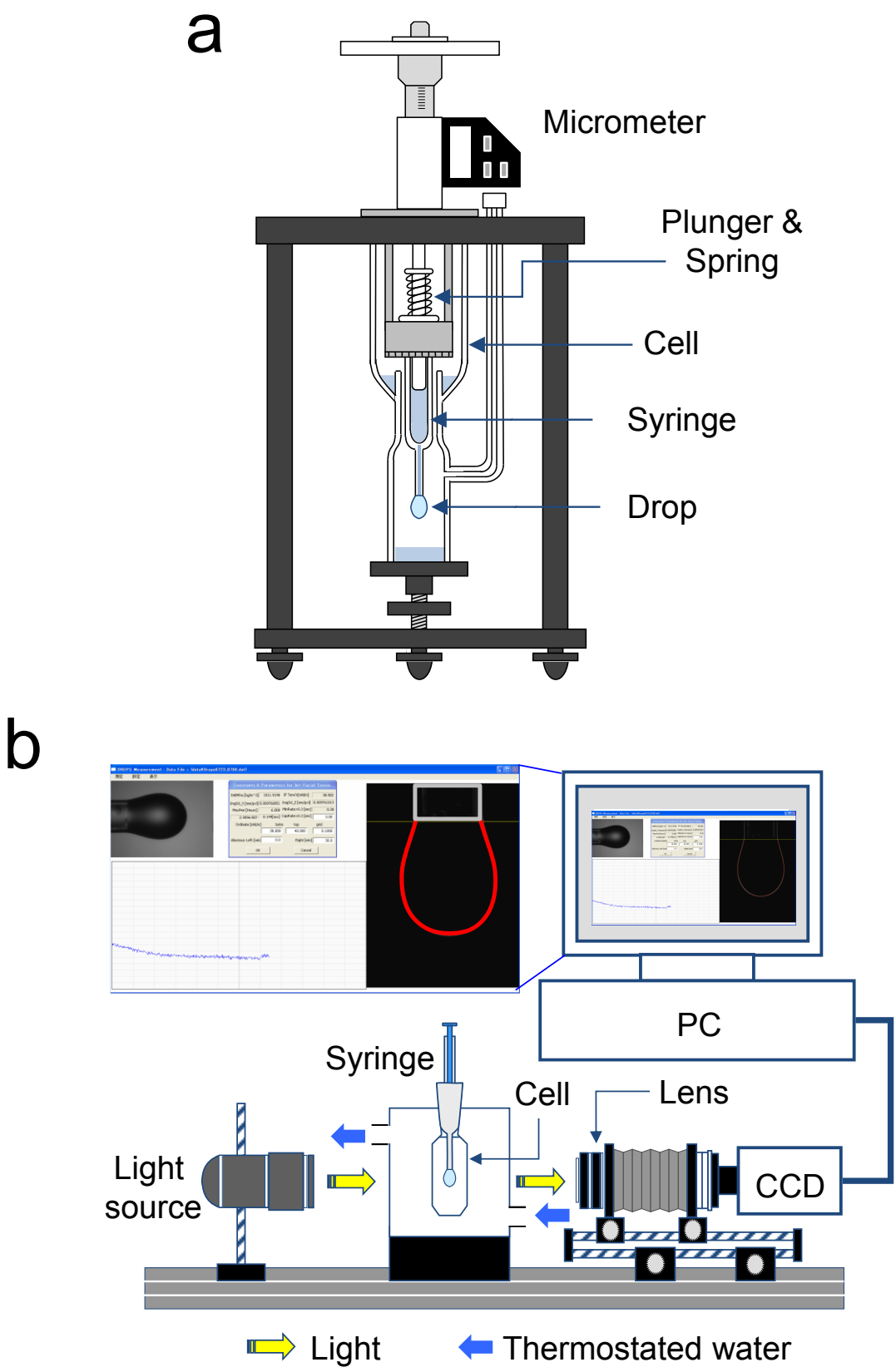

Figure 2-1. The apparatuses for (a) drop volume and (b) pendant drop methods.

shape of sample solution hung on the tip of capillary lighted by a light source was enlarged and captured by the CCD camera equipped with optical lenses. Then, the γ value was calculated by PC in real time through drop shape analysis based on Young-Laplace equation during measurement.

In both techniques, the temperature was kept constant with circulating thermostated water around the sample cells, and the measurement was conducted at 298.15 K under atmospheric pressure. The experimental error of the surface tension was within 0.05 mN m^{-1} in both techniques. In the study of this thesis, the drop volume technique was mainly adopted, whereas the pendant drop technique was used especially for estimating the time required to reach the adsorption equilibrium.

2-3. Total-reflection XAFS measurement

TR-XAFS experiment was performed using the synchrotron radiation at BL-7C of the Photon Factory in the National Laboratory for High Energy Physics (Tsukuba, Japan) [11]. The apparatus devised by Watanabe et al. [12] was used and the schematic of that is shown in Fig. 2-2(a) and (b).

X-ray beam radiated from the electron storage ring was monochromatized by a double-crystal Si (111) monochromator then tilted by a mirror to make incident angle of the X-ray be 1 mrad so as to satisfy the total reflection condition at the solution surface. Energy of X-ray was scanned to cover the Br-K edge from 13391 to 13663 eV. The X-ray beam was shaped as 50 μm × 6 mm by using a slit. The gap of slit is quite narrow, so sagittal focus by using monochromator was conducted to obtain the X-ray having strong light intensity. The gas-ionization chamber placed in front of the solution cell counts the incident beam intensity, I_0, by using flowing N_2 gas. The

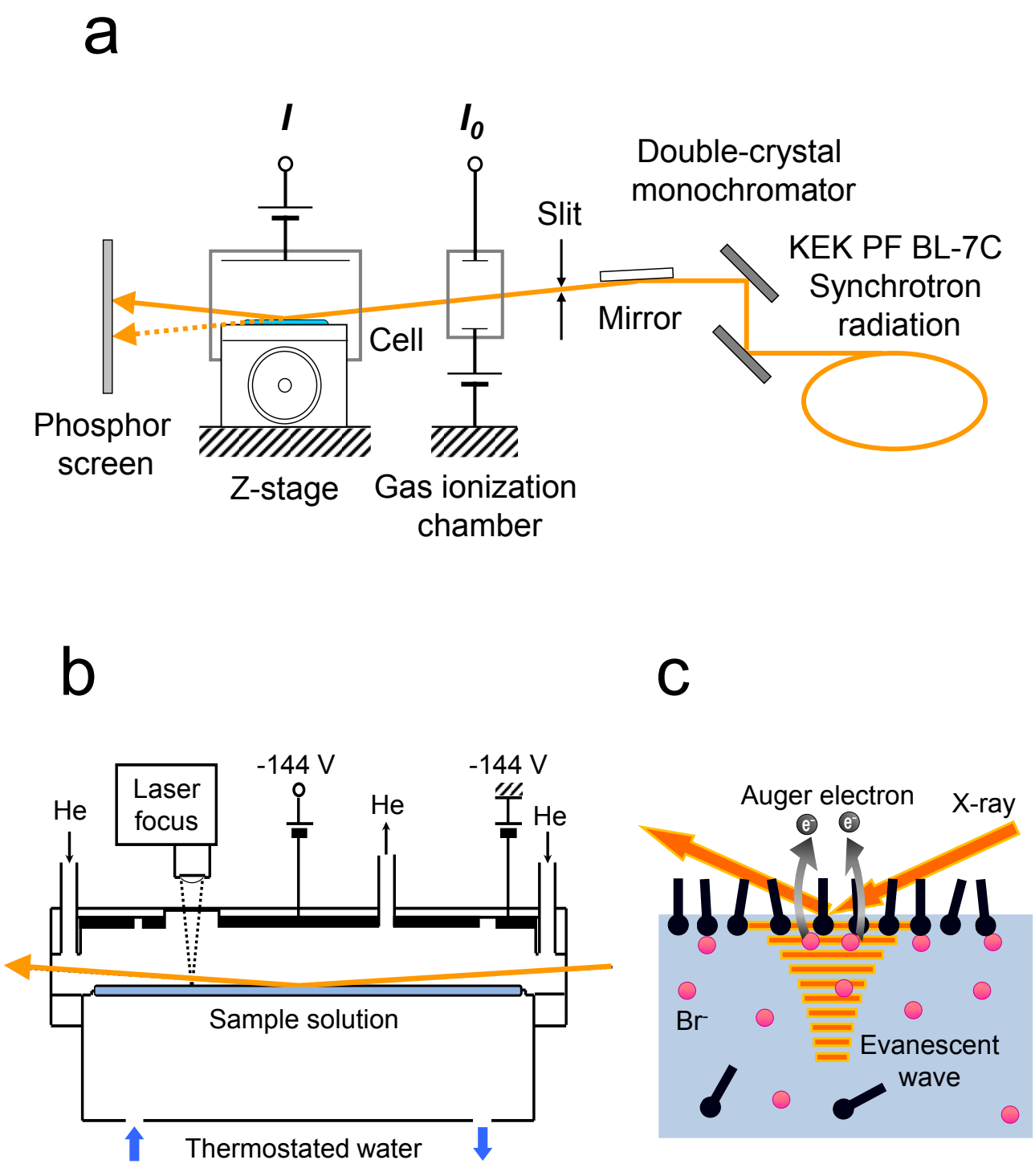

Figure 2-2. The apparatus for total reflection XAFS method: (a) the overall picture, (b) the sample cell and (c) the enlarged view of solution surface.

solution cell itself was filled with He gas flowing at a constant rate (1 L min^{-1}) as shown in Fig. 2-2(b). The cell wall equipped with the electrode collects helium ions generated by Auger electrons from bromide ions due to evanescent wave at the surface (Fig. 2-2(c)). Then the signal intensity, *I*, was detected by the total conversion He^+ ion-yield method [13]. The size of foot print is about 5 cm × 6 mm, and in order to realize the reflection of X-ray at hypothetically flat surface at the center of trough, a large size of trough (22cm × 6 cm) was used. Furthermore, the height of the solution surface was checked by laser focus displacement meter and the height was automatically controlled by z-stage stepping motor during measurement. The solution temperature was kept constant at 298.15K by circulating the thermostated water. To reduce the noise due to the earth shake the laboratory table was lifted by tubes for tires. Dusts and bubbles on surface of sample solution were removed carefully by using a pipette before the measuring. In order to estimate the incidence angle to the solution surface a phosphor screen and digital camera on the wall of the station hatch were used. The distance between the marked positions of X-ray of direct and reflected at the solution surface the angle was calculated. The XAFS spectrum was obtained by plotting I / I_0 against X-ray energy. The detail experimental procedure and set-up were summarized in our previous reports [14, 15].

2-4. References

1. Aratono, M.; Okamoto, T.; Motomura, K. *Bull. Chem. Soc. Jpn*. **1987**, 60, 2361.
2. Imai, Y.; Shimamoto, K.; Takiue, T.; Matsubara, H.; Aratono, M. *Colloid Polym. Sci.* **2010**, 288, 1005.
3. Voeks, J. F.; Tartar, H. V. *J. Phys. Chem.* **1956**, 59, 1190.

4. Shimamoto, K.; Onohara, A.; Takumi, H.; Watanabe, I.; Tanida, H.; Matsubara, H.; Takiue, T.; Aratono, M. *Langmuir* **2009**, 25, 9954.

5. Aratono, M.; Shimamoto, K.; Onohara, A.; Murakami, D.; Tanida, H.; Watanabe, I.; Ozeki, T.; Matsubara, H.; Takiue, T. *Anal. Sci.* **2008**, 24, 1279.

6. 松木　均、荒殿　誠、金品昌史、表面、**1996**、34、160.

7. Motomura, K.; Iwanaga, S.; Hayami, Y.; Uryu, S.; Matuura, R. *J. Colloid and Interface Sci*. **1981**, 80, 32.

8. Harkins, W. D.; Brown, F. E. *J. Am. Chem. Soc.* **1919**, 41, 499.

9. Lando, J. L.; Oakly, H. T. *J. Colloid Interface Sci.* **1967**, 25, 526.

10. Sakamoto, H.; Murao, A.; Hayami, Y. *The Journal of the Institute of Image Information and Television Engineers* 56 (2002) 1643.

11. Nomura, M.; Koyama, A.; Sakurai, M. *KEK report 91-1: Design and Performance of Beamline 7C at the Photon Factory*; Photon Factory: Tsukuba, Japan, 1991.

12. Watanabe, I.; Tanida, H. *Anal. Sci*. **1995**, 11, 525.

13. Yanase, E.; Watanabe, I.; Harada, M.; Takahashi, M.; Dake, Y.; Hiroshima, Y. *Anal. Sci*. **1999**, 15, 255.

14. Watanabe, I.; Tanida, H.; Kawauchi, S.; Harada, M.; Nomura, M. *Rev. Sci. Instrum*. **1997**, 68, 3307.

15. Takiue, T.; Kawagoe, Y.; Muroi, S.; Murakami, R.; Ikeda, N.; Aratono, M.; Tanida, H.; Sakane, H.; Harada, M.; Watanabe, I. *Langmuir* **2003**, 19, 10803.

Chapter 3 Counterion distribution in Single Surfactant Systems Investigated by Total Reflection XAFS

3-1. Introduction

As shown in Chapter 1, counterion distribution could be greatly influenced by both the nature and chemical structure of counterion and hydrophilic head group of surfactants. It has been also shown in several studies that counterions are concentrated and the binding ratio of counterions is increased with surface density of adsorbed molecules [1-5], which suggests that the surface charge density fundamentally influences counterion distribution. To investigate the specific ion effects from the viewpoint of counterion distribution, therefore, it is highly required to have the relation between the binding ratio and surface charge density. The binding ratio is evaluated from the analysis of the TR-XAFS spectra and the surface charge density from the surface density of surfactant ions.

For this purpose, the surface densities of surfactant ions $\Gamma^{\mathrm{H}}_{\mathrm{surfactant\ ion}}$ of DTAB, HTAB, DTAB in the presence of added NaBr and DeMIMBr were collected from our previous studies [6-9] and plotted against the molality of surfactant m_1 as shown in Fig. 3-1. The results will be cited later.

In this Chapter, first the procedure to obtain the bound ratio through EXAFS analysis is presented and then comparing the ratio of bound-Br vs. the surface density of surfactant ions curves for these surfactants, the relation between counterion distribution and surface charge density is discussed from the viewpoint of the effects of chain length, the added electrolyte and the hydrophilic head group.

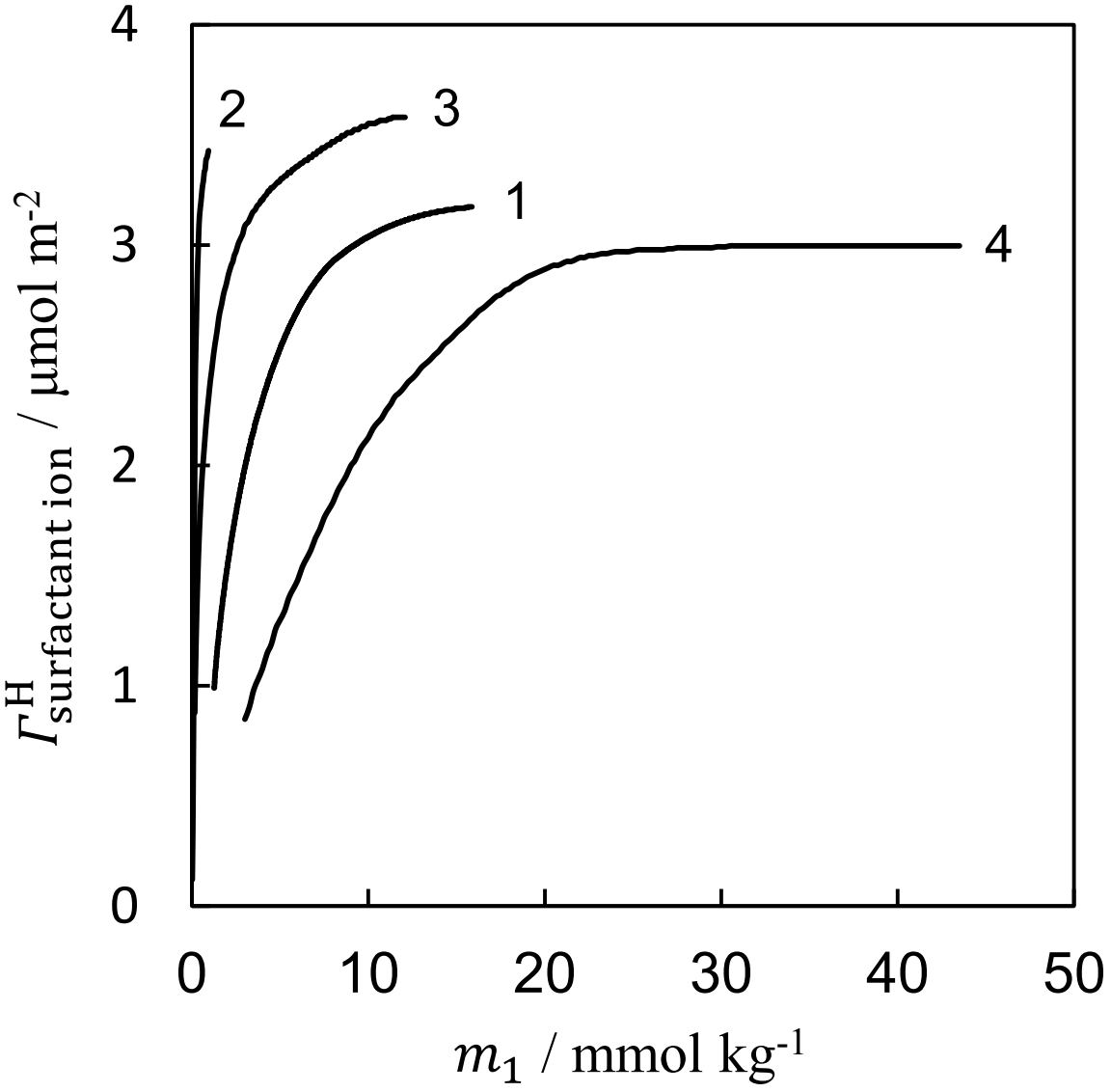

Figure 3-1. Surface density of surfactant ion vs. molality of surfactant for the single surfactant systems: (1) DTAB, (2) HTAB, (3) DTAB with 10 mmol kg-1 NaBr and (4) DeMIMBr.

3-2. Determination of the ratio of bound-Br through EXAFS analysis

The representatives of the TR-XAFS spectra are displayed for the DTAB system at four concentrations in Fig. 3-2. The spectra for other systems have been already demonstrated in the previous studies [8, 9]. In order to examine the distribution of Br^- ions from the standpoint of their solvation structure, the normalized EXAFS interference function $\chi(k)$ in k space, which we call EXAFS χ spectra, defined by

$$\chi(k) = \frac{\mu(k) - \mu_0(k)}{\mu_0(k)} \qquad (3-1)$$

$$k = \sqrt{\frac{2m}{\hbar^2}(E - E_0)} \qquad (3-2)$$

should be calculated from the TR-XAFS spectra according to usual procedure [10, 11]. Here, $\mu(k)$ is the experimental absorption coefficient due to the K-shell excitation evaluated by subtracting the background absorption due to the other shells and atoms $\mu_b(k)$ from I/I_0 where $\mu_b(k)$ is estimated with Victreen's formula: $AE^{-3} - BE^{-4} - C$. $\mu_0(k)$ is the absorption coefficient of a hypothetical isolated bromide atom containing the contribution from the multielectron excitation structure, k is the photoelectron wavenumber, m is the electron mass, E is the incident X-ray energy, and E_0 is the threshold energy which is determined to be the midpoint of the edge jump. The obtained EXAFS χ spectra were shown in Fig. 3-3 for the four systems. k^3 was multiplied for the convenience of the solvation structure analysis. It is said that the amplitude of χ spectra is decreased with increasing the molality and meanwhile, the isosbestic points are clearly observed. This means the EXAFS χ spectra of surfactant adsorbed films at different molalities can be expressed as a linear combination of two specific χ spectra, χ_1 and χ_2, as

$$\chi = (1 - \alpha)\chi_1 + \alpha\chi_2. \qquad (3-3)$$

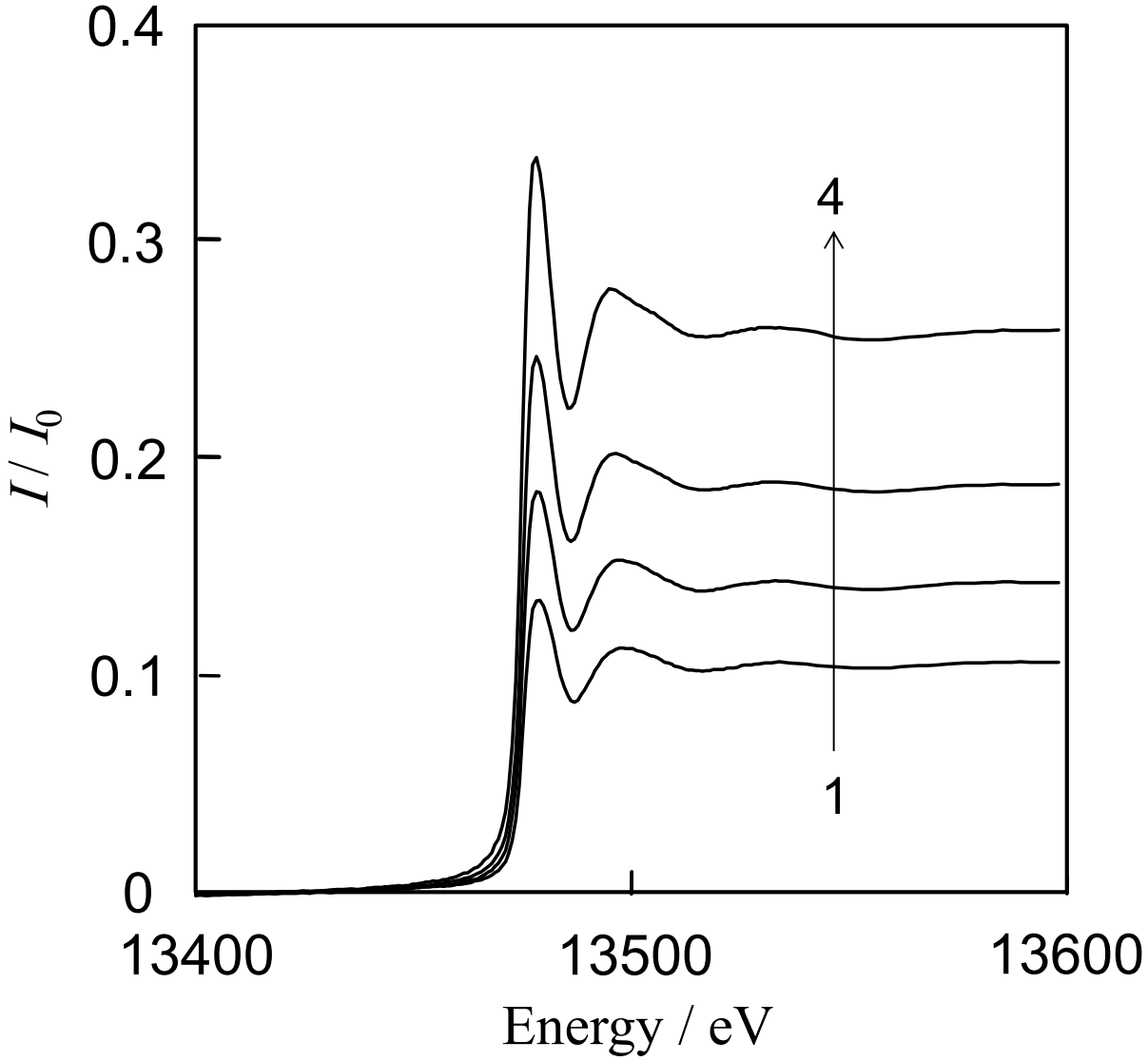

Figure 3-2. TR-XAFS spectra for DTAB system at m_1 = (1) 1.75, (2) 2.50, (3) 9.35 and (4) 30 mmol kg^{-1}.

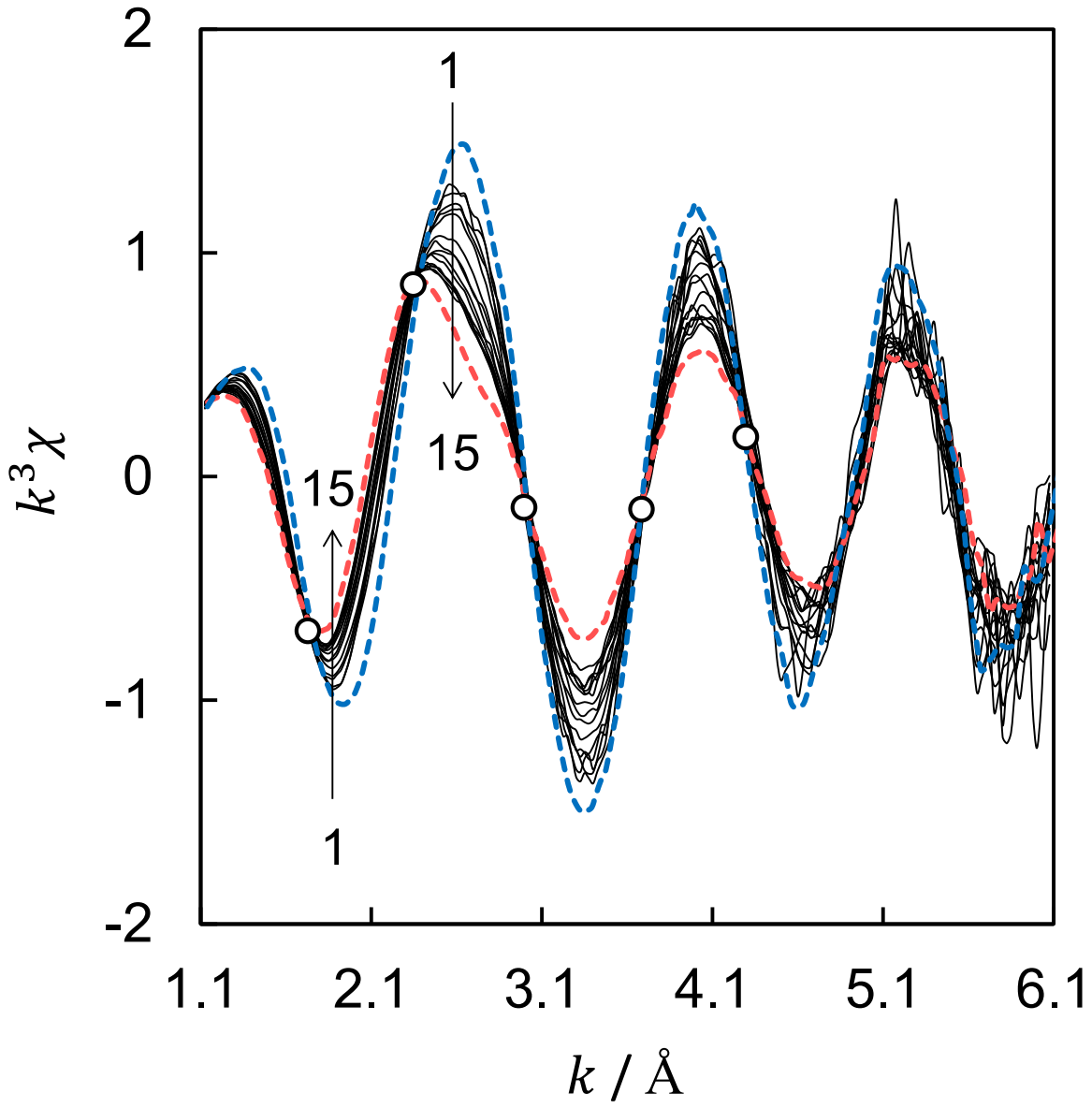

Figure 3-3(a). EXAFS $k^3\chi$ spectra of Br^- ion in the adsorbed film of DTAB pure system at m_1 / mmol kg^{-1} = (1) 1.38, (2) 1.50, (3) 1.63, (4) 1.75, (5) 2.00, (6) 3.00, (7) 3.50, (8) 4.00 (9) 5.00, (10) 6.25, (11) 7.50, (12) 8.75, (13) 10.0, (14) 12.5 and (15) 15.0. Open circles are the isosbestic points observed. Blue and red dashed curves represent respectively two specific $k^3\chi$ spectra χ_1 and χ_2 obtained through factor analysis.

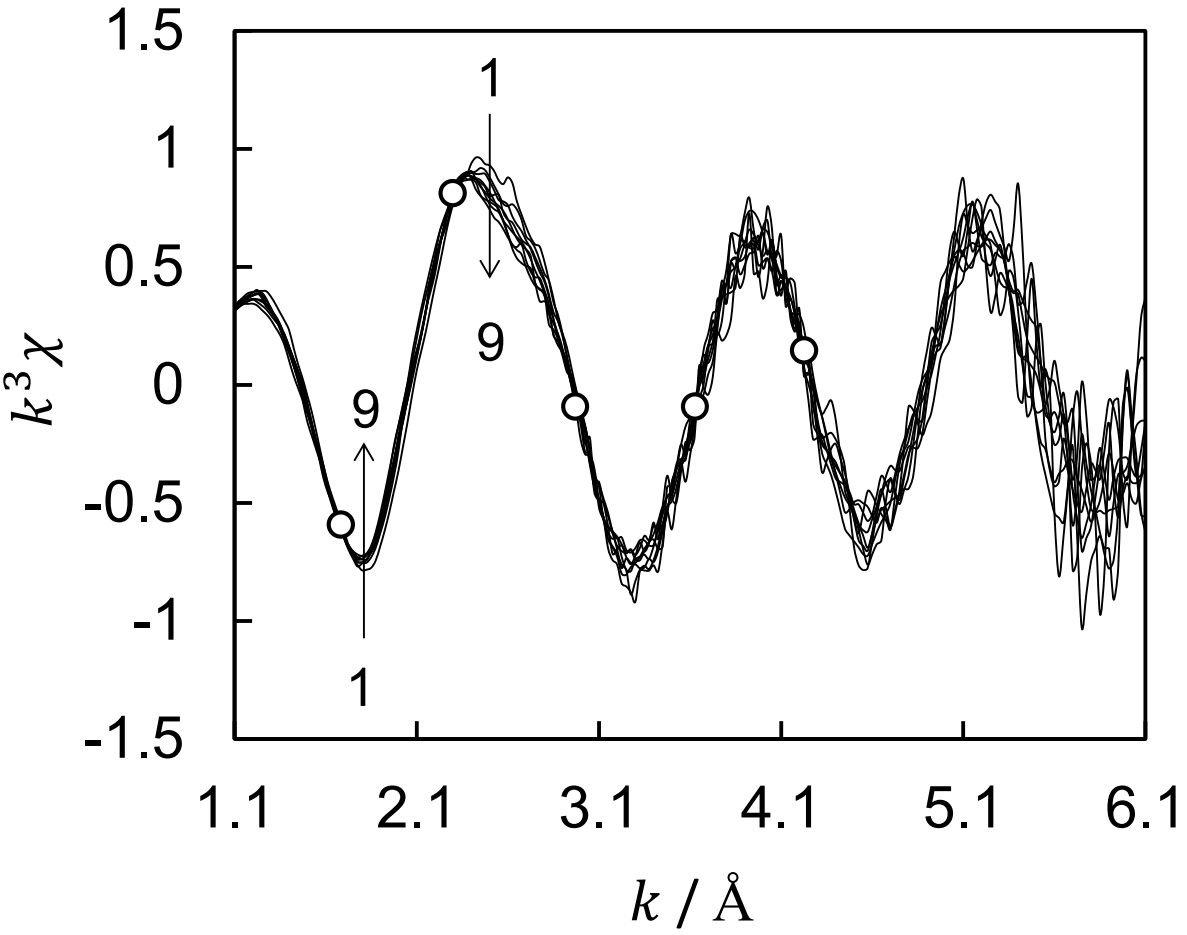

Figure 3-3(b). EXAFS $k^3\chi$ spectra of Br^- ion in the adsorbed film of HTAB pure system at m_1 / mmol kg^{-1} = (1) 0.30, (2) 0.40, (3) 0.50, (4) 0.60, (5) 0.70, (6) 0.80, (7) 0.85, (8) 0.90 and (9) 0.93. Open circles are the isosbestic points observed.

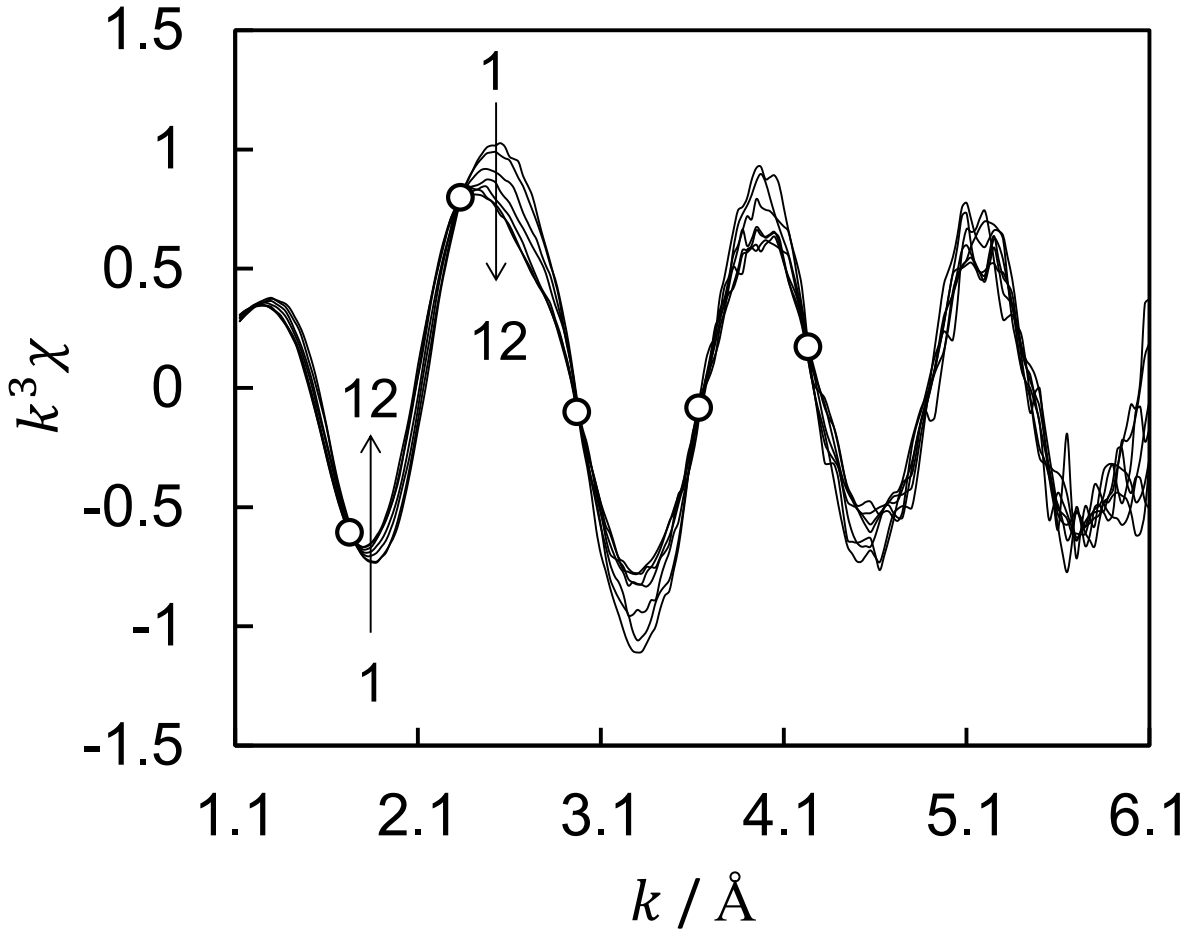

Figure 3-3(c). EXAFS $k^3\chi$ spectra of Br^- ion in the adsorbed film of DTAB with 10 mmmol kg^{-1} NaBr at m_1 / mmol kg^{-1} = (1) 0.64, (2) 0.96, (3) 1.99, (4) 4.00, (5) 7.01, (6) 10.3 and (7) 11.9. Open circles are the isosbestic points observed.

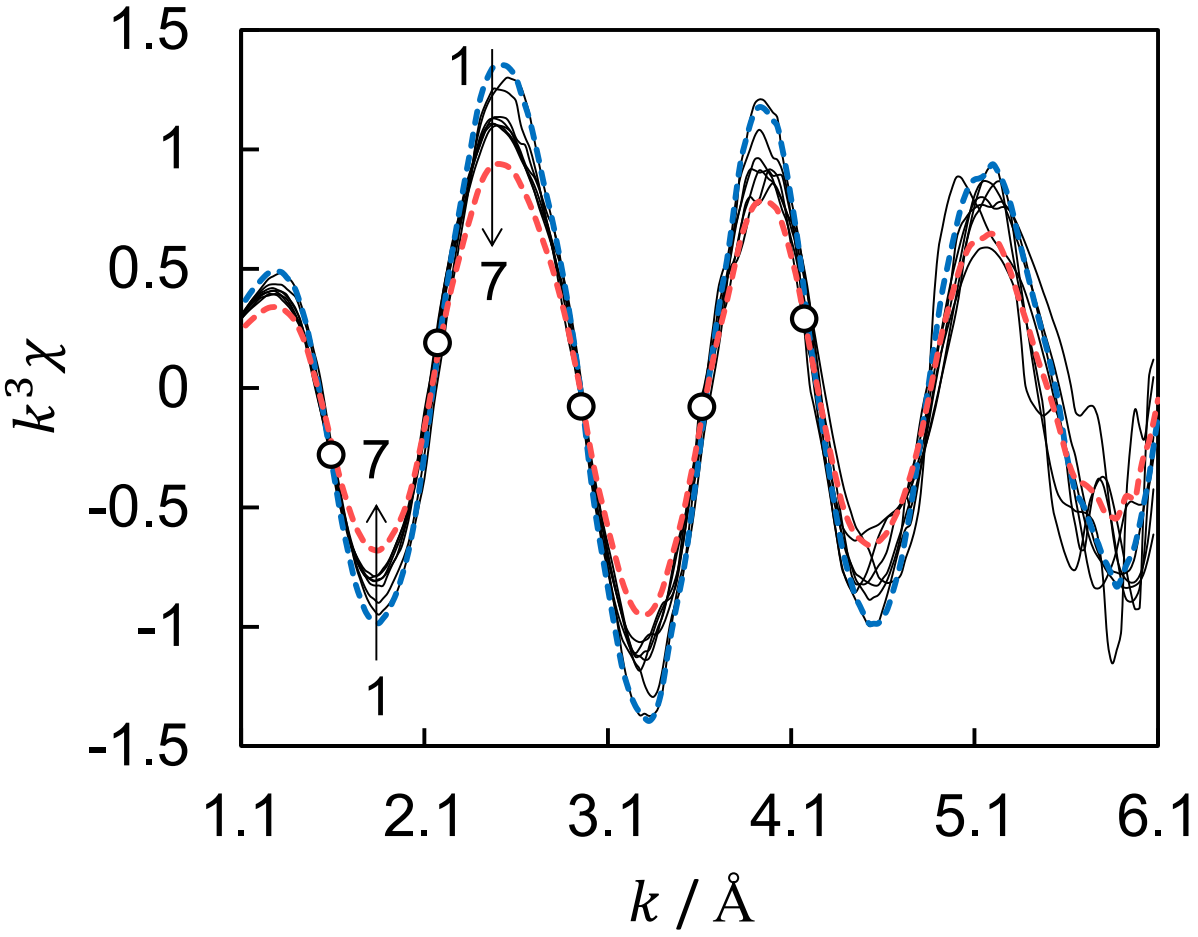

Figure 3-3(d). EXAFS $k^3\chi$ spectra of Br^- ion in the adsorbed film of DeMIMBr at m_1 / mmol kg^{-1} = (1) 6.00, (2) 10.0, (3) 24.0, (4) 32.0, (5) 36.0, (6) 40.0 and (7) 44.0. Open circles are the isosbestic points observed. Blue and red dashed curves represent respectively two specific $k^3\chi$ spectra χ_1 and χ_2 obtained through factor analysis.

Here χ_1 and χ_2 were the extracted from the experimental EXAFS χ spectra using factor analysis [12] and shown in Fig. 3-3 for the DTAB and DeMIMBr systems. $(1-\alpha)$ and α are the fractions of each spectrum components.

To extract the structure parameters from the two specific spectra, curve fitting was conducted for χ_1 and χ_2 using the following equation [13],

$$\chi(k) = \sum \frac{B_j F_j(k_j)}{k_j r_j^2} \exp\left(-2\sigma_j^2 k_j^2\right) \sin\left[2k_j r_j + \phi_j(k_j) - k_j^3 C_{3j}\right] \qquad (3-4)$$

$$k_j = \sqrt{k^2 - \frac{2m}{\hbar^2}\Delta E_{0j}} \qquad (3-5)$$

where the subscript j indicates the kind of the co-ordination shell. The back scattering amplitude of photoelectron $F(k)$ and the total phase shift ϕ were generated by the computer program FEFF version 8.10 for $r_{\mathrm{Br-O}} = 3.2$ Å [14]. The anharmonicity C_3 was fixed at 34.4×10^{-4} Å^3 [15]. Four kinds of parameters were estimated from the fitting procedure: the distance between absorbing and scattering atoms r, the Debye-Waller-like factor σ, the absorption edge shift ΔE_0 and the amplitude factor $B = SN$ where S is the amplitude reduction factor and N the number of scattering atoms.

Table 1(a) summarizes the result of the curve fitting using Eqs. 3-4 and 3-5 for obtained χ_1 and χ_2 spectra of the DTAB pure system demonstrated in Fig. 3-3(a). It is realized that only one coordination shell was extracted for χ_1 whereas two for χ_2. Taking into account that χ_1 is quite similar in shape to that obtained for dilute KBr (less than 1 M) aqueous solution [16] and the distance of about 3.2 Å between Br atom and scattering atom reasonably correspond to that between Br atom and oxygen atom of the hydrated Br ions obtained by other techniques [17, 18], Br^- in the χ_1 state is referred to as free-Br because it is free from coordination to any other atoms than water

Table 3-1(a). EXAFS curve fitting results for the DTAB single system.

		shell	B	N	r / Å	σ / Å	ΔE_0	R (%)
χ_1	Free Br	1	4.73	6.0	3.2	0.20	-3.05	4.70
χ_2	Bound Br	1	2.50	3	3.2	0.19	-5.63	7.97
		2	3.10	4	4.1	0.38	5.68	

Table 3-1(b). EXAFS curve fitting results for the DeMIMBr single system.

		shell	B	N	r / Å	σ / Å	ΔE_0	R (%)
χ_1	Free Br	1		6.0	3.2	0.20	-1.41	5.31
χ_2	Bound Br	1		4	3.2	0.19	-1.87	4.18
		2		3	4.2	0.39	9.35	

molecules. The number of scattering atoms N for χ_1 was assumed to be six because this value is generally accepted as the probable value [17, 18]. In the χ_2 state, N was determined using the value of the amplitude reduction factor S obtained for χ_1, and about four scattering atoms were also observed around about 4.1 Å in the second shell instead. Referring to the results of χ_1, it can be concluded that the hydration number of Br^- ion in the χ_2 state is about three, and the four atoms in the second shell are probably attributable to the atoms in the hydrophilic group of surfactant ion e.g., one N and three C since its distance is approximately the average of Br-N and Br-C in the crystal of DTAB [19]. Therefore, we call the bromide ions in the χ_2 state the bound-Br where Br^- is partially bound to other atoms in addition to water molecules. Similar results are obtained also for χ_1 and χ_2 for the DeMIMBr system as shown in Table 1(b).

3-3. Counterion distribution in the DTAB, HTAB, DTAB-NaBr and DeMIMBr systems

To investigate the counterion distribution, the ratio of bound-Br α for the DTAB, HTAB and DTAB-NaBr systems and that for the DeMIMBr system were evaluated respectively by the reference to χ_1 and χ_2 spectra for the DTAB and DeMIMBr single surfactant systems, and they are plotted against the surface density of surfactant ion (see Fig. 3-1) in Fig. 3-4. It is clearly shown that the ratio of bound Br is increased with surface density for all systems. Although a qualitative trend itself that α could increase with increasing the surface density of surfactant ion was suggested by other researches as mentioned in 3.1, it should be noted that the counterion distribution was evaluated experimentally and quantitatively without any models of electrical double

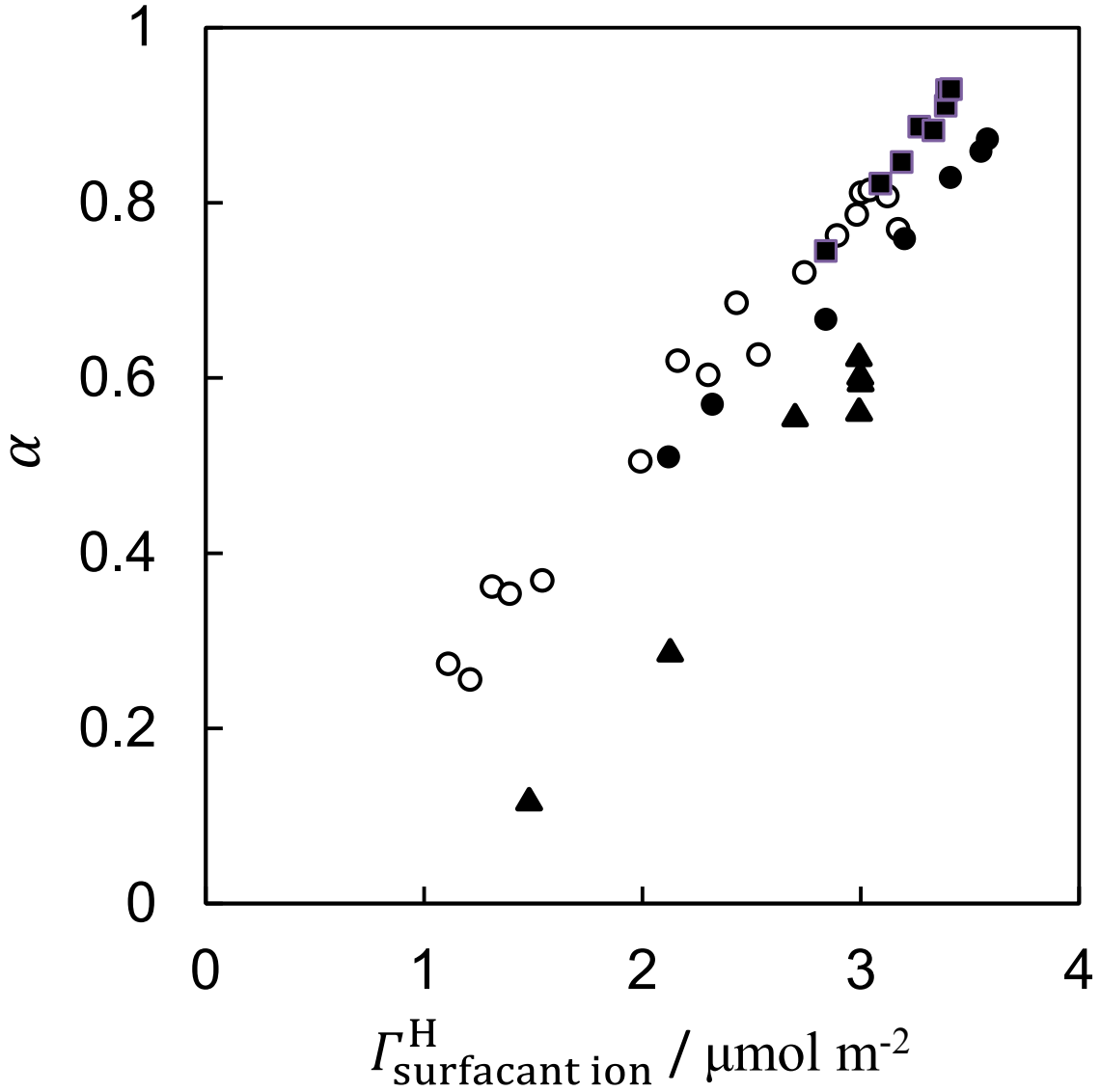

Figure 3-4. The ratio of bound-Br vs. the surface density of surfactant ion for DTAB (open circle) HTAB (filled square), DTAB with 10 mmol kg^{-1} NaBr (filled circle), and DeMIMBr (filled triangle) systems.

layer through TR-XAFS technique followed by the well confirmed EXAFS analysis.

Let us look at closely the results. The value of α for HTAB (filled squares) is almost coincident with and that for DTAB with 10 mmol kg^{-1} NaBr (filled circles) seems to be only a little smaller than that for DTAB (open circles) at a fixed surface density. These results indicate that the difference in chain length and adding electrolyte are not so much influential on counterion distribution when the head group is the same as each other. However, it should be noted here that the value of α is evidently smaller for DeMIMBr than for DTAB at the same surface density, which in turn the surface density of surfactant ion is larger for DeMIMBr than for DTAB at the same binding ratio α. This may because imidazolium cations can take a kind of stacking alignment because of the plain ring structure of their head groups. Taking account of the experimental finding that EXAFS $k^3\chi$ spectrum of the adsorbed film could be expressed by the sum of two kinds of spectra, the adsorbed films consist of only two states of free and bound Br ions, and on average there is no intermediate situation for adsorbed surfactant molecules. The most conceivable situation deduced from these observations is that the adsorbed molecules are definitely not homogeneously dispersed but a part of them are molecularly dispersed around the domains (islands or clusters) with the bound Br ions . Therefore it is indicated that the arrangement of hydrophilic headgroups in the adsorbed film and thus the distribution of surface charge due to surfactant ions could greatly influence counterion distribution in the electrical double layer.

3-4. References

1. Kalinin, V. V.; Radke, C. J. *Colloids and Surfaces A* **1996**, 114, 337.
2. Para, G.; Warszynski, P. *Colloids and Surfaces A* **2007**, 300, 346.
3. Hantal, G.; Partay, L. B.; Varga, I.; Jedlovszky, P.; Gilanyi, T. *J. Phys. Chem. B* **2007**, 111, 1769.
4. Shapovalov, V.; Brezesinski, G. *J. Phys. Chem. B* **2006**, 110, 10032.
5. Alargova, R. G.; Danov, K. D.; Petkov, J. P.; Kralchevsky, P. A.; Broze, G.; Mehreteab, A. *Langmuir* **1997**, 13, 5544.
6. Li, H. H.; Imai, Y.; Hayami, Y.; Takiue, T.; Matsubara, H.; Aratono, M. *J. Colloid and Interface Sci.* **2011**, 359, 189.
7. Kashimoto, K.; Matsubara, H.; Takahara, H.; Nakano, T.; Takiue, T.; Aratono, M. *Colloid. Polym. Sci.* **2004**, 283, 329. T. Nakano, Master thesis entitled *Synergism in the Adsorbed Films and Micelles of Binary Cationic Surfactant Mixtures with Different Hydrophobic Chain Length*; Department of Chemistry, Graduate School of Sciences, Kyushu University: Fukuoka, Japan, 2005.
8. Kashimoto, K.; Takata, Y.; Matsuda, T.; Ikeda, N.; Matsubara, H.; Takiue, T.; Aratono, M.; Tanida, H.; Watanabe, I. *Langmuir* **2006**, 22, 8403.
9. Aratono, M.; Shimamoto, K.; Onohara, A.; Murakami, D.; Tanida, H.; Watanabe, I.; Ozeki, T.; Matsubara, H.; Takiue, T. *Anal. Sci.* **2008**, 24, 1279.
10. Sakane, H.; Miyanaga, T.; Watanabe, I.; Matsubayashi, N.; Ikeda, S.; Yokoyama, Y. *J. Appl. Phys.* **1993**, 32, 4641.
11. Tanida, H.; Sakane, H.; Watanabe, I. *J. Chem. Soc. Dalton Trans.* **1994**, 15, 2321.
12. Ozeki, T.; Kihara, H.; Hikime, S. *Anal. Chem.* **1987**, 59, 945.
13. Frenkel, A. I.; Rehr, J. J. *Phys. Rev. B* **1993**, 48, 585.

14 Ankudinov, A. L.; Rehr, J. J. *Phys. Rev. B* **2000**, 62, 2437.

15. Sawa, Y.; Miyanaga, T.; Tanida, H.; Watanabe, I. *J. Chem. Soc. Faraday Trans.* **1995**, 91, 4389.

16. Watanabe, I.; Tanida, H. *Anal. Sci*. **1995**, 11, 525.

17. Ohtaki, H.; Radnai, T. *Chem. Rev.* **1993**, 93, 1157.

18. Raugei, S.; Klein, M. *J. Chem. Phys.* **2002**, 116, 196.

19. Kamitori, S.; Sumimoto, Y.; Vongbupnimit, K.; Noguchi K.; Okuyama, K. *Mol. Crist. Liq. Cryst.* **1997**, 300, 31.

Chapter 4 Miscibility and Distribution of Binary Counterions in the Surfactant Adsorbed Films

4-1. Introduction

In Chapter 3, the relation between counterion distribution and surface charge density was explored on the basis of the ratio of bound-Br evaluated by the solvation structure analysis of TR-XAFS method. This chapter is concerned with the systems containing two kinds of counterions with the common surfactant ion to investigate the specific ion effect more closely.

In the mixed surfactant systems containing common surfactant ions but different counterions, the counterion distribution such as preferential binding of counterion to the surfactant ion and their miscibility at interfaces are expected to provide information on the specific ion effect. In our previous study, taking advantage of the phase diagram of adsorption (PDA) through surface tension measurement and thermodynamic analysis, we examined the miscibility by calculating the composition of counterions and surfactant ions in the adsorbed films, and then by evaluating the excess Gibbs energy of adsorption on the basis of the criterion of ideal mixing [1]. We have previously studied miscibility of Cl^- and Br^- in the adsorbed film of dodecyltrimethylammonium bromide (DTAB) and dodecyltrimethylammonium chloride (DTAC) [2]. In this system, although it was shown that the composition of Br^- ion in the adsorbed film $\hat{X}_2^{\mathrm{H}}$ was larger than that in the bulk phase $\hat{X}_2$, an ideal mixing was observed. In such a case the excess Gibbs free energy of adsorption $\hat{g}^{\mathrm{H,E}}$ is almost zero as shown in Fig. 4-1. In contrast to the DTAB-DTAC system, we recently found nonideal mixing behavior in the adsorbed film of the DTAB-$DTABF_4$ and HMIMBr-$HMIMBF_4$ systems

[3, 4]. This is clearly demonstrated by $\hat{g}^{\mathrm{H,E}}$ as a function of $\hat{X}_2^{\mathrm{H}}$ in Fig. 4-1. The negative $\hat{g}^{\mathrm{H,E}}$ of the DTAB-$DTABF_4$ system shows the preferable mixing of counterions at the surface in terms of free energy, whereas the positive one of the HMIMBr-$HMIMBF_4$ system the unpreferable mixing of them. These results were explained from the difference in size, surface activity of counterions and specific hydrogen bonding between $HMIM^+$ ion and BF_4^- ion.

In this chapter, the total reflection X-ray absorption fine structure (TR-XAFS) measurement was applied to above mentioned three systems to investigate the counterion distribution in the electrical double layer with the aid of the ratio of bound-Br. The ion binding could be also investigated complementarily by other technique like X-ray reflectometry that gives us an electron density profile [5, 6] and surface potential, surface tension, or X-ray reflectivity followed by a model fitting [7-9]. However, the TR-XAFS measurement is an element-selective (Br-selective in the present study) and thus can provide the ratio of free- and bound-Br ions regardless of the existence of other counterions. Furthermore, the bromide ion used as probe for the TR-XAFS measurement in this thesis is in almost the center of the Hofmeister series (SO_4^{2-} HPO_4^{2-} OAc^- cit^- OH^- Cl^- Br^- NO_3^- ClO_3^- BF_4^- I^- ClO_4^- SCN^- PF_6^-) [10]. In this respect, this technique is especially advantageous for investigating the preferential binding of the counterions in mixed systems.

The ratio of free- and bound-Br ions was determined as a function of the surface tension and the surface composition of surfactants. From the comparison among the DTAB-DTAC, DTAB-$DTABF_4$ and HMIMBr-$HMIMBF_4$ systems, the relation between the miscibility and distribution of counterions at the solution surface are discussed from the view point of the specific ion effect.

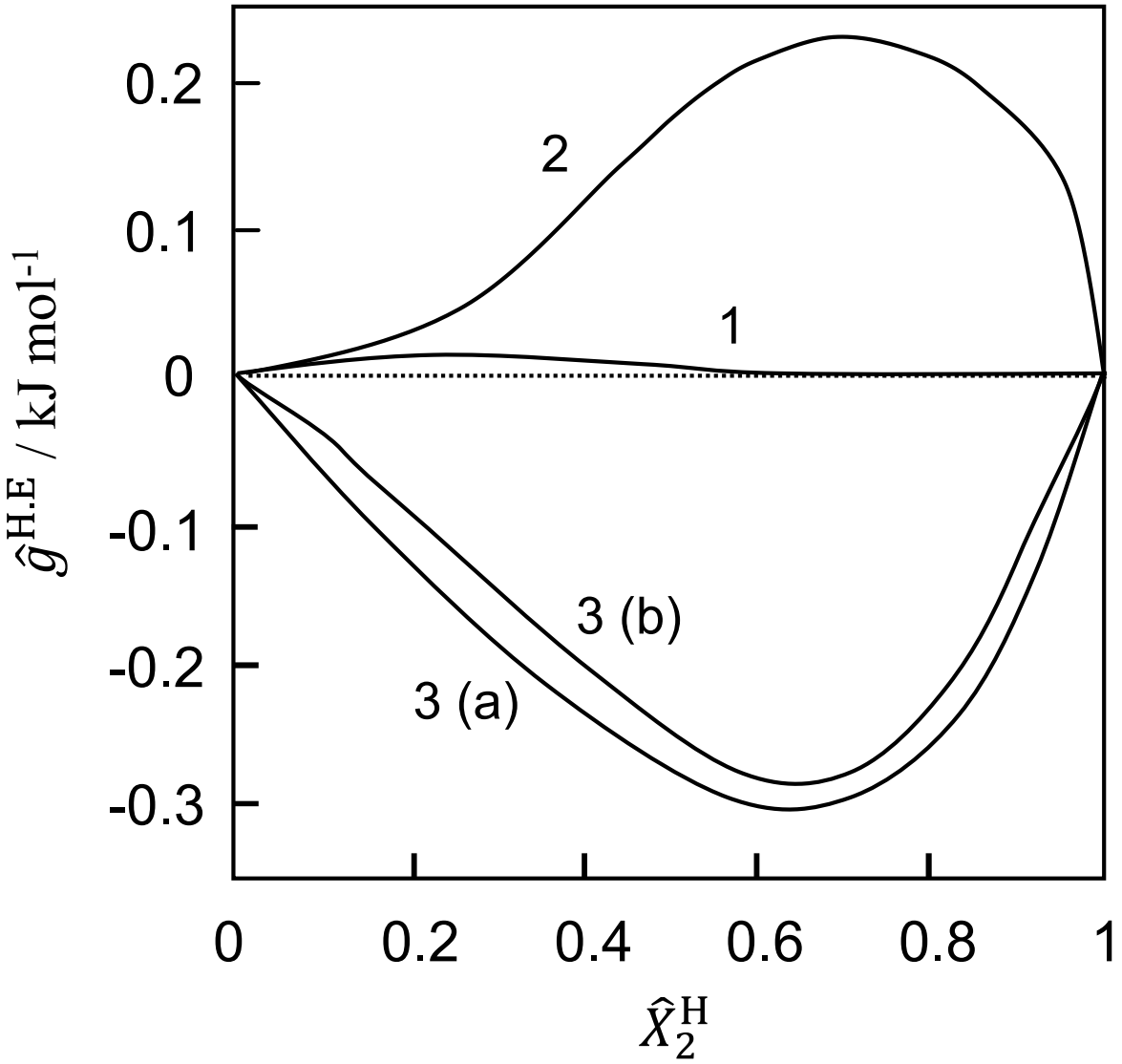

Figure 4-1. Excess Gibbs energy of adsorption vs. surface composition curves for (1) DTAB-DTAC (45.0 mN m^{-1}), (2) HMIMBr-$HMIMBF_4$ (45.0 mN m^{-1}), and (3) DTAB-$DTABF_4$ ((a) 45.0 and (b) 55.0 mN m^{-1}).

4-2. Determination of surface compositions of counterions through Jump value analysis.

TR-XAFS measurement was applied to the DTAB-$DTABF_4$ mixed adsorbed films at different total concentration of surfactants $\hat{m}$ and composition of $DTABF_4$ in the bulk solution $\hat{X}_2$ that give a constant surface tension. $\hat{m}$ and $\hat{X}_2$ are respectively defined by

$$\hat{m} = 2m_1 + 2m_2 \qquad (4-1)$$

and

$$\hat{X}_2 = 2m_2/\hat{m} \qquad (4-2)$$

where m_1 and m_2 are the molalities of DTAB and $DTABF_4$, respectively. Here the coefficients 2 are for taking account of the dissociation of ionic surfactants. The selected combination of $\hat{m}$ and $\hat{X}_2$ that give 55.0 mN m^{-1} and 45.0 mN m^{-1} were marked by open circles in Fig. 4-2 and these conditions were determined referring to the phase diagram shown as curves in Fig. 4-2 constructed in advance through surface tension measurement and thermodynamic analysis [3].

The solid and dashed lines represent the relation between $\hat{m}$ and $\hat{X}_2$ and that between $\hat{m}$ and $\hat{X}_2^{\mathrm{H}}$ at the given surface tension, respectively. Here $\hat{X}_2^{\mathrm{H}}$ is the surface composition that expresses the mole fraction of $DTABF_4$ in the mixed adsorbed film in equilibrium with bulk solution defined by,

$$\hat{X}_2^{\mathrm{H}} = 2\Gamma_2^{\mathrm{H}}/(2\Gamma_1^{\mathrm{H}} + 2\Gamma_2^{\mathrm{H}}). \qquad (4-3)$$

where, Γ_1^{H} and Γ_2^{H} are the surface excess of DTAB and that of $DTABF_4$, respectively. Here coefficients 2 are also for considering the dissociation of ionic surfactants. The value of $\hat{X}_2^{\mathrm{H}}$ can be calculated by applying the thermodynamic equation

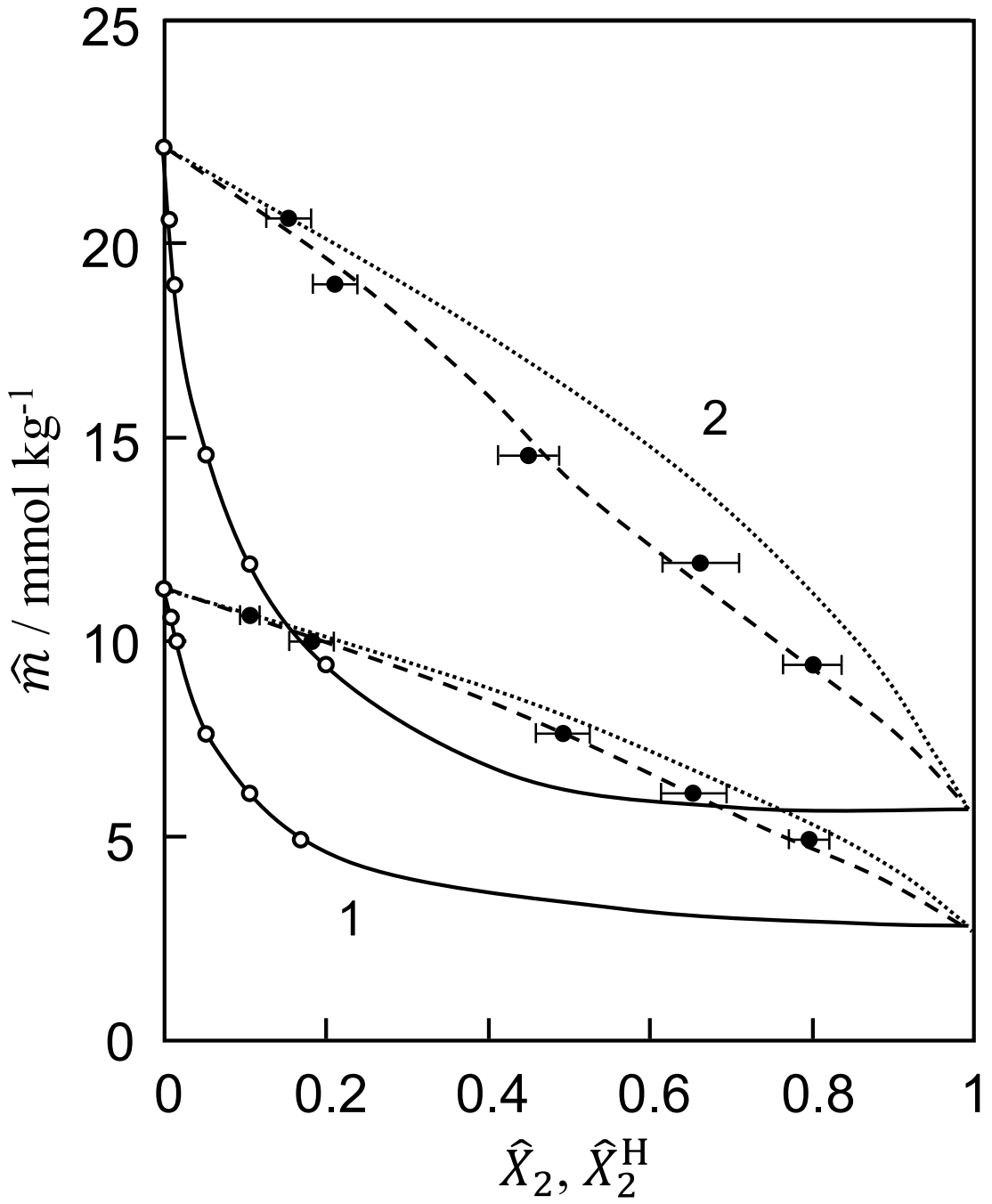

Figure 4-2. Total molality vs. bulk and surface composition curves of DTAB-$DTABF_4$ system at (1) 55.0 and (2) 45.0 mN m^{-1}. (——) $\hat{m}$ vs. $\hat{X}_2$, (- - -) $\hat{m}$ vs. $\hat{X}_2^{\mathrm{H}}$, and (·····) $\hat{m}$ vs. $\hat{X}_2^{\mathrm{H}}$ of ideal mixing. Filled circles show the surface compositions evaluated from TR-XAFS measurements at several ($\hat{m}$ vs. $\hat{X}_2$) combinations shown by open circles.

$$\hat{X}_2^{\mathrm{H}} = \hat{X}_2 - \frac{2\hat{X}_1\hat{X}_2}{\hat{m}}\left(\frac{\partial \hat{m}}{\partial \hat{X}_2}\right)_{T,p,\gamma} \qquad (4-4)$$

to the $\hat{m}$ vs. $\hat{X}_2$ curves [1]. These curves show the relation between the composition in the adsorbed film and that in the bulk phase, therefore we call them the phase diagram of adsorption (PDA).

We evaluated the surface composition also from TR-XAFS measurement. Examples of TR-XAFS spectra measured at the given $\hat{m}$ and $\hat{X}_2$ by open circles in Fig. 4-2 were shown in Fig. 4-3(a) and (b). In both figures, it is seen that the absorption of X-ray was increased with increasing the bulk composition of Br^- ion. The vertical distance between the best fitted linear lines in the lower and higher energy regions at the inflection point of the TR-XAFS spectrum (see the insert in Fig. 4-3(a)) is related to the amount of Br^- ions near the surface by the next equation [11]:

$$J = kS\int_0^\infty C(z)P(z)dz = kSP(0)\int_0^\infty C(z)\exp\left(-\frac{z}{\lambda}\right)dz \qquad (4-5)$$

where k is a proportional constant, S the footprint at the air/solution interface, $P(0)$the intensity of the incident X-ray, and λ is the penetration depth of the evanescent wave. Here λ is experimentally estimated to be about 9 nm for the present system [12]. The Debye length of the electrical double layer for surfactant adsorbed films examined in this study is estimated to be less than about 2 nm [13], therefore measured J values include the contribution from Br^- ions in the bulk solution. We subtracted this contribution by using the J value of NaBr solution having the same Br^- concentration of the surfactant solutions J_{NaBr}, and the value only attributable to Br^- ions in the adsorbed film J_{film} was evaluated. Assuming that J_{film} is proportional to the thermodynamic surface excess Γ_1^{H} with a proportional constant, one can also evaluate the surface composition of surfactants using J_{film} and the total surface density $\hat{\Gamma}^{\mathrm{H}}$ calculated from

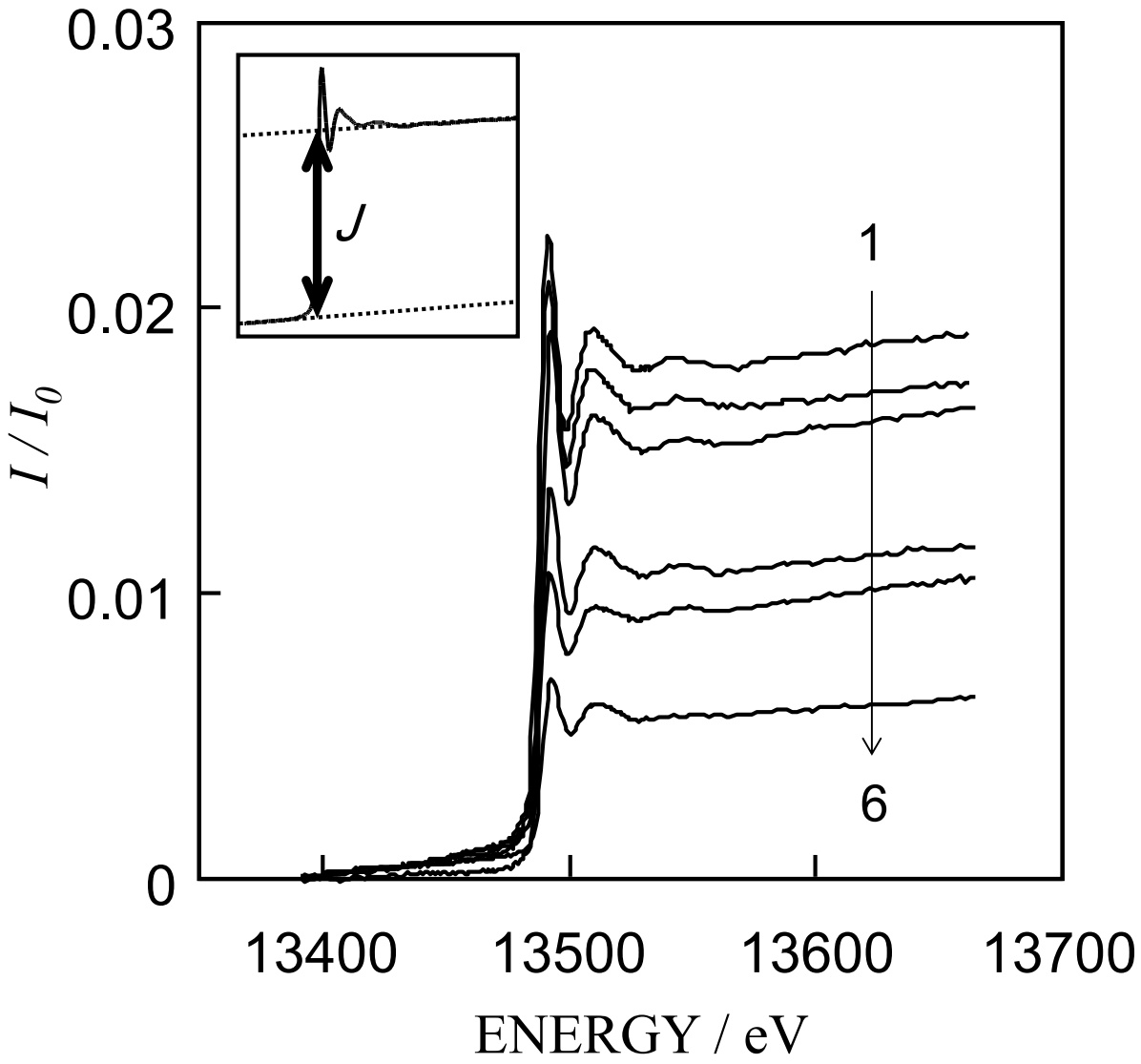

Figure 4-3(a). TR-XAFS spectra for DTAB-DTABF$_4$ system at 55.0 mN m^{-1} and ($\hat{X}_2$, $\hat{m}$ / mmol kg^{-1}) = (1) (0, 11.25), (2) (0.008, 10.5), (3) (0.013, 9.86), (4) (0.050, 7.64), (5) (0.100, 6.26), and (6) (0.200, 5.00). The I / I_0 values at 13391 eV were set at 0 for all spectra.

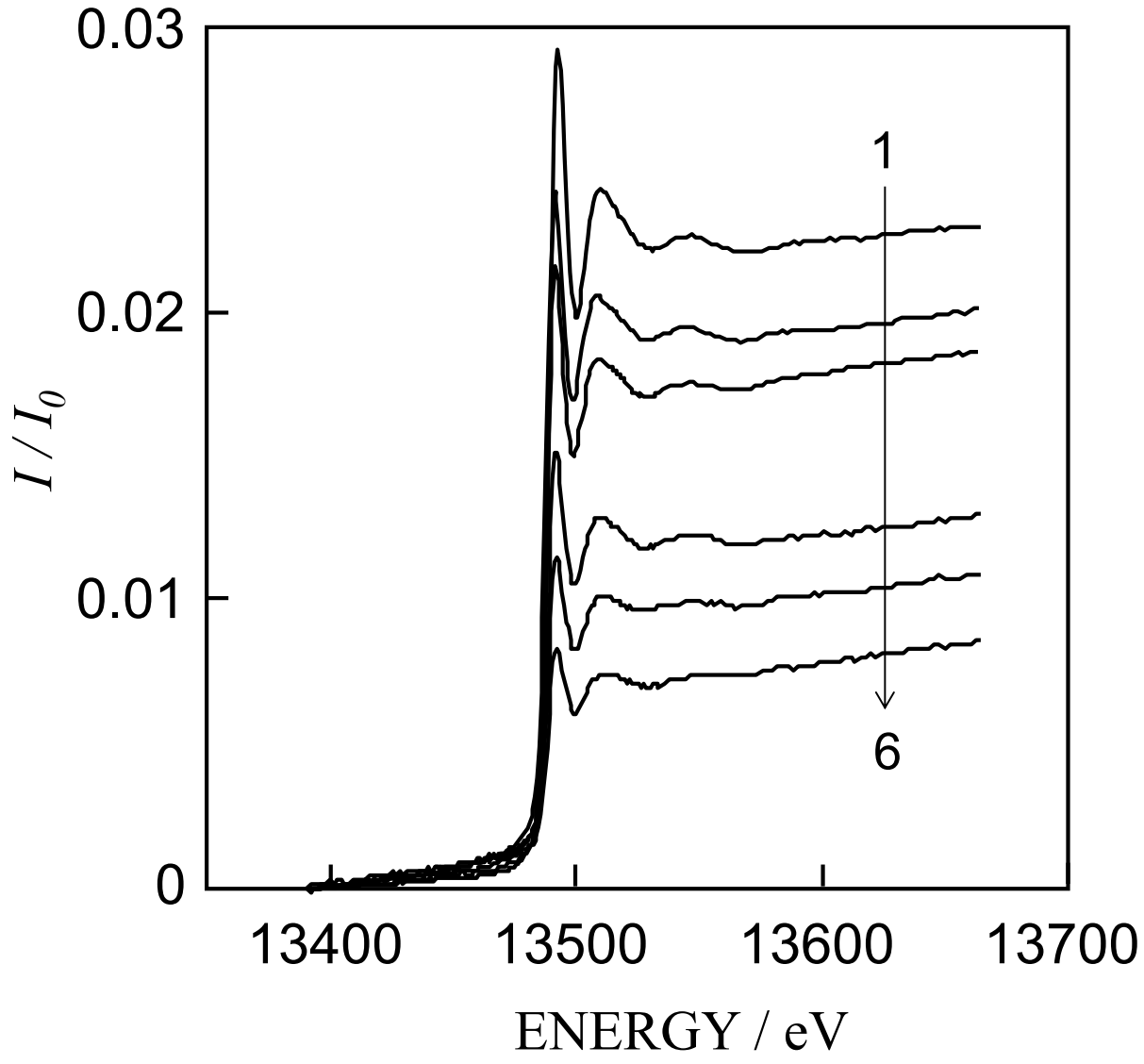

Figure 4-3(b). TR-XAFS spectra for DTAB-DTABF$_4$ system at 45.0 mN m^{-1} and ($\hat{X}_2$, $\hat{m}$ / mmol kg^{-1}) = (1) (0, 22.00), (2) (0.008, 20.40), (3) (0.013, 18.70), (4) (0.050, 14.40), (5) (0.100, 11.60), and (6) (0.200, 9.20). The I / I_0 values at 13391 eV were set at 0 for all spectra.

the surface tension vs. $\hat{m}$ curves at given $\hat{X}_2$ [4]. The results were plotted as filled circles in Fig. 4-2 and a reasonable coincidence between the surface compositions obtained by the thermodynamics and TR-XAFS guarantees the reliability of the present experiment.

From Fig 4-2, it is shown that BF_4^- ion is richer in the adsorbed film than in the bulk phase, which is expected because the affinity of counterions to the surface obeys the order of the Hofmeister series [10]. Similar results were also obtained by other researchers [14, 15]. We also evaluated the miscibility of counterions in reference to the thermodynamic criterion. The dotted curves in Fig. 4-2 represent the $\hat{m}$ vs. $\hat{X}_2^{\mathrm{H}}$ curves in the thermodynamically ideal mixing [1]. The negative deviation of $\hat{m}$ vs. $\hat{X}_2^{\mathrm{H}}$ curves from the ideal mixing yields the negative $\hat{g}^{\mathrm{H,E}}$ in Fig. 4-1 and indicates that the surface composition of Br^- ions was enhanced from the ideal mixing although BF_4^- ions have higher affinity to the surface. It should be noted here that the surface composition evaluated by Eq. 4-4 counts all the (excess) BF_4^- ions and Br^- ions in the surface region, that is, mixing of counterions evaluated by PDA is that for any kinds of counterions in the electrical double layer (Stern and diffuse layer). In the following section, we examine the state of counterion mixing from the view point of counterion distribution through EXAFS analysis.

4-3. Miscibility and distribution of binary counterions in the DTAB-DTAC, DTAB-DTABF$_4$ and HMIMBr-HMIMBF$_4$ systems

In order to examine the distribution of Br^- ions from the solvation structure of Br^- ions, the EXAFS χ spectra were constructed in the same procedure shown in Chapter 3, and they are shown in Fig. 4-4. In the DTAB-DTABF$_4$ mixed system, the signal

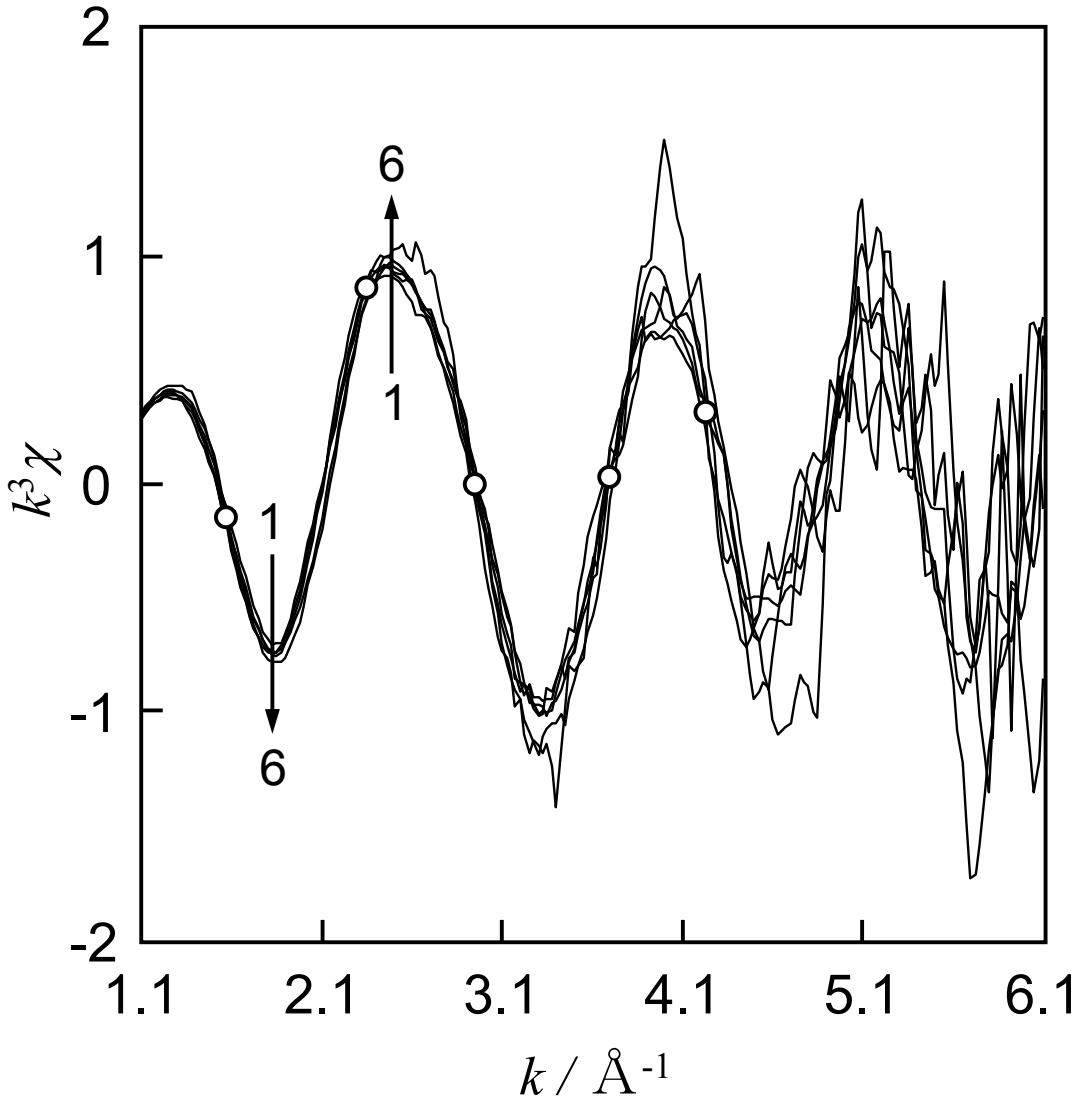

Figure 4-4(a). EXAFS $k^3\chi$ spectra of Br^- ion in the adsorbed film of DTAB-$DTABF_4$ system at 55.0 mN m^{-1} and ($\hat{X}_2$, $\hat{m}$ / mmol kg^{-1}) = (1) (0, 11.25), (2) (0.008, 10.5), (3) (0.013, 9.86), (4) (0.050, 7.64), (5) (0.100, 6.26), and (6) (0.200, 5.00). Open circles are the isosbestic points determined.

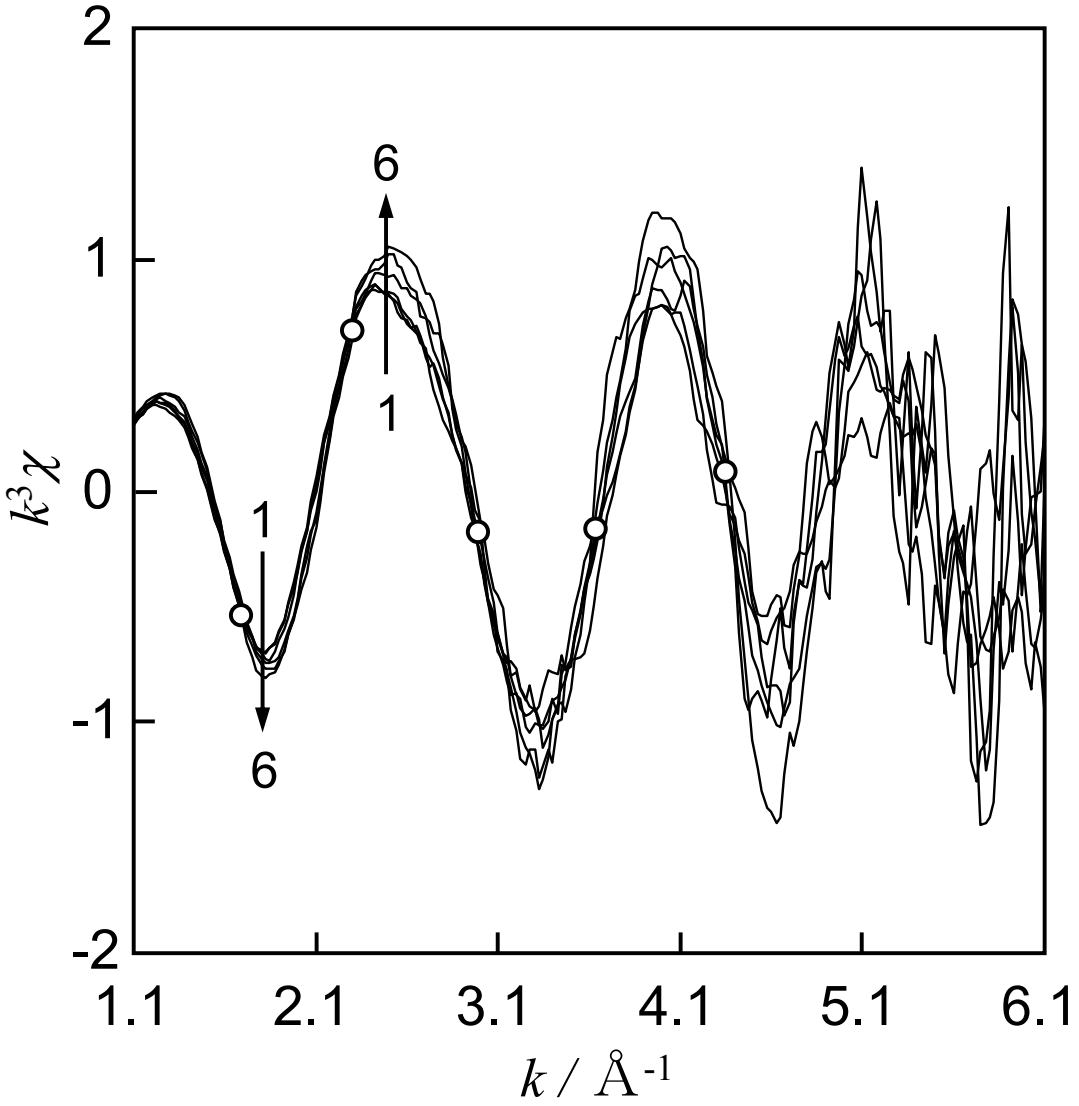

Figure 4-4(b). EXAFS $k^3\chi$ spectra of Br^- ion in the adsorbed film of DTAB-$DTABF_4$ system at 45.0 mN m^{-1} and ($\hat{X}_2$, $\hat{m}$ / mmol kg^{-1}) = (1) (0, 22.00), (2) (0.008, 20.40), (3) (0.013, 18.70), (4) (0.050, 14.40), (5) (0.100, 11.60), and (6) (0.200, 9.20). Open circles are the isosbestic points determined.

intensity is smaller than that of the DTAB pure system due to the smaller amount of Br^- ions at surface, so χ spectra were rather noisy especially at the high k region. However, the isosbestic points are clearly observed. Hence, in this mixed system, we evaluated α for each spectrum at the region where k is smaller than 4 with the reference to χ_1 and χ_2 for the DTAB pure system evaluated in Chapter 3. In Fig. 4-5, the α values obtained are plotted against the counterion composition in the adsorbed film together with the previously obtained results for the DTAB-DTAC and the HMIMBr-HMIMBF$_4$ systems [4, 16].

The dependence of α on $\hat{X}_2^{\mathrm{H}}$ is quite different among three systems and provides us information on the relation between counterion distribution and miscibility of counterion. For the case of ideal mixing (DTAB-DTAC system), the ratio of bound-Br increases with decreasing the surface tension, thus with increasing total surface density of counterions, but is not so changed with decreasing the surface composition of Br^- ions. That is, the mixing of Cl^- ions has practically no influences to the distribution of Br^- ions in the adsorbed film. Hence, we considered such behavior of counterion distribution as a criterion for the ideal mixing.

When the PDA shows positive deviation from the ideal mixing and unpreferable mixing is observed (HMIMBr-HMIMBF$_4$ system), on the other hand, the α is almost zero irrespective of surface tension and surface composition examined. This implies that almost all Br^- ions are not in the vicinity of hydrophilic head groups but in the diffuse layers and fully hydrated by six water molecules. For neat ionic liquids having cationic imidazolium head group, there are several experimental reports on their surface structures studied by sum frequency spectroscopy and X-ray reflectivity [17], direct recoil spectrometry [18], X-ray photoelectron spectroscopy [19] and neutron

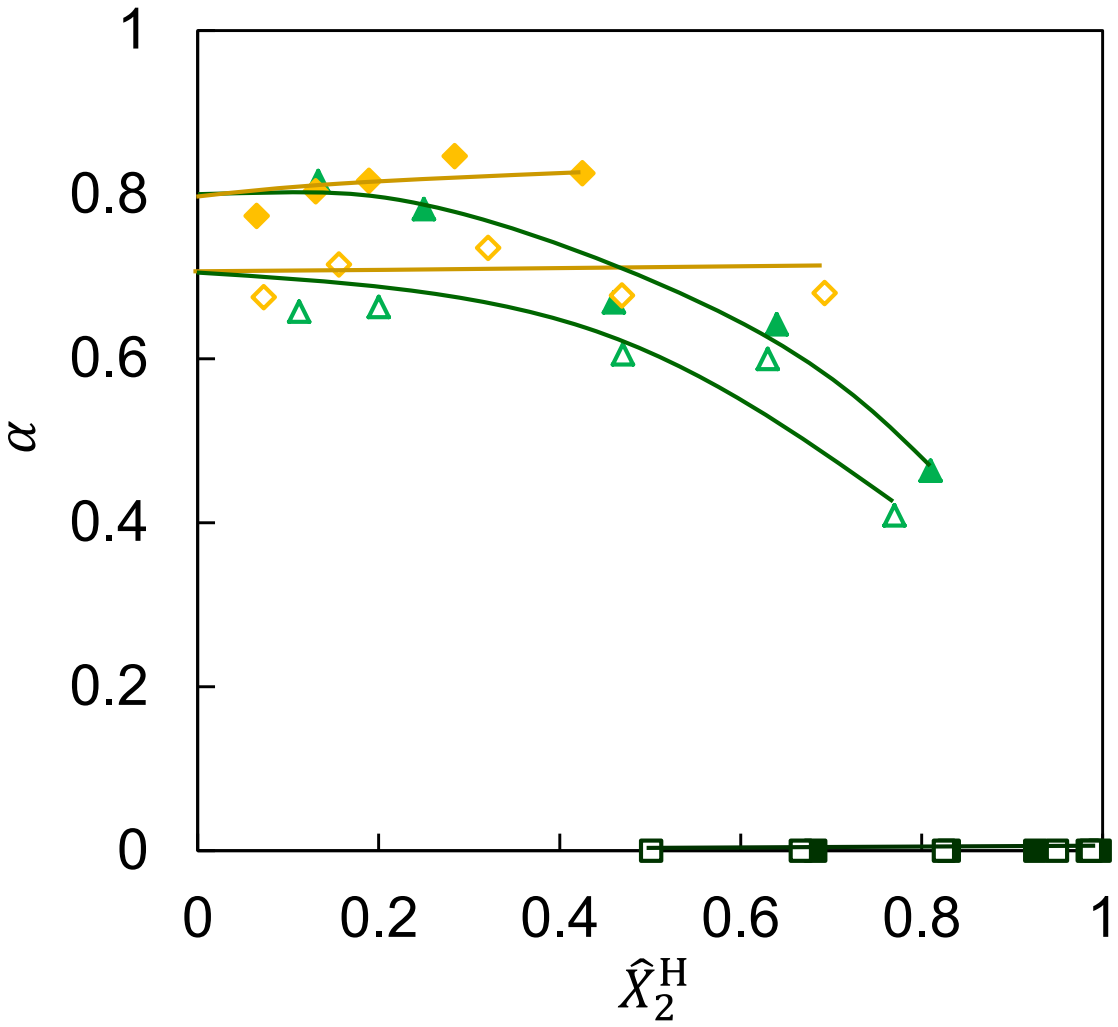

Figure 4-5. The ratio of bound Br vs. overall counterion composition in the adsorbed film obtained for DTAB-DTAC (diamond), HMIMBr-HMIMBF$_4$ (square), and DTAB-DTABF$_4$ (triangle) systems. Open and filled symbols respectively represent the data at 55.0 and 45.0 mN m^{-1}.

reflectometry [20]. These experiments indicated that the BF_4^- ion occupies the surface at the same level of the imidazolium ring of the cation, whereas the single atomic anion such as Br^- distributes below the cation layer. This is now understood as the result of the difference in hydrogen-bonding capability between imidazolium cation and counterions: the imidazolium cation forms one-hydrogen-bonded ion pair with Br^- ions but two-hydrogen-bonded ion pair with BF_4^- ions [21]. The strong hydrogen-bonding between $HMIM^+$ and BF_4^- ions in the adsorbed film was also suggested in our previous papers [22]. Therefore, one of the plausible reasons for the positive excess Gibbs energy in the HMIMBr-$HMIMBF_4$ system is the decrease of mixing entropy in the adsorbed film due to the exclusion of Br^- ions from the Stern layer by the preferential binding of BF_4^- ions to imidazolium cations.

When the PDA is negatively deviated from the ideal mixing and improved preferable mixing is observed (DTAB-$DTABF_4$ system), the α value decreases monotonically with increasing $\hat{X}_2^{\mathrm{H}}$ from that of the DTAB pure system. This means that BF_4^- ion could occupy the vicinity of head groups of surfactant ions preferentially to Br^- ion as the surface composition of BF_4^- ion increases. However, since DTA^+ ion does not form the specific hydrogen bonding with BF_4^- ion, the preferential binding in the DTAB－$DTABF_4$ system may arise only from the lower adsorption energy when the hydration state of BF_4^- ion changes from the fully hydrated to the bound state [18, 19, 21]. According to the PDA shown in Fig 4-2, however, the composition of Br^- ion in the adsorbed film is larger than that of the ideal mixing in spite of the preferential binding of BF_4^- ion to the hydrophilic head groups. Therefore, another interaction leads $\hat{g}^{\mathrm{H,E}}$ negative. It is seen in Fig. 4-1 that deviation from the ideal mixing i.e. the absolute value of $\hat{g}^{\mathrm{H,E}}$ becomes larger with decreasing surface tension. The

dependence of $\hat{g}^{\mathrm{H,E}}$ on γ is related to the excess occupied area expressed by next equation [23],

$$\hat{a}^{\mathrm{H,E}} = -(\partial \hat{g}^{\mathrm{H,E}}/\partial\gamma)_{T,p,\hat{X}_2^{\mathrm{H}}} \qquad (4-6)$$

In the DTAB-$DTABF_4$ system $\hat{a}^{\mathrm{H,E}}$ becomes negative, and this means the more effective packing of components is realized in the adsorbed film. Taking into account that the counterions are concentrated in the electrical double layer, one of the plausible interactions is the mixing of counterions of different radius in the vicinity of head groups and/or in the diffuse double layer, which was also observed in our previous study [24]. The importance of mixing entropy of different kinds of counterions at Stern layer is also suggested by other authors [25]. Therefore we conclude that negative $\hat{g}^{\mathrm{H,E}}$ is caused by the balance between the decreasing of enthalpy due to preferential binding of BF_4^- ions having surface activity and the increase of entropy due to effective mixing of different-size counterions.

4-4. References

1. Aratono, M.; Villeneuve, M.; Takiue, T.; Ikeda, N.; Iyota, H. *J. Colloid and Interface Sci.* **1998**, 200, 161.
2. Yamanaka, M.; Amano, T.; Ikeda, N.; Aratono, M.; Motomura, K. *Colloid Polym. Sci.* **1992**, 270, 682.
3. Li, H. H.; Imai, Y.; Hayami, Y.; Takiue, T.; Matsubara, H.; Aratono, M. *J. Colloid and Interface Sci.* **2011**, 359, 189.
4. Shimamoto, K.; Onohara, A.; Takumi, H.; Watanabe, I.; Tanida, H.; Matsubara, H.; Takiue, T.; Aratono, M. *Langmuir* **2009**, 25, 9954.
5. Shapovalov, V. L.; Brezesinski, G. *J. Phys. Chem. B* **2006**, 110, 10032.

6. Koelsch, P.; Viswanath, P.; Motschmann, H.; Shapovalov, V. L.; Brezesinski, G.; Möhwald, H.; Horinek, D.; Netz, R. R.; Giewekemeyer, K.; Salditt, T.; Schollmeyer, H.; Klitzing, R.; Daillant, J.; Guenoun, P. *Colloids and Surfaces A* **2007**, 303, 110.
7. Warszynski, P.; Barzyk, W.; Lunkenheimer, K.; Fruhner, H. *J. Phys. Chem. B* **1998**, 102, 10948.
8. Kralchevsky, P. A.; D. Danov, K.; Broze, G.; Mehreteab, A. *Langmuir* **1999**, 15, 2351.
9. Luo, G.; Malkova, S.; Yoon, J.; Schultz, D. G.; Lin, B.; Meron, M.; Benjamin, I.; Vanysek, P.; Schlossman, M. L. *Science* **2006**, 311, 216.
10. Kunz W. (ed), *Specific ion effects*; World Scientific Publishing Co.: Singapore, 2011.
11. Takiue, T.; Kawagoe, Y.; Muroi, S.; Murakami, R.; Ikeda, N.; Aratono, M.; Tanida, H.; Sakane, H.; Harada, M.; Watanabe, I. *Langmuir* **2003**, 19, 10803.
12. Watanabe, I.; Tanida, H.; Kawauchi, S.; Harada, M.; Nomura, M. *Rev. Sci. Instrum*. **1997**, 68, 3307.
13. Israelachvili, J. N. *Intermolecular and Surface Forces, 2nd Ed.*; Academic press: London, 1992.
14. Para, G.; Jarek, P.; Warszynski, P. *Adv. in Colloid and Interface Sci*. **2006**, 122, 39.
15. Dey, J.; Thapa, U.; Ismail, K. *J. Colloid and Interface Sci*. **2012**, 367, 305.
16. Aratono, M.; Kashimoto, K.; Matsuda, T.; Muroi, S.; Takata, Y.; Ikeda, N.; Takiue, T. *Langmuir* **2005**, 21, 7398.
17. Jeon, Y.; Sung, J.; Bu, W.; Vaknin, D.; Ouchi, Y.; Kim, D. *J. Phys. Chem. C* **2008**, 112, 19649.
18. Law, G.; Watson, P. R.; Carmichael, A. J.; Seddon, K. R. *Phys. Chem. Chem. Phys.* **2001**, 3, 2879.

19. Lockett, V.; Sedev, R.; Bassell, C.; Ralston, J. *Phys. Chem. Chem. Phys.* **2008**, 10, 1330.

20. Bowers, J.; Vergara-Gutierrez, M. C.; Webster, J. R. P. *Langmuir* **2004**, 20, 309.

21. Dong, K.; Zhang, S.; Wang, D.; Yao, X. *J. Phys. Chem. A* **2006**, 110, 9775.

22. Matsubara, H.; Onohara, A.; Imai, Y.; Shimamoto, K.; Takiue, T.; Aratono, M. *Colloids and Surfaces A* **2010**, 370, 113.

23. Takiue, T.; Matsuo, T.; Ikeda, N.; Motomura, K.; Aratono, M. *J. Phys. Chem. B* **1998**, 102, 5840.

24. Hayami, Y.; Nomura, T.; Villeneuve, M.; Takiue, T.; Aratono, M. *Colloid Polym. Sci*. **2002**, 280, 146.

25. Takata, Y.; Tagashira, H.; Hyono, A.; Ohshima, H. *Entropy* **2010**, 12, 983.

Chapter 5 Valence and Size Effects on Miscibility and Distribution of Binary Counterions in Surfactant Adsorbed Films

5-1. Introduction

The valence effect have been one of the most basic problems in the specific ion effects since the discovery of Hofmeister series over one hundred years ago but even today this is not sufficiently clarified. Strong electrostatic interaction due to multi-valence of counterion facilitates the binding of counterions to surfactant ions at the solution surface and sometimes brings about charge inversion [1, 2] and multilayer formation [3, 4]. On the other hand, it is also suggested that multivalent counterions are hydrated strongly and the hydration shell is kept to some extent at the air/water surface [5, 6]. The study on Langmuir film for investigating the effect of size and valence of counterions by Shapovalov et al. also clarified that at high surface charge densities (> 0.6 C m^{-2}), smaller monovalent counterions adsorbs to the solution surface preferentially to the larger hydrated multivalent ion in the aspect of competitive adsorption [21, 22]. This tendency is confirmed also theoretically by several researchers [9-12]. In the system containing multivalent ion, the electrostatic interaction and hydration effect due to higher valence could be especially depending on the surface charge density.

In this chapter, the TR-XAFS measurement and surface tensiometry were extended to the DTAB-DTA_2SO_4 mixed system containing multivalent ions to investigate the effect of valence and size on the distribution and miscibility of counterions in the electrical double layer. The ratio of the number of bound-Br ions was determined as a function of the surface composition of counterions and surface density of surfactant ion,

and the relation between the miscibility and distribution of counterions at the solution surface are discussed from the view point of the specific ion effect.

5-2. Surface tension data and thermodynamic equations for the DTAB-DTA_2SO_4 system.

Surface tension γ of the DTAB-DTA_2SO_4 mixed aqueous solution was measured at 298.15 K under atmospheric pressure as a function of the total molality of surfactants $\hat{m}$ and the bulk composition of DTA_2SO_4 $\hat{X}_2$ defined respectively by,

$$\hat{m} = \hat{m}_1 + \hat{m}_2 = m_{\mathrm{DTA}} + m_{\mathrm{Br}} + m_{\mathrm{SO_4}} \qquad (5-1)$$

$$\hat{X}_2 = \hat{m}_2/\hat{m} \qquad (5-2)$$

where $\hat{m}_1$ and $\hat{m}_2$ are the molalities of DTAB and DTA_2SO_4 defined by $\hat{m}_1 = m_{1,\mathrm{DTA}} + m_{\mathrm{Br}} = 2m_1$ and $\hat{m}_2 = m_{2,\mathrm{DTA}} + m_{\mathrm{SO4}} = 3m_2$. Here m_1 and m_2 are the usually-employed molalities of DTAB and DTA_2SO_4, respectively. The surface tension γ of the aqueous solution of the DTAB-DTA_2SO_4 mixtures is plotted against $\hat{m}$ at nine fixed bulk compositions of DTA_2SO_4 $\hat{X}_2$ in Fig. 5-1.

In all curves, the break point corresponding to cmc was observed. It should be noted that not only SO_4^{2-} ions but also hydrosulfate ions HSO_4^- possibly exist in the aqueous solution due to hydrolysis. The dissociation constant for HSO_4^- K_d (1.2×10^{-2} mol dm^{-3}) [13] shows that almost all HSO_4^- ions are dissociated and SO_4^{2-} ions exist in the solution in the molality region of this study. Furthermore, Br^- and SO_4^{2-} ions are not expected to associate with DTA^+ ions (for example ion pairs or small aggregations) below cmc because the equivalent conductivity of the DTAB aqueous solution and that for DTA_2SO_4 decrease linearly with increasing the square root of normality below cmc at which the distinct break point is observed [14]. Such linear

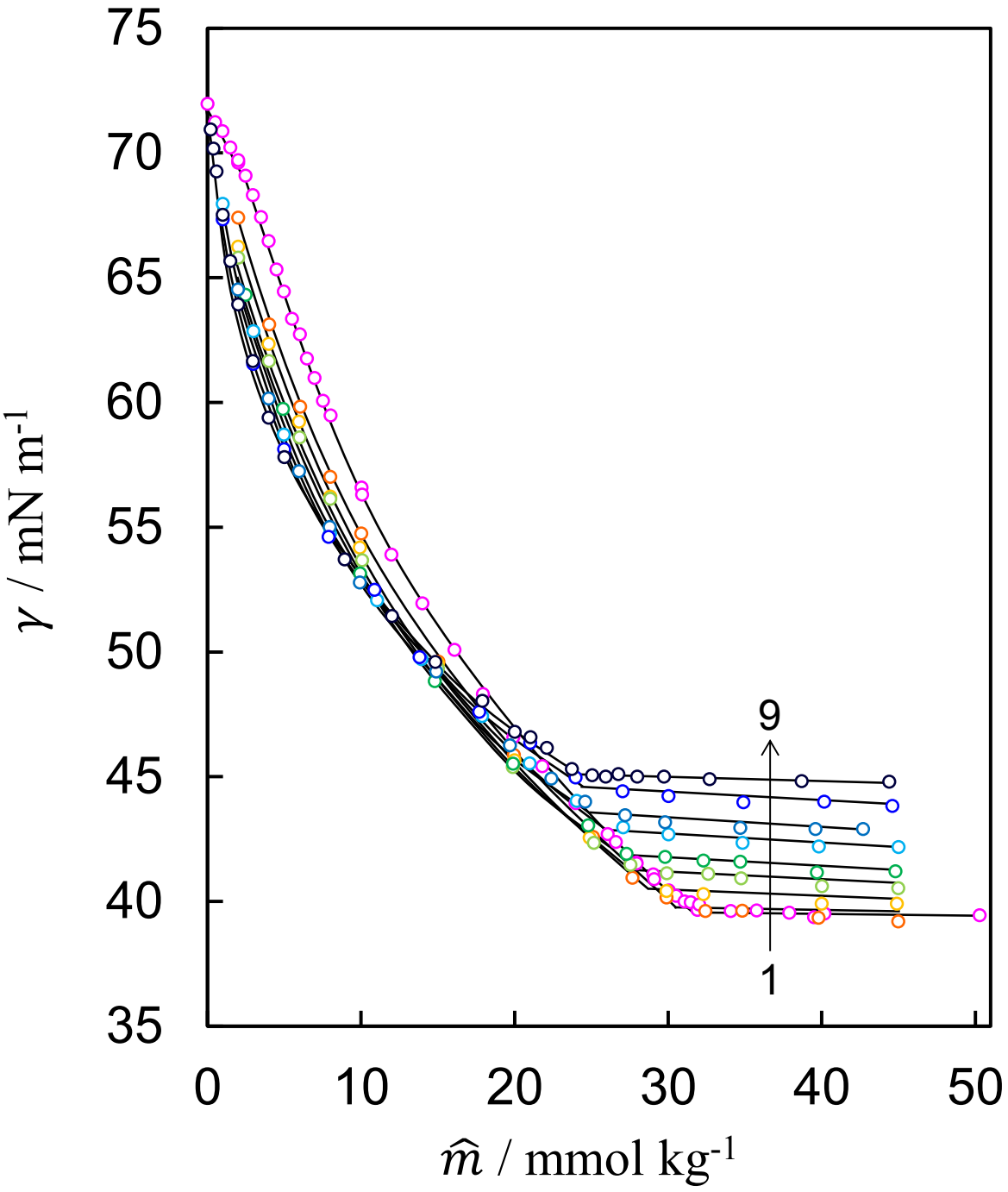

Figure 5-1. Surface tension vs. total molality of DTAB-DTA_2SO_4 mixtures at constant bulk compositions $\hat{X}_2$= (1) 0 (DTAB), (2) 0.0999, (3) 0.199, (4) 0.350, (5) 0.495, (6) 0.646, (7) 0.748, (8) 0.899, (9) 1 (DTA_2SO_4).

decreasing is observed in the strong electrolyte aqueous solution, which is experimentally confirmed by Kohlrausch [15] and theoretically explained by researchers [16, 17].

Here, let us briefly summarize the thermodynamic equations employed in the analysis of the surface tension data of the DTAB-DTA_2SO_4 system. As shown above, the ion species existing in the aqueous solution are expected to be DTA^+, Br^- and SO_4^{2-}. In this study, the bulk aqueous solution is assumed to be ideally dilute. In this case, the surface tension γ is expressed as a function of the total molality $\hat{m}$ defined by Eq. 5-1 and the bulk compositions of DTA_2SO_4 $\hat{X}_2$ defined by eq. 5-2 as

$$\mathrm{d}\gamma = -\frac{RT\hat{\Gamma}^{\mathrm{H}}}{\hat{m}}\mathrm{d}\hat{m} + \frac{RT\hat{\Gamma}^{\mathrm{H}}\left(\hat{X}_2 - \hat{X}_2^{\mathrm{H}}\right)\left(1+\hat{X}_2\right)}{\hat{X}_1\hat{X}_2\left(3+\hat{X}_2\right)}d\hat{X}_2 \qquad (5-3)$$

at constant temperature and pressure [18]. Here the total surface density of ions $\hat{\Gamma}^{\mathrm{H}}$ and the surface composition of DTA_2SO_4 $\hat{X}_2^{\mathrm{H}}$, are respectively defined similarly to Eqs. 5-1 and 5-2 by

$$\hat{\Gamma}^{\mathrm{H}} = \hat{\Gamma}_1^{\mathrm{H}} + \hat{\Gamma}_2^{\mathrm{H}} = \Gamma_{\mathrm{DTA}}^{\mathrm{H}} + \Gamma_{\mathrm{Br}}^{\mathrm{H}} + \Gamma_{\mathrm{SO_4}}^{\mathrm{H}} \qquad (5-4)$$

$$\hat{X}_2^{\mathrm{H}} = \hat{\Gamma}_2^{\mathrm{H}}/\hat{\Gamma}^{\mathrm{H}} \qquad (5-5)$$

where $\hat{\Gamma}_1^{\mathrm{H}}$ and $\hat{\Gamma}_2^{\mathrm{H}}$ are the surface (excess) densities of ions attributable to DTAB and DTA_2SO_4 respectively, which are defined by $\hat{\Gamma}_1^{\mathrm{H}} = \Gamma_{1,\mathrm{DTA}}^{\mathrm{H}} + \Gamma_{\mathrm{Br}}^{\mathrm{H}} = 2\Gamma_{\mathrm{Br}}^{\mathrm{H}}$, and $\hat{\Gamma}_2^{\mathrm{H}} = \Gamma_{2,\mathrm{DTA}}^{\mathrm{H}} + \Gamma_{\mathrm{SO_4}}^{\mathrm{H}} = 3\Gamma_{\mathrm{SO_4}}^{\mathrm{H}}$ from the electroneutrality condition for each surfactant in the adsorbed film. $\hat{\Gamma}^{\mathrm{H}}$ and $\hat{X}_2^{\mathrm{H}}$ are evaluated by applying

$$\hat{\Gamma}^{\mathrm{H}} = -(\hat{m}/RT)(\partial\gamma/\partial\hat{m})_{T,p,\hat{X}_2} \qquad (5-6)$$

and

$$\hat{X}_2^{\mathrm{H}} = \hat{X}_2 - \frac{\hat{X}_1\hat{X}_2\left(3+\hat{X}_2\right)}{\hat{m}\left(1+\hat{X}_2\right)}\left(\frac{\partial\hat{m}}{\partial\hat{X}_2}\right)_{T,p,\gamma} \qquad (5-7)$$

to the surface tension data. The diagram constructed from the $\hat{m}$ vs. $\hat{X}_2$ and $\hat{m}$ vs.

$\hat{X}_2^{\mathrm{H}}$ curves at a given surface tension is called the phase diagram of adsorption (PDA) and provides the relation between the bulk and surface compositions at equilibrium. Furthermore, the mean activity coefficients of the DTAB and DTA_2SO_4 $\hat{f}_{i\pm}^{\mathrm{H}}$ in the adsorbed films are respectively estimated from the surface compositions using the relations,

$$\left(\hat{X}_1\right)^{1/2}(\hat{m}/\hat{m}_1^0) = \hat{f}_{1\pm}^{\mathrm{H}}\left(\hat{X}_1^{\mathrm{H}}\right)^{1/2} \qquad (5-8)$$

$$\left(\hat{X}_2\right)^{1/3}(\hat{m}/\hat{m}_2^0) = \hat{f}_{2\pm}^{\mathrm{H}}\left(\hat{X}_2^{\mathrm{H}}\right)^{1/3} \qquad (5-9)$$

where $\hat{m}_i^0$ is the molality of surfactant *i* that yields the given surface tension in the respective single systems. The $\hat{m}$ vs. $\hat{X}_2^{\mathrm{H}}$ relation expressing the criterion of ideal mixing at the surface is obtained by eliminating bulk compositions from these two equations when $\hat{f}_{1\pm}^{\mathrm{H}} = \hat{f}_{2\pm}^{\mathrm{H}} = 1$ as

$$\hat{m}^3 - (\hat{m}_1^0)^2\left(1-\hat{X}_2^{\mathrm{H}}\right)\hat{m} - (\hat{m}_2^0)^3\hat{X}_2^{\mathrm{H}} = 0 \qquad (5-10)$$

where one of the three solutions of Eq. 5-10 provides the physicochemically meaningful value for the molality. Here $\hat{f}_{i\pm}^{\mathrm{H}}$ is defined as the ratio of the mean activity coefficient in the mixture $\gamma_{i\pm}^{\mathrm{H}}$ to that in the single system $\gamma_{i\pm}^{\mathrm{H,0}}$ by

$$\hat{f}_{i\pm}^{\mathrm{H}} = \gamma_{i\pm}^{\mathrm{H}}/\gamma_{i\pm}^{\mathrm{H,0}} \qquad (5-11)$$

and thus the excess Gibbs energy of adsorption per mole of surfactants $\hat{g}^{\mathrm{H,E}}$ is estimated from $\hat{X}_i^{\mathrm{H}}$ and $\hat{f}_{i\pm}^{\mathrm{H}}$ by using

$$\hat{g}^{\mathrm{H,E}} = RT\left(\hat{X}_1^{\mathrm{H}}\ln\hat{f}_{1\pm}^{\mathrm{H}} + \hat{X}_2^{\mathrm{H}}\ln\hat{f}_{2\pm}^{\mathrm{H}}\right). \qquad (5-12)$$

The thermodynamics relevant to the above equations has been published in ref. 18. It should be noted that the surface density of surfactant ion $\Gamma_{\mathrm{DTA}}^{\mathrm{H}}$ and the surface composition of counterions $\hat{Y}_2^{\mathrm{H}}$ are sometimes more useful than $\hat{\Gamma}^{\mathrm{H}}$ and $\hat{X}_2^{\mathrm{H}}$ for clarifying the miscibility of ions in the surface, because $\Gamma_{\mathrm{DTA}}^{\mathrm{H}}$ and $\hat{Y}_2^{\mathrm{H}}$ give us more

directly the information on the surface charge density depending on the numbers of adsorbed surfactant ions and the mixing state of counterions in the adsorbed film. $\Gamma_{\mathrm{DTA}}^{\mathrm{H}}$ and $\hat{Y}_2^{\mathrm{H}}$ are evaluated from $\hat{\Gamma}^{\mathrm{H}}$ and $\hat{X}_2^{\mathrm{H}}$ by the equations

$$\Gamma_{\mathrm{DTA}}^{\mathrm{H}} = (1/2)\hat{\Gamma}^{\mathrm{H}}\hat{X}_1^{\mathrm{H}} + (2/3)\hat{\Gamma}^{\mathrm{H}}\hat{X}_2^{\mathrm{H}} \qquad (5-13)$$

and

$$\hat{Y}_2^{\mathrm{H}} = \Gamma_{\mathrm{SO_4}}^{\mathrm{H}}/\left(\Gamma_{\mathrm{Br}}^{\mathrm{H}} + \Gamma_{\mathrm{SO_4}}^{\mathrm{H}}\right) = 2\hat{X}_2^{\mathrm{H}}/\left(3 - \hat{X}_2^{\mathrm{H}}\right). \qquad (5-14)$$

Also the corresponding bulk composition of counterions $\hat{Y}_2$ to $\hat{Y}_2^{\mathrm{H}}$ is defined and calculated by

$$\hat{Y}_2 = m_{\mathrm{SO_4}}/\left(m_{\mathrm{Br}} + m_{\mathrm{SO_4}}\right) = 2\hat{X}_2/\left(3 - \hat{X}_2\right). \qquad (5-15)$$

Similarly to the adsorbed film, the composition of DTA_2SO_4 in the micelle

$$\hat{X}_2^{\mathrm{M}} = \hat{N}_2^{\mathrm{M}}/\hat{N}^{\mathrm{M}} \qquad (5-16)$$

is evaluated by applying the following equation [18]

$$\hat{X}_2^{\mathrm{M}} = \hat{X}_2 - \frac{\hat{X}_1\hat{X}_2\left(3 + \hat{X}_2\right)}{\hat{C}\left(1 + \hat{X}_2\right)}\left(\frac{\partial \hat{C}}{\partial \hat{X}_2}\right)_{T,p} \qquad (5-17)$$

to the critical micelle concentration $\hat{C}$ vs. $\hat{X}_2$ curve. Also, the excess Gibbs energy of micelle formation is evaluated by applying the following equation

$$\hat{g}^{\mathrm{M,E}} = RT\left(\hat{X}_1^{\mathrm{M}} \ln \hat{f}_{1\pm}^{\mathrm{M}} + \hat{X}_2^{\mathrm{M}} \ln \hat{f}_{2\pm}^{\mathrm{M}}\right) \qquad (5-18)$$

to the phase diagram of micelle formation (PDM), where the activity coefficients is defined similarly to those for adsorbed film. The excess Gibbs energy in the adsorbed film at cmc $\hat{g}^{\mathrm{H,E,C}}$ is obtained by extrapolating $\hat{g}^{\mathrm{H,E}}$ vs. γ curves at fixed surface composition to the surface tension at cmc, and the comparison of $\hat{g}^{\mathrm{H,E,C}}$ and $\hat{g}^{\mathrm{M,E}}$ provides information on the difference of the miscibility between the adsorbed film and micelle, being coexisting in equilibrium.

5-3. Effect of counterions on adsorption of surfactant ions.

In order to examine the effect of counterions on the adsorption of surfactant ions, the surface density of DTA^+ Γ_{DTA}^{H} for the single surfactant systems of DTAB and DTA_2SO_4 were evaluated by applying eqs. 5-6 and 5-13 to the γ vs. $\hat{m}$ curves in Fig 5-1. The results are plotted against $\hat{m}$ in Fig. 5-2 which demonstrates that the Γ_{DTA}^{H} values are higher for DTA_2SO_4 at lower molalities (also at lower ionic strength), while they are higher for DTAB at larger ones. Adsorption behavior is affected by some factors such as electrostatic interaction between ionic species, hydration and size of counter ions, van der Waals interaction between hydrophobic chains, and so on. Among these, the electrostatic interaction works even when the distance between ionic species is comparatively large, while the others become essential when the distance between the relevant species is comparatively short. Therefore, it is expected that that divalent SO_4^{2-} ions shield the repulsion between DTA^+ ions in the adsorbed film more effectively than monovalent Br^- ions even in the lower molality (and thus lower Γ_{DTA}^{H}) region, and thus DTA_2SO_4 gives a higher Γ_{DTA}^{H} at a given ionic strength where the degree of shielding of the charge in the bulk solution is the same. This is in accord with the present results in Fig. 5-2.

On the other hand, in the high molality region where the surface density is relatively high and the average distance between ion species is smaller, the effect of size and hydration of counterions and van der Waals interaction between hydrocarbon chains become more influential. Here it should be remembered that about 80 % of bromide ions are partially dehydrated and bound to DTA^+ ions to form ion pairs in DTAB system at saturation adsorption [19], hydration free Gibbs energy $\Delta_{hyd}G$ for SO_4^{2-} (-1080 kJ mol^{-1}) is more negative than that for Br^- (-315 kJ mol^{-1}) [20], and the radius of SO_4^{2-}

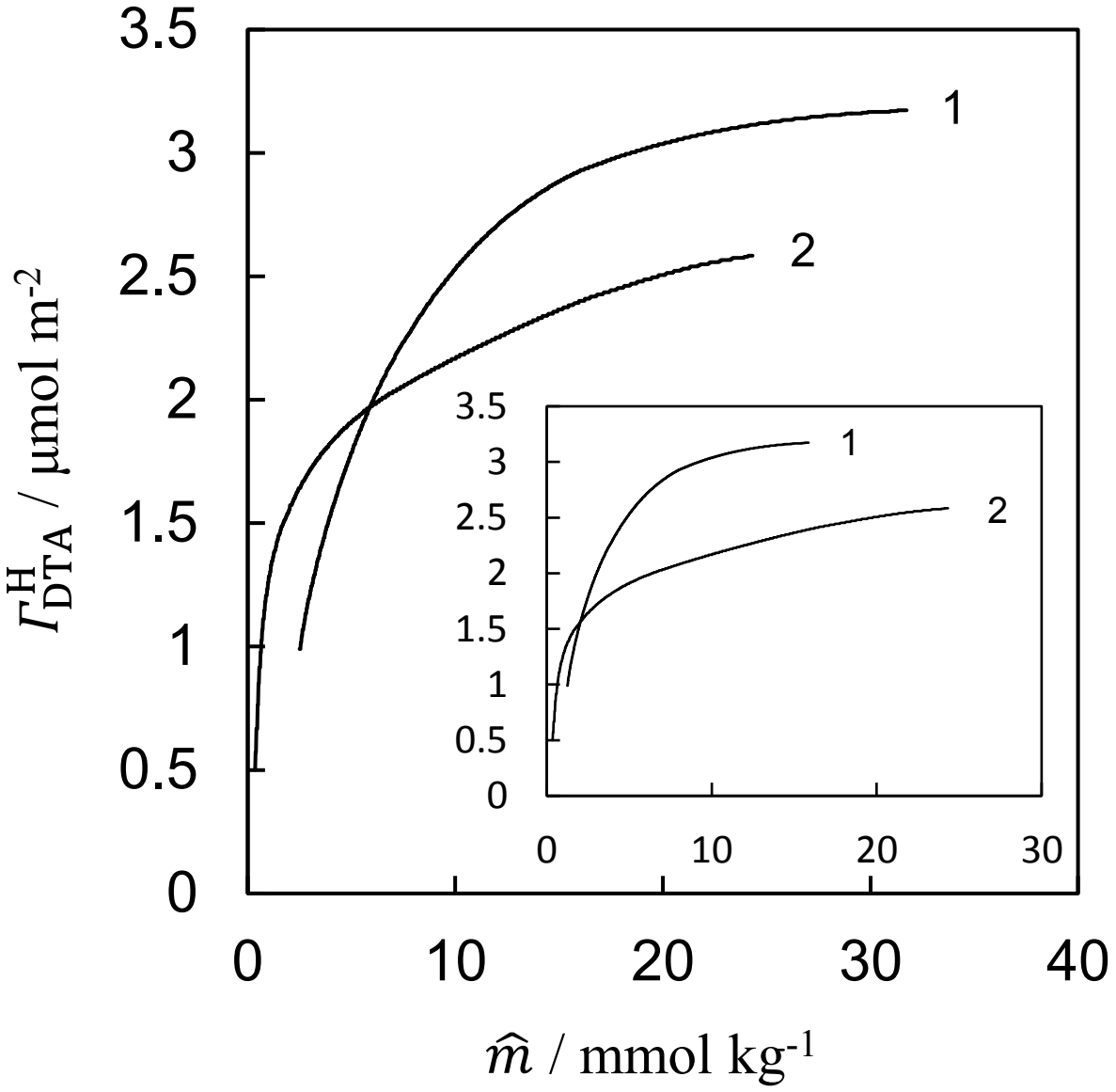

Figure 5-2. Surface density of surfactant ion vs. molality for the single surfactant system: (1) DTAB, (2) DTA_2SO_4. Surface density of surfactant ion is plotted also against ionic strength in the insert.

ions (2.40 Å and 2.78 Å for bare and hydrated states respectively) are much larger than that of Br^- ions (1.96Å and 2.31 Å) [20]. The properties of these counterions are shown in Table 1. Furthermore a large proportion of SO_4^{2-} ions keep their hydration shell in the adsorbed films, although some of SO_4^{2-} ions could be partially dehydrated and bound to DTA^+ ions due to the strong electrostatic interaction between DTA^+ and SO_4^{2-}, which is supported by the results of Shapovalov et al. [7, 8] as shown in introduction section and also by the results of Eliad et al. for the porous carbon electrode [21] that gives one of the direct evidences clarifying SO_4^{2-} ions keep their hydration shell in the electrical double layer. All these experimental findings support that the $\Gamma_{\mathrm{DTA}}^{\mathrm{H}}$ values of DTAB are higher than those of DTA_2SO_4 at the higher molalities.

5-4. Miscibility of counterions.

In order to investigate the miscibility of counterions, the surface composition of counterions $\hat{Y}_2^{\mathrm{H}}$ was evaluated. First, $\hat{X}_2^{\mathrm{H}}$ was estimated by applying Eq. 5-7 to the $\hat{m}$ vs. $\hat{X}_2$ curves at constant surface tension, it was converted to $\hat{Y}_2^{\mathrm{H}}$ by using Eq. 5-14, and then PDAs were constructed by plotting the $\hat{m}$ vs. $\hat{Y}_2$ and $\hat{m}$ vs. $\hat{Y}_2^{\mathrm{H}}$ curves together and they are shown in Fig. 5-3. At 65.0 and 55.0 mN m^{-1}, the surface composition of SO_4^{2-}, $\hat{Y}_2^{\mathrm{H}}$, is larger than bulk composition $\hat{Y}_2$, and this supports that SO_4^{2-} interact with DTA^+ more strongly through electrostatic interaction in the adsorbed film. This is in accord with the results in Fig. 5-2 that the $\Gamma_{\mathrm{DTA}}^{\mathrm{H}}$ values of DTA_2SO_4 are higher than those of DTAB at the lower molalities, thus, at the higher surface tensions. It should be noted here that the surface composition of $\hat{Y}_2^{\mathrm{H}}$ is smaller than $\hat{Y}_2^{\mathrm{H}}$ of ideal mixing $\hat{Y}_2^{\mathrm{H,id}}$ in the adsorbed film, that is, the molality in the real mixture

Table 5-1. The radius and hydration Gibbs free energy of counterions evaluated by Marcus.[20]

ion	R_{bare} / Å	R_{hyd} / Å	ΔG_{hyd} / kJ mol^{-1}
SO_4^{2-}	2.40	2.78	-1080
Cl^-	1.81	2.24	-340
Br^-	1.96	2.31	-315
BF_4^-	2.32	2.55	-190

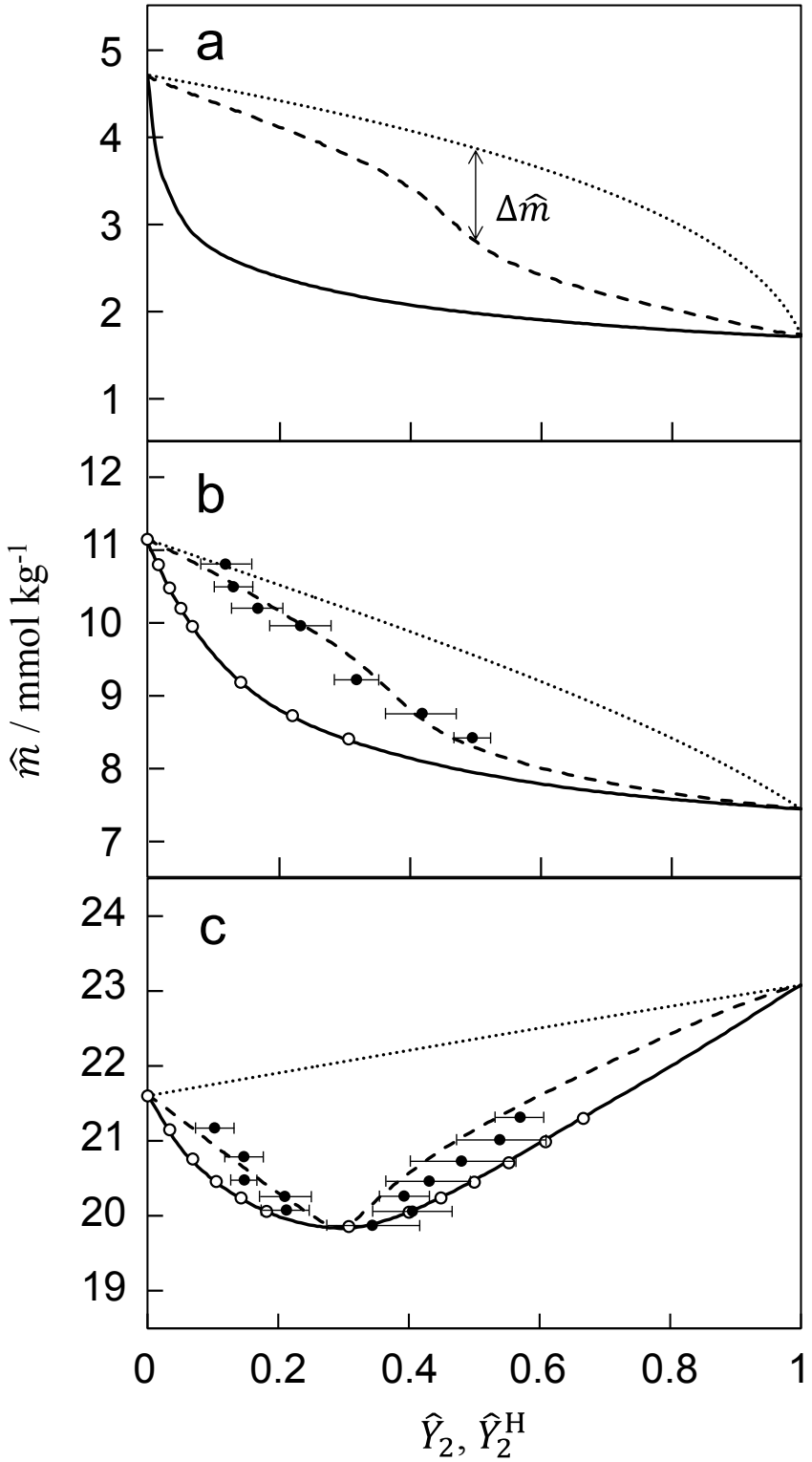

Figure 5-3. Total molality vs. bulk and surface composition curves of DTAB-DTA_2SO_4 system at (a) 65.0, (b) 55.0 and (c) 45.5 mN m^{-1}. (——) $\hat{m}$ vs. $\hat{Y}_2$ (- - - -) $\hat{m}$ vs. $\hat{Y}_2^{\mathrm{H}}$, and (·····) $\hat{m}$ vs. $\hat{Y}_2^{\mathrm{H}}$ of ideal mixing. Filled circles show the surface compositions evaluated from TR-XAFS measurements at several ($\hat{m}$ vs. $\hat{Y}_2$) combinations shown by open circles.

being required to give $\hat{Y}_2^{\mathrm{H,id}}$ is lower by $\Delta\hat{m}$ than that in the ideal mixture as shown in Fig 5-3(a). This means that the chemical potential of constituents in the real mixture, which gives $\hat{Y}_2^{\mathrm{H}} = \hat{Y}_2^{\mathrm{H,id}}$, are lower than those in the ideal mixture and thus the mixing of counterions is favorable in terms of free energy. It should be noted here from Figure 5-3(c) that $\hat{Y}_2^{\mathrm{H}}$ is smaller than $\hat{Y}_2$ in high $\hat{Y}_2^{\mathrm{H}}$ region, which shows the adsorbed films could be enriched in Br^- ion compared to the bulk solution when the density of the adsorbed film are increased. For highly charged Langmuir films, the X-ray reflectivity measurement showed that at high surface charge density (> 0.6 C m^{-2}) small univalent counterions are participated in the electrical double layer preferentially even to bulky divalent ones due to size effect, whereas below 0.3 C m^{-2} the participation of divalent ions was preferable as expected from the classical Gouy-Chapman model [7]. Although the present PDAs are those for Gibbs adsorbed films and the $\Gamma_{\mathrm{DTA}}^{\mathrm{H}}$ value in the PDAs is ranging from 1.5 to 3.2 $\mu\mathrm{mol\,m^{-2}}$ and thus from 0.14 to 0.31 C m^{-2} in surface charge density, the trend that the surface becomes rich in small univalent counterions with increasing surface charge density (from the first diagram to the third in Fig. 5-3) is the same as that of the Langmuir monolayer. The phase diagram of micelle formation which shows the relation between the counterion composition in the micelle and that in the bulk solution in equilibrium was also constructed and shown in Fig. 5-4. In contrast to adsorbed film, it was found that counterions are almost ideally mixed in the micelle.

To investigate the miscibility more quantitatively, the excess Gibbs energy of adsorption $\hat{g}^{\mathrm{H,E}}$ was evaluated by applying Eqs. 5-8, 5-9 and 5-12 to the PDA, and $\hat{g}^{\mathrm{H,E}}$ at the cmc $\hat{g}^{\mathrm{H,E,C}}$ and that of micelle formation $\hat{g}^{\mathrm{M,E}}$ were also evaluated. They are plotted against $\hat{Y}_2^{\mathrm{H}}$, $\hat{Y}_2^{\mathrm{H.C}}$ and $\hat{Y}_2^{\mathrm{M}}$, respectively in Fig. 5-5.

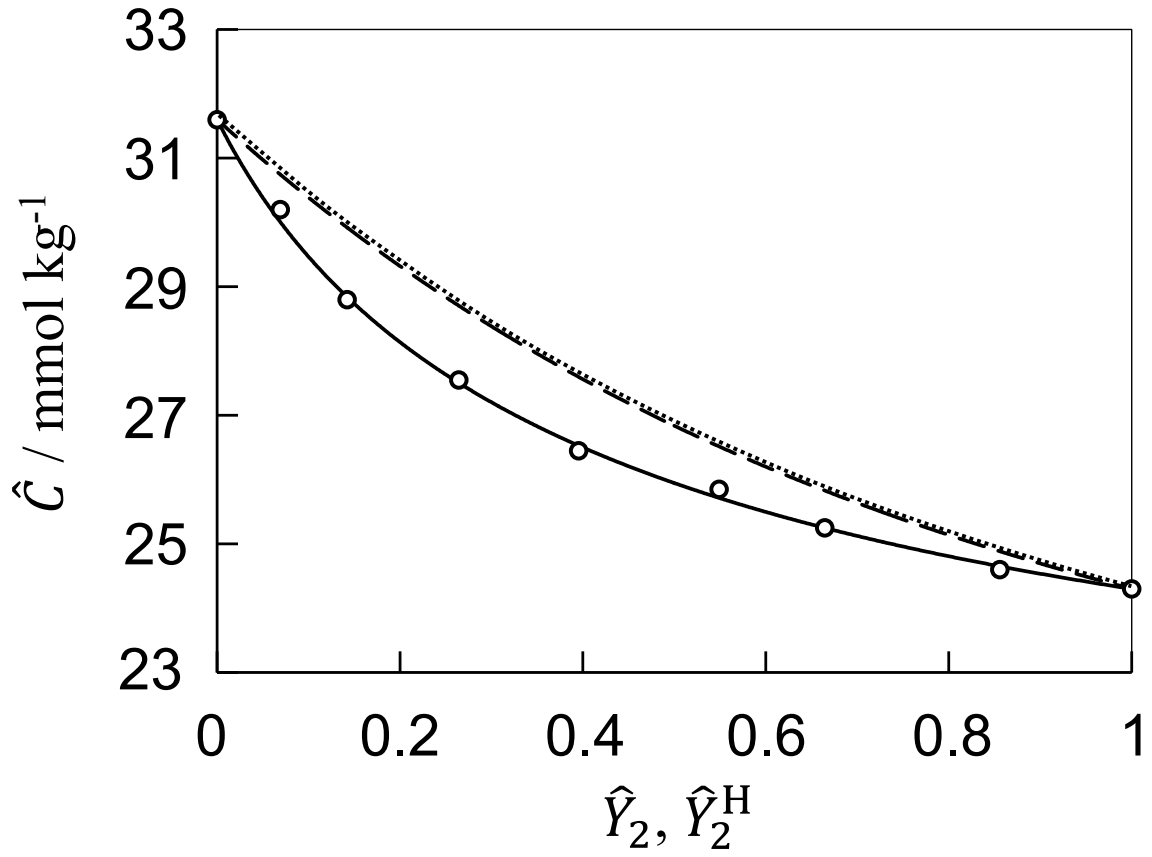

Figure 5-4. cmc vs. bulk and micelle composition curves of DTAB-DTA_2SO_4 system. (—○—) $\hat{C}$ vs. $\hat{Y}_2$ (- - -) $\hat{C}$ vs. $\hat{Y}_2^{\mathrm{M}}$, and (·····) $\hat{C}$ vs. $\hat{Y}_2^{\mathrm{M}}$ of ideal mixing.

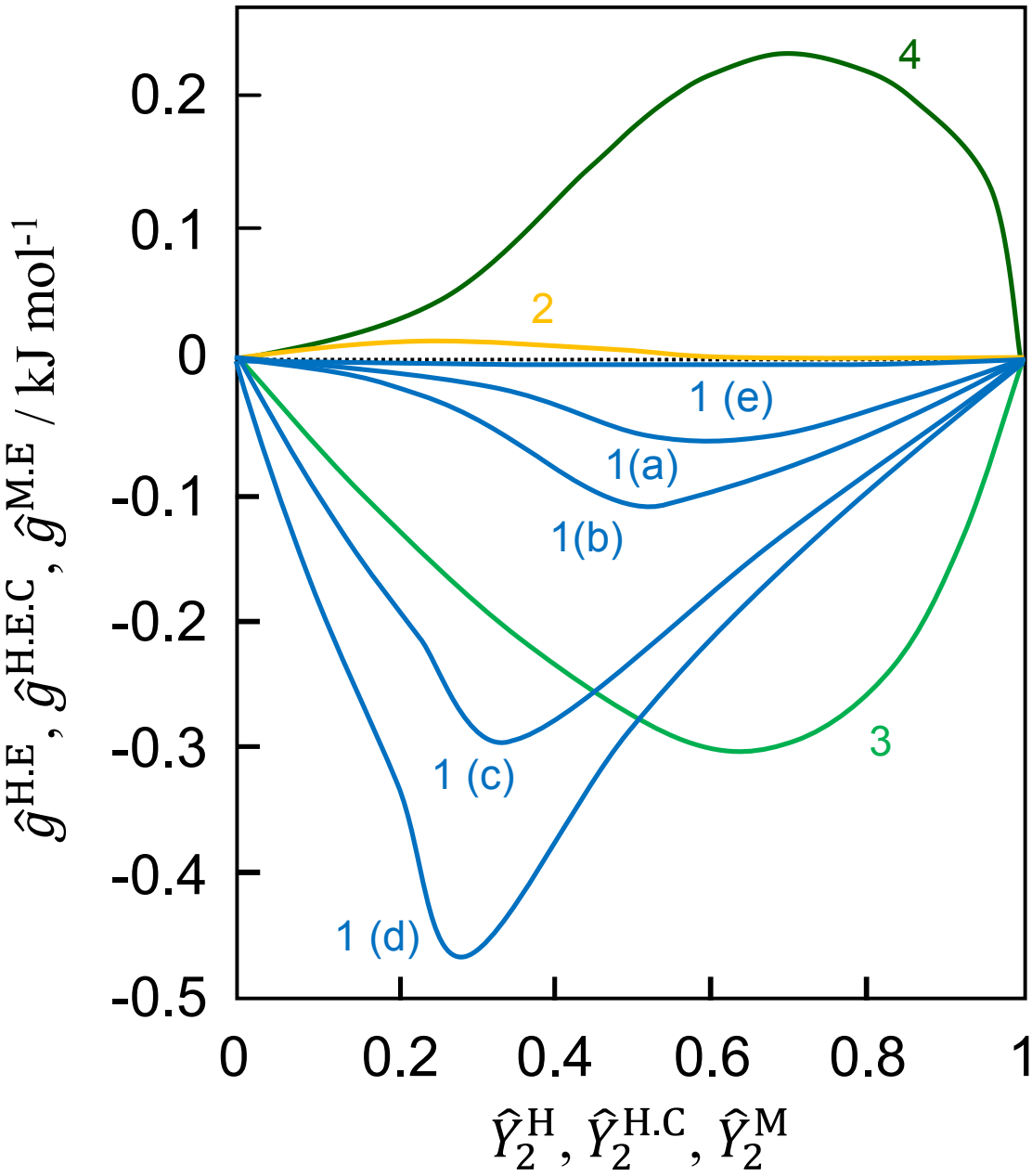

Figure 5-5. Excess Gibbs energy in the adsorbed film and micelle vs. composition of counterions curves for (1) DTAB-DTA_2SO_4 ((a) 65.0 mN m^{-1}, (b) 55.0 mNm^{-1}, (c) 45.5 mN m^{-1}, (d) surface tension at cmc and (e) micelle) (2) DTAB-DTAC (45.0 mN m^{-1}), (3) DTAB-$DTABF_4$ (45.0 mN m^{-1}) and (4) HMIMBr-$HMIMBF_4$ (45.0 mN m^{-1}). For all binary mixed systems, the composition of zero represents the single systems containing Br^- ions.

The curves of 1(a) to 1(d) clearly show that $\hat{g}^{\mathrm{H,E}}$ are negative and thus the mixing of counterions in the adsorbed film is preferable, whereas $\hat{g}^{\mathrm{M,E}}$ (curve 1(e)) is almost zero and thus the mixing in the micelle is an ideal one. Furthermore $\hat{g}^{\mathrm{H,E}}$ becomes more negative as the surface tension decreases, from which the excess molar occupied area is evaluated by the next equation [22],

$$\hat{a}^{\mathrm{H,E}} = -(\partial \hat{g}^{\mathrm{H,E}}/\partial \gamma)_{T,p,\hat{X}_2^{\mathrm{H}}} \qquad (5-19)$$

In the DTAB-DTA_2SO_4 system, $\hat{a}^{\mathrm{H,E}}$ is apparently negative, and therefore, the components are packed more closely or/and more effectively than the ideal mixing in the adsorbed film. Taking into account that the counterions are concentrated in the electrical double layer and the radius of SO_4^{2-} and Br^- ions are different from each other, one of the plausible reasons for preferable mixing is that the spaces among SO_4^{2-} ions are effectively occupied by Br^- ions. This is also supported by the fact that $\hat{g}^{\mathrm{H,E,C}}$ is much smaller than $\hat{g}^{\mathrm{M,E}}$ which comes from that the edge like space at the surface of spherical micelle is enough for counterions to be distributed freely compared to the planar surface of adsorbed film. Similar results were obtained also in our previous works for DTAB-$DTABF_4$ and sodium dodecylsulfate (SDS)-tetramethylammonium dodecylsulfate (TMADS) mixed systems where a large difference in the size of counterions is realized [18, 23] as already shown in Chapter 4. This section revealed that the surface density and the miscibility of counterions are greatly influenced not only by the electrostatic interaction between DTA^+ and counterions but also by the difference in size of counterions. In the following sections, the preferable counterion mixing will be examined more closely from the viewpoint of counterion distribution in the adsorbed film by means of the total reflection XAFS.

5-5. TR-XAFS spectra of the DTAB-DTA_2SO_4 system for evaluating the surface composition and ratio of bound-Br

The TR-XAFS measurement was conducted at the ($\hat{Y}_2$, $\hat{m}$) combinations at the given surface tensions marked with open circles in Fig. 5-3, and the obtained spectra are shown in Fig. 5-6(a) and (b). The surface composition obtained in the same procedure in Chapter 4 are plotted by filled circles in Fig. 5-3 and the coincidence between the surface compositions obtained from the thermodynamic analysis and those from TR-XAFS measurement is generally satisfactory.

In order to examine the distribution of Br^- ions from the standpoint of their solvation structure, EXAFS χ spectra was calculated from the TR-XAFS spectra in the same procedure shown in Chapter 3. Fig. 5-7(a) and (b) show the obtained EXAFS χ spectra. k^3 was multiplied for the convenience of the solvation structure analysis. In the DTAB-DTA_2SO_4 mixed system, the isosbestic points are observed as shown by the open circles in Fig. 5-7, although the signal intensity is smaller than that of the DTAB pure system due to the smaller amount of Br^- ions at surface and χ spectra were more noisy especially at the high *k* region. Hence, in this mixed system, we evaluated α for each spectrum with *k* being smaller than 4 by the least square method with Eq. 3-3 and the reference to χ_1 and χ_2 for the DTAB single surfactant system in Fig. 3-3(a).

5-6. Relation between distribution and miscibility of counterions

In Fig. 5-8, the α values are plotted against the surface composition of counterions (in the whole electrical double layer) together with the results for the DTAB-DTAC, DTAB-$DTABF_4$ and HMIMBr-$HMIMBF_4$ systems [19].

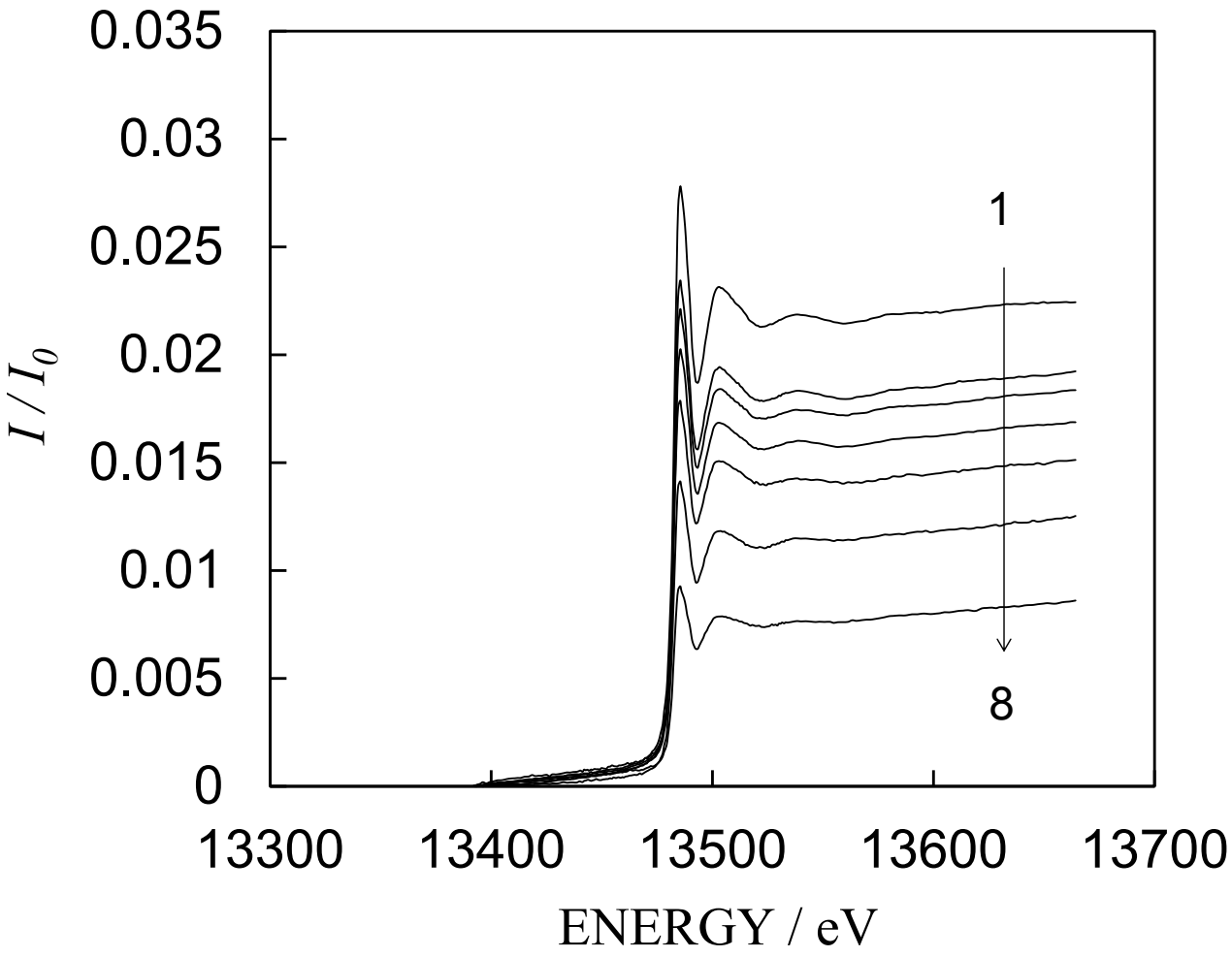

Figure 5-6(a). TR-XAFS spectra for DTAB-DTA_2SO_4 system at 55.0 mN m^{-1} and ($\hat{Y}_2$, $\hat{m}$ / mmol kg^{-1}) = (1) (0, 11.2), (2) (0.0168, 10.8), (3) (0.0339, 10.5), (4) (0.0513, 10.2), (5) (0.0690, 9.95), (6) (0.143, 9.18), (7) (0.222, 8.72) and (8) (0.308, 8.40). The I / I_0 values at 13391 eV were set at 0 for all spectra.

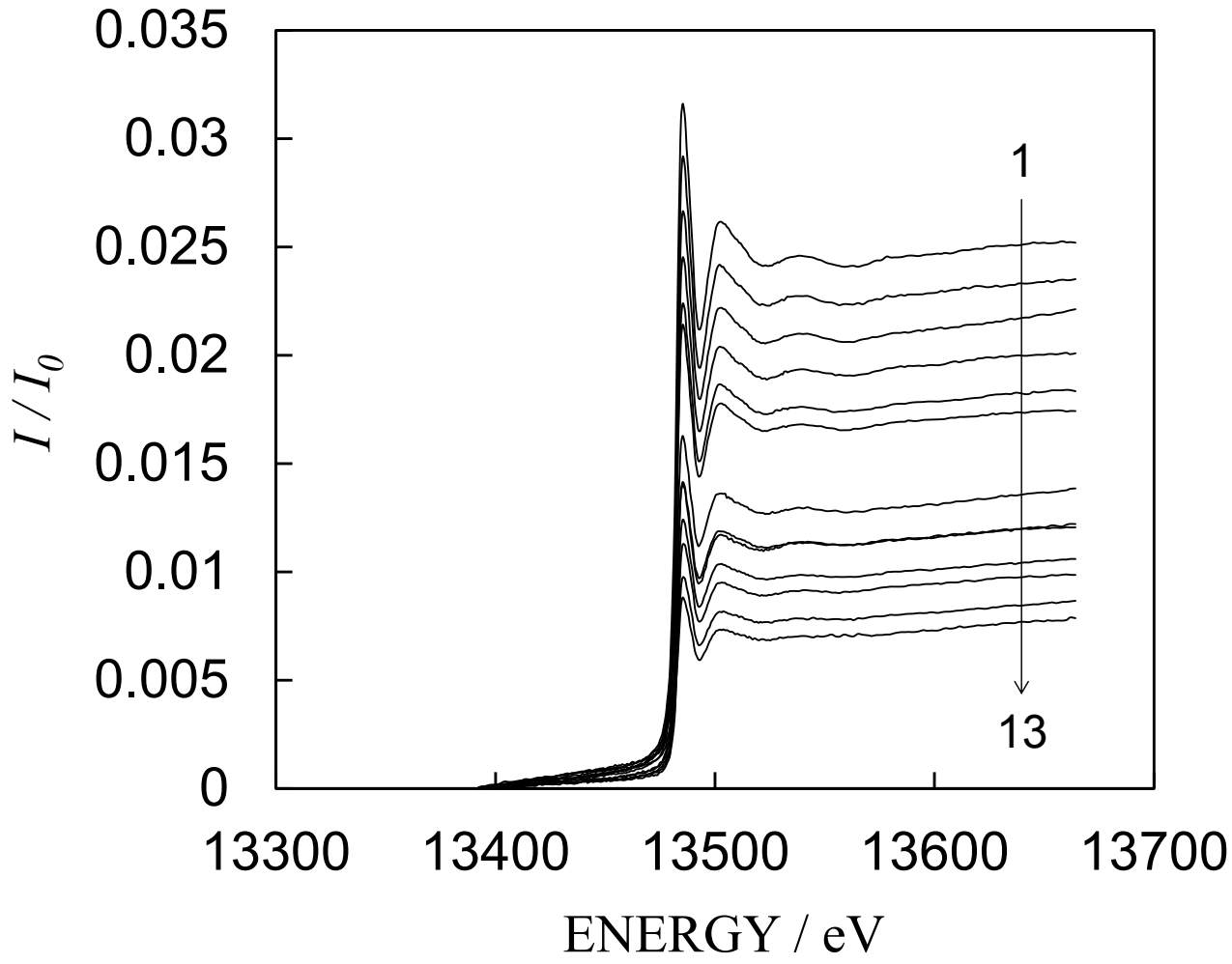

Figure 5-6(b). TR-XAFS spectra for DTAB-DTA_2SO_4 system at 55.0 mN m^{-1} and 45.5 mN m^{-1} and ($\hat{Y}_2$, $\hat{m}$ / mmol kg^{-1}) = (1) (0, 21.6), (2) (0.0339, 21.15), (3) (0.0690, 20.8), (4) (0.105, 20.5), (5) (0.143, 20.2), (6) (0.182, 20.1), (7) (0.308, 19.9), (8) (0.400, 20.1), (9) (0.449, 20.1), (10) (0.500, 20.5), (11) (0.553, 20.7), (12) (0.609, 21.0) and (13) (0.667, 21.3). The I / I_0 values at 13391 eV were set at 0 for all spectra.

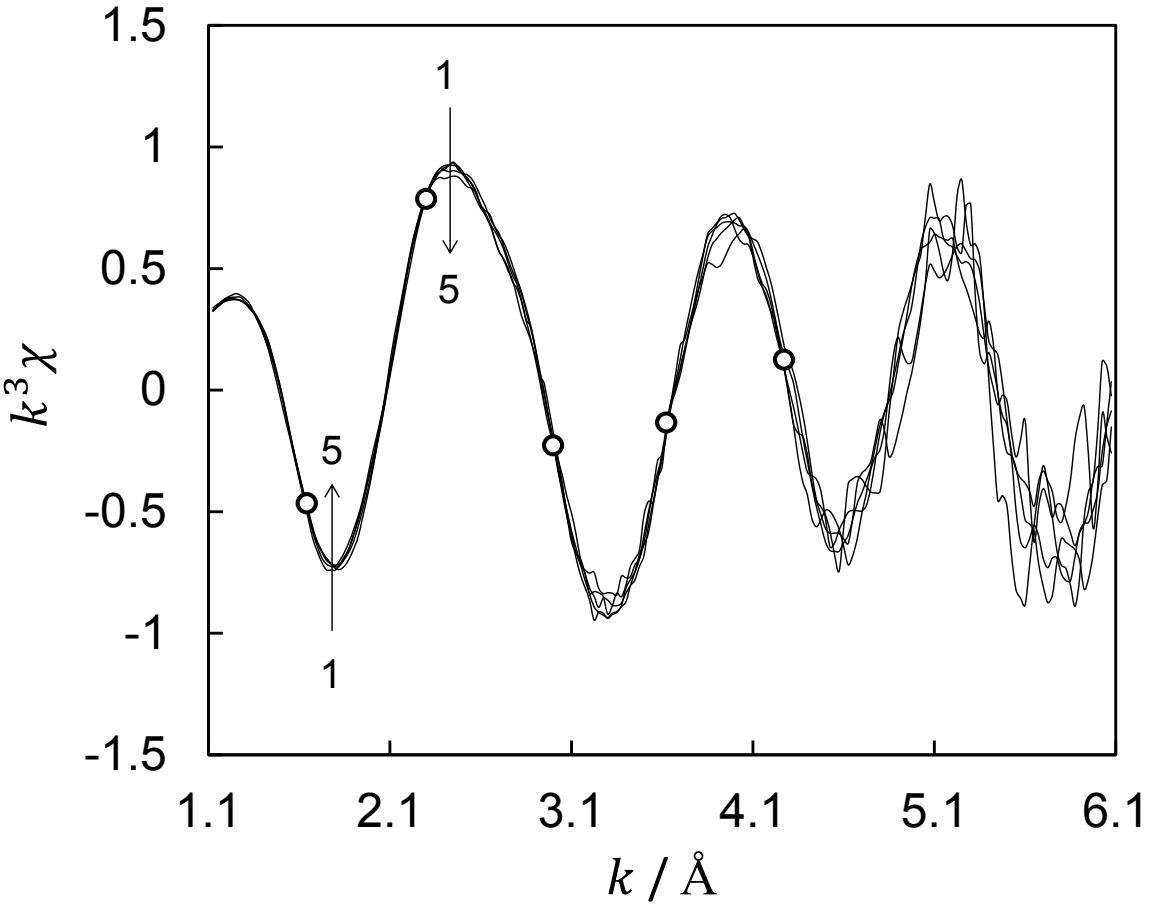

Figure 5-7(a). EXAFS $k^3\chi$ spectra of Br^- ion in the adsorbed film of DTAB-DTA_2SO_4 system at 55.0 mN m^{-1} and ($\hat{Y}_2$, $\hat{m}$ / mmol kg^{-1}) = (1) (0, 11.2), (2) (0.0168, 10.8), (3) (0.0339, 10.5), (4) (0.0513, 10.2), (5) (0.0690, 9.95). Open circles are the isosbestic points observed.

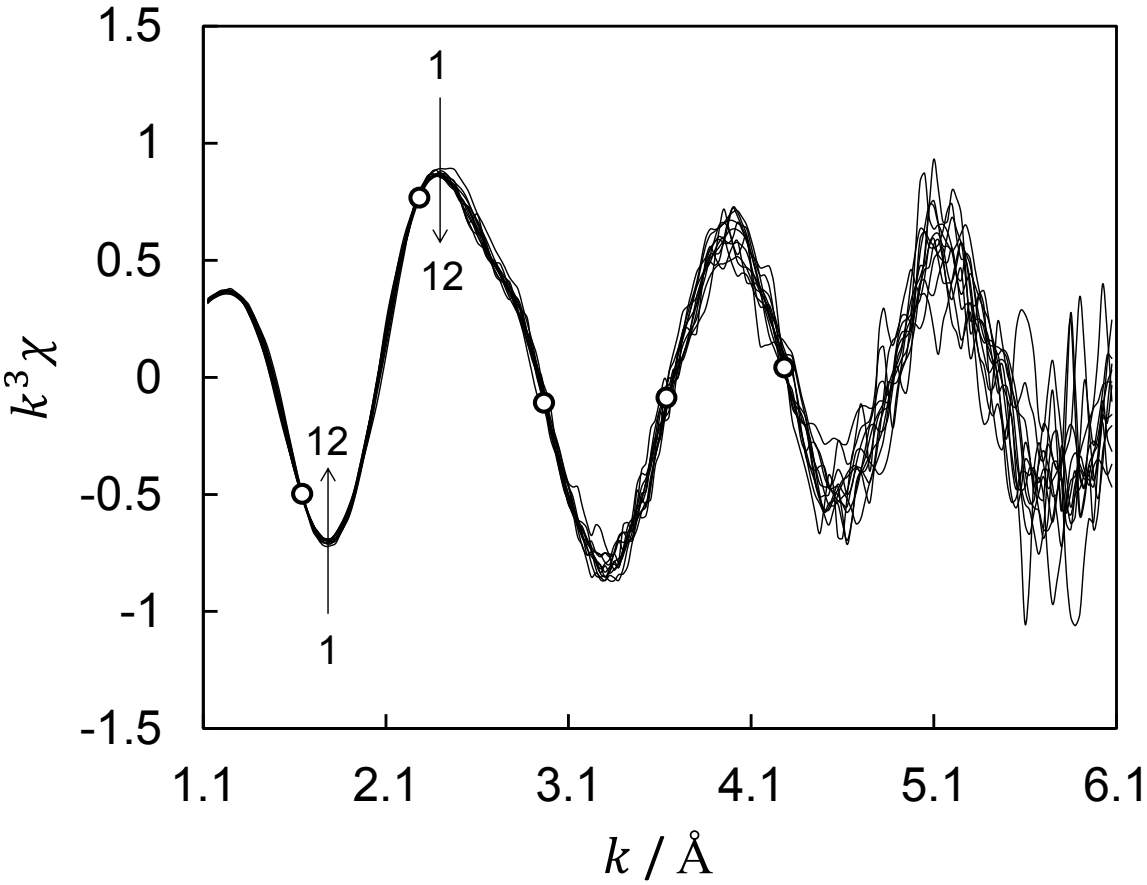

Figure 5-7(b). EXAFS $k^3\chi$ spectra of Br^- ion in the adsorbed film of DTAB-DTA_2SO_4 system at 45.5 mN m^{-1} and ($\hat{Y}_2$, $\hat{m}$ / mmol kg^{-1}) = (1) (0, 21.6), (2) (0.0339, 21.15), (3) (0.0690, 20.8), (4) (0.105, 20.5), (5) (0.143, 20.2), (6) (0.182, 20.1), (7) (0.308, 19.9), (8) (0.400, 20.1), (9) (0.449, 20.1), (10) (0.500, 20.5), (11) (0.553, 20.7) and (12) (0.609, 21.0). Open circles are the isosbestic points observed.

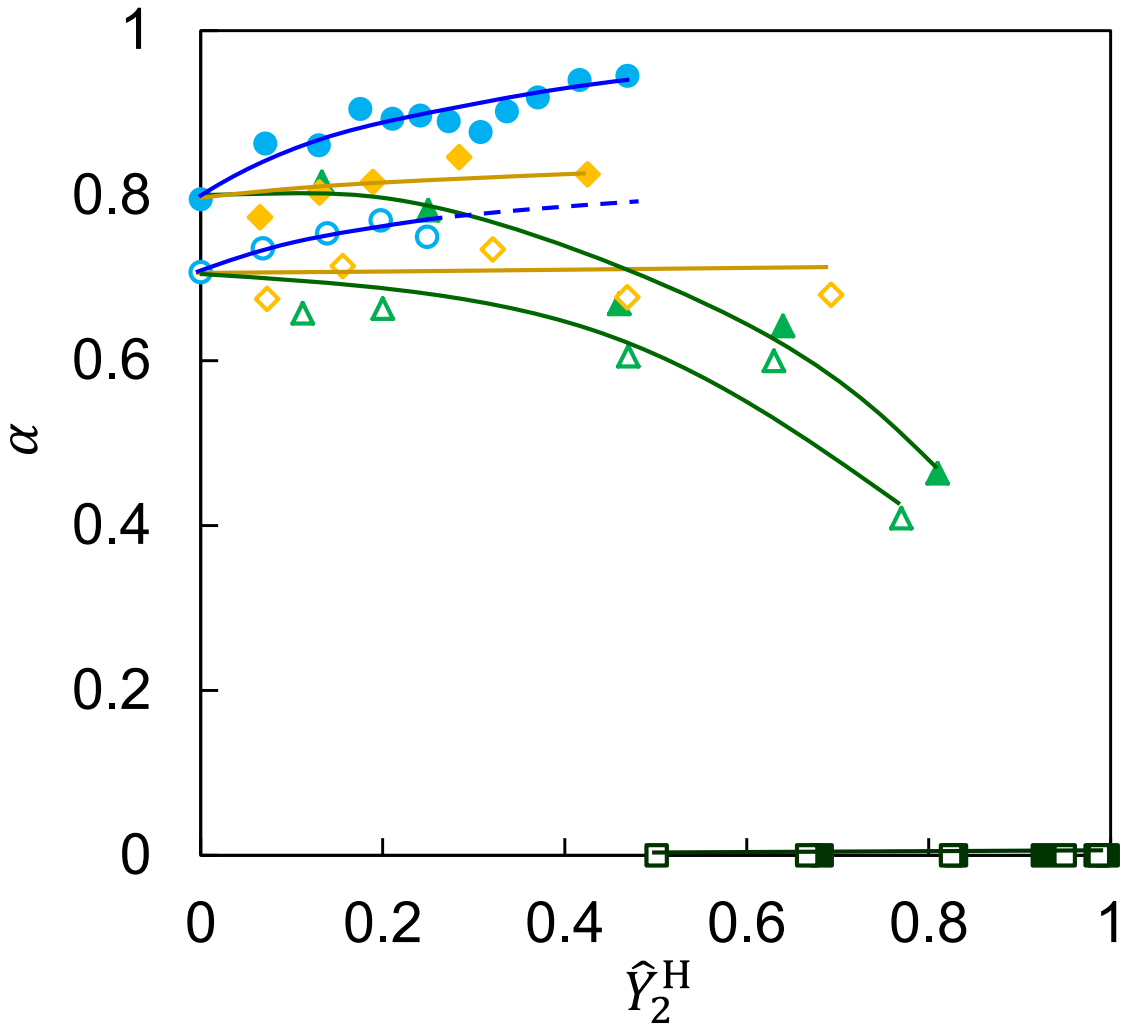

Figure 5-8. The ratio of bound-Br vs. the surface composition obtained for DTAB-DTA_2SO_4 (circle) DTAB-DTAC (diamond), DTAB-$DTABF_4$ (triangle), and HMIMBr-$HMIMBF_4$ (square) systems. Open symbols respectively represent the data at 55.0 and filled symbols at 45.0 mN m^{-1} (45.5 mN m^{-1} for the DTAB-DTA_2SO_4 system). For all binary mixed systems, the composition of zero represents the single systems containing Br^- ions.

The dependence of α on $\hat{Y}_2^{\mathrm{H}}$ is quite different among four systems and provides us information on the relation between the distribution and miscibility of counterions. It should be noted in Fig. 5-8 that because α is plotted against $\hat{Y}_2^{\mathrm{H}}$ at given surface tensions, the surface densities of surfactant ions are changed with $\hat{Y}_2^{\mathrm{H}}$. Because the surface charge density due to surfactant ions is unequivocally connected to the counterion distribution as shown in chapter 3, α vs. $\Gamma^{\mathrm{H}}_{\mathrm{surfactant\ ion}}$ (Fig. 5-9) was also newly constructed by combining the results in Fig. 5-8 with the $\Gamma^{\mathrm{H}}_{\mathrm{DTA}}$ vs. $\hat{Y}_2^{\mathrm{H}}$ curves at given surface tensions (Fig. 5-10) that were estimated by Eqs. 5-6 and 5-13. For other systems than the DTAB-DTA_2SO_4, the surface densities of surfactant ions were estimated from our previous data [24-26]. In Fig. 5-9(a). the α vs. $\Gamma^{\mathrm{H}}_{\mathrm{surfactant\ ion}}$ plots of the DTAB single system is also included. It was observed that although the α values of the DTAB-DTAC systems are a little scattered, the α vs. $\Gamma^{\mathrm{H}}_{\mathrm{surfactant\ ion}}$ plots at given $\hat{Y}_2^{\mathrm{H}}$ are essentially on and very near the line of the DTAB single system. However, the α vs. $\Gamma^{\mathrm{H}}_{\mathrm{surfactant\ ion}}$ plots of the DTAB-DTA_2SO_4 system are clearly deviated to the above and those of the DTAB-$DTABF_4$ system to the below of the line of the DTAB single system. The situation is schematically demonstrated in Fig. 5-9(b), where the dotted lines are connecting the α values at fixed $\hat{Y}_2^{\mathrm{H}}$ at intervals of 0.1. To understand the α vs. $\Gamma^{\mathrm{H}}_{\mathrm{surfactant\ ion}}$ plots in Fig. 5-9, it is helpful to examine them by two ways; the first is how the α value changes with $\Gamma^{\mathrm{H}}_{\mathrm{surfactant\ ion}}$ at constant $\hat{Y}_2^{\mathrm{H}}$ (along the dotted lines) and the second is how it changes with $\hat{Y}_2^{\mathrm{H}}$ at constant $\Gamma^{\mathrm{H}}_{\mathrm{surfactant\ ion}}$ (Fig. 5-11).

Furthermore, combining the information of $\hat{g}^{\mathrm{H,E}}$ with that of α, the relation between the miscibility and distribution of binary counterions in the adsorbed film is more closely examined from the viewpoints of the hydration and size of counterions and

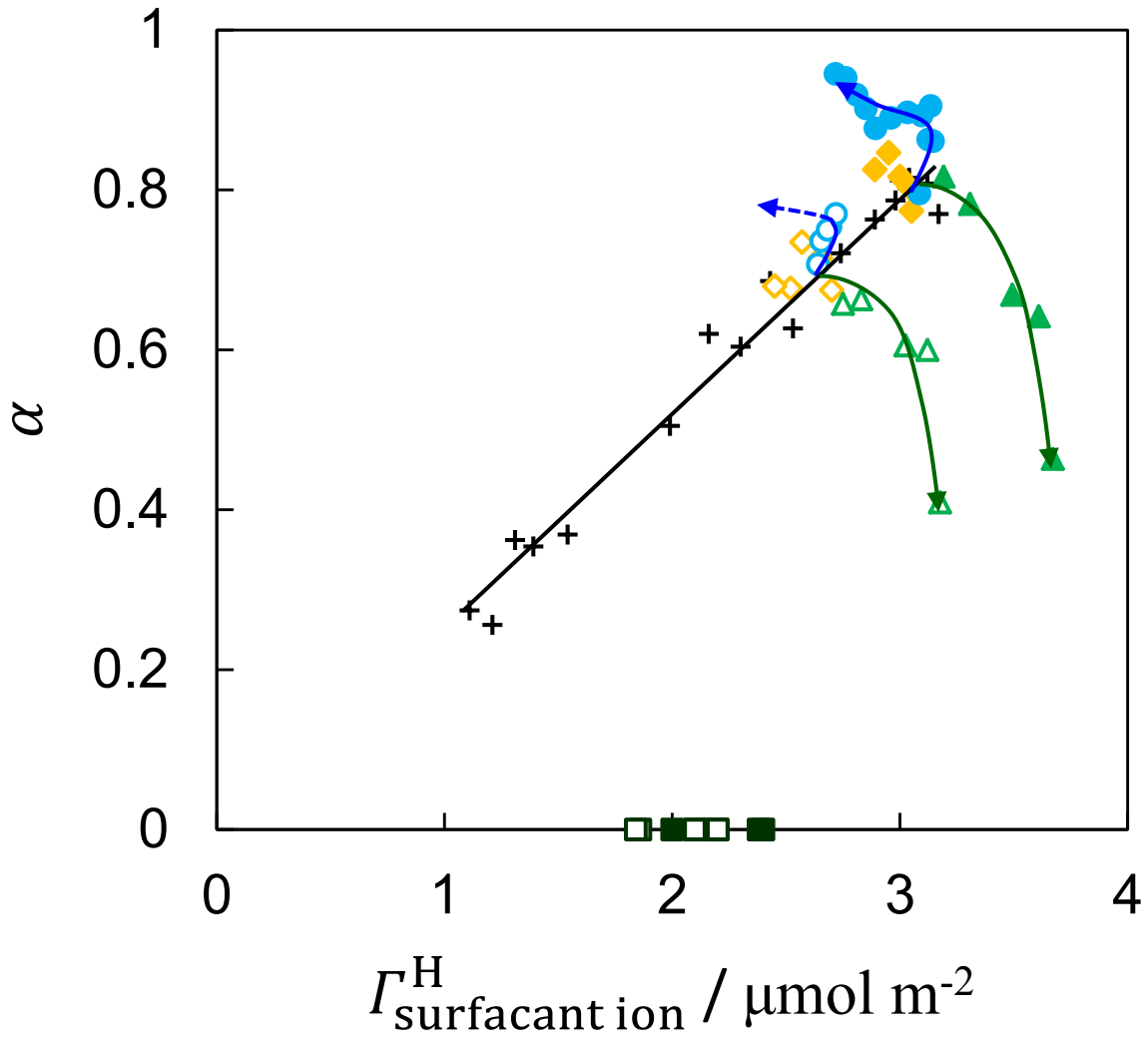

Figure 5-9(a). The ratio of bound-Br vs. the surface density of surfactant ion for DTAB-DTA_2SO_4 (circle) DTAB-DTAC (diamond), DTAB-$DTABF_4$ (triangle), and HMIMBr-$HMIMBF_4$ (square) systems. Open symbols respectively represent the data at 55.0, and filled symbols at 45.0 mN m^{-1} (45.5 mN m^{-1} for the DTAB-DTA_2SO_4 system). Cross symbols and solid line represent the data for DTAB single system. Solid curves were drawn by using those in Figure 9 and 11, and arrows represent the increase in $\hat{Y}_2^{H}$.

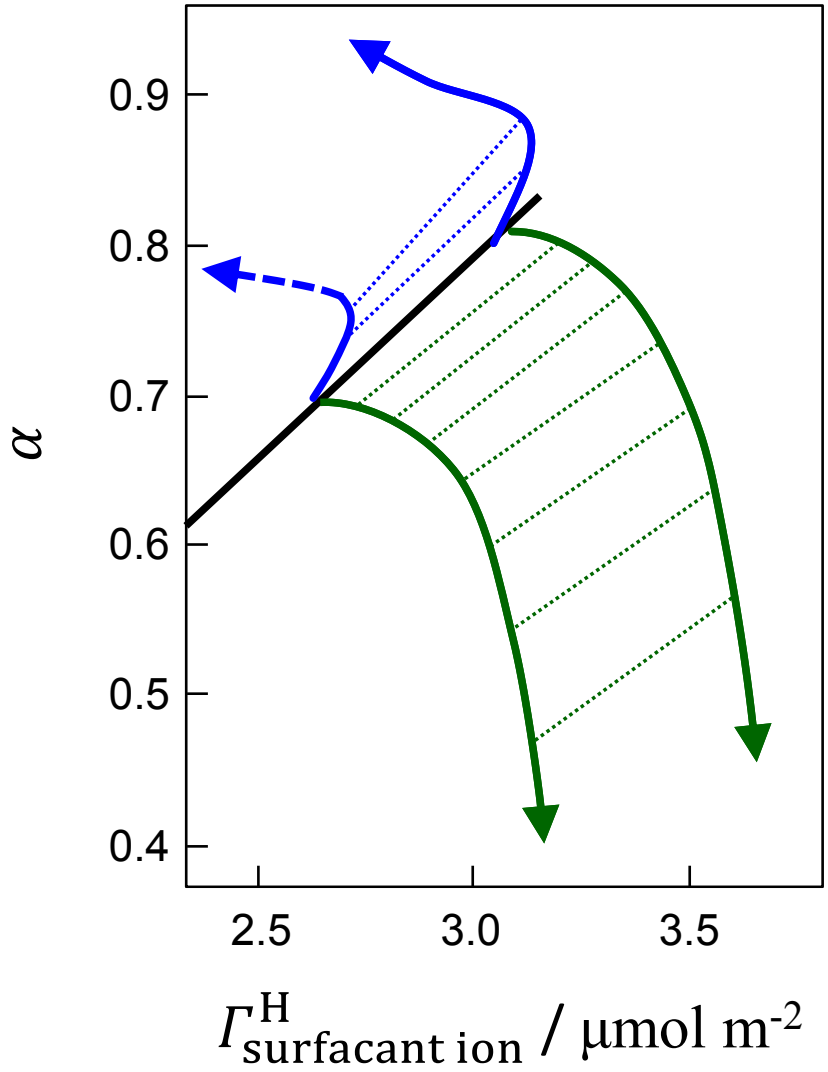

Figure 5-9(b). The enlarged view of Figure 5-9(a) where dotted lines connect the α values at fixed $\hat{Y}_2^{H}$ at intervals of 0.1.

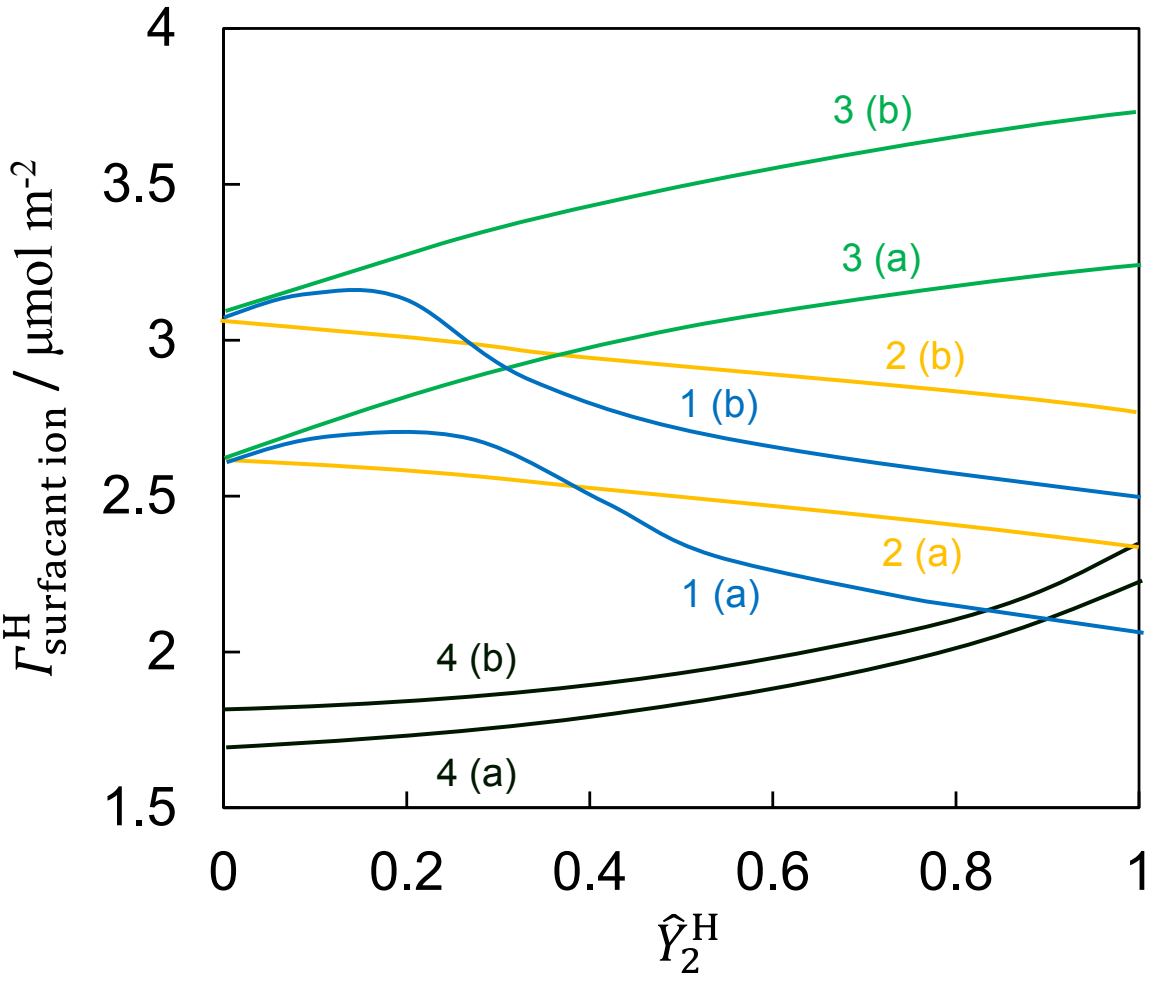

Figure 5-10. The surface density of surfactant ion vs. the surface composition of counterions for (1) DTAB-DTA_2SO_4, (2) DTAB-DTAC, (3) DTAB-$DTABF_4$ and (4) HMIMBr-$HMIMBF_4$ systems. (a) and (b) represent respectively the data at 55.0 and 45.0 mN m^{-1} (45.5 mN m^{-1} for the DTAB-DTA_2SO_4 system). For all binary mixed systems, the composition of zero represents the single systems containing Br^- ions.

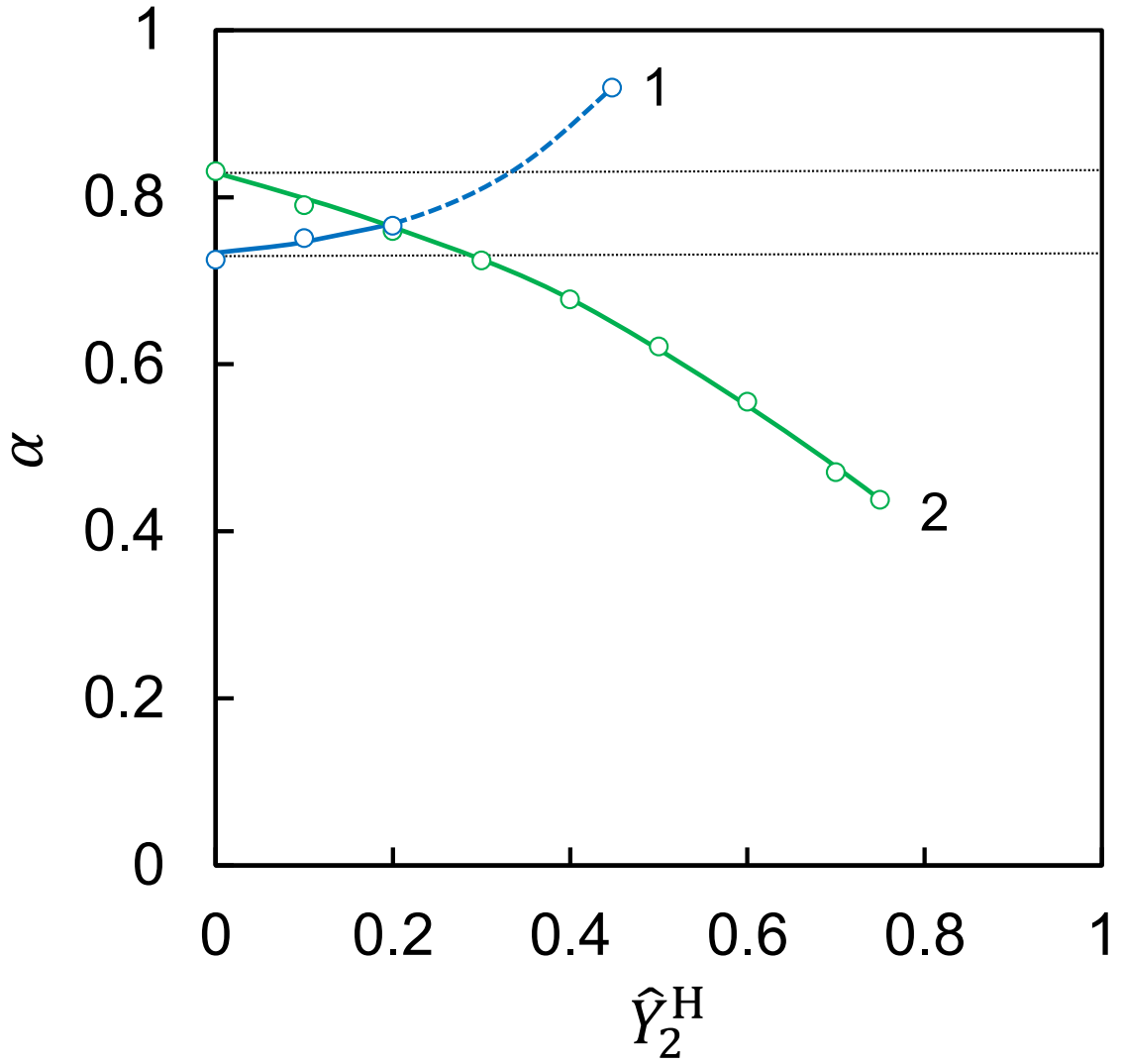

Figure 5-11. The ratio of bound-Br vs. the surface composition curves at constant $\Gamma_{\mathrm{DTA}}^{\mathrm{H}}$ for (1) DTAB-DTA_2SO_4 (2.75 μmol m^{-2}) and (2) DTAB-$DTABF_4$ (3.15 μmol m^{-2}) obtained from Figure 5-9. Dotted lines represent the ratio of bound-Br in ideal mixing expected from the data for the DTAB-DTAC system.

the specific interaction between counterion and surfactant ion [19]. Therefore, let us reexamine the counterion miscibility of the DTAB-DTAC, DTAB-$DTABF_4$, HMIMBr-$HMIMBF_4$ and DTAB-DTA_2SO_4 systems on the basis of the α vs. $\Gamma^{\mathrm{H}}_{\text{surfactant ion}}$ plots in Fig. 5-9 and $\hat{g}^{\mathrm{H,E}}$ in Fig. 5-5.

For the case of the DTAB-DTAC system, the hydration free energy and the size of counterions are not so different from each other as shown in Table 1, and the mixing of Cl^- ions has practically no essential influences on the distribution of Br^- ions in the adsorbed film. This is demonstrated in the fact that the α vs. $\Gamma^{\mathrm{H}}_{\text{surfactant ion}}$ plots at given $\hat{Y}^{\mathrm{H}}_2$ are essentially on and very near the line of the DTAB single system as already shown in Fig. 5-9(a). This implies that the α values are determined solely by $\Gamma^{\mathrm{H}}_{\mathrm{DTA}}$ irrespective of $\hat{Y}^{\mathrm{H}}_2$ as shown in Fig. 5-11 by dotted lines. Remembering that $\hat{g}^{\mathrm{H,E}}$ of the DTAB-DTAC system is almost zero as shown in Fig. 5-5 and thus the counterions are ideally mixed in the adsorbed film, therefore, one of the criterions for the ideal mixing from the viewpoint of the counterion distribution in the adsorbed films is that the α vs. $\Gamma^{\mathrm{H}}_{\text{surfactant ion}}$ plots at any $\hat{Y}^{\mathrm{H}}_2$ are sitting around the one of the DTAB single system. For the HMIMBr-$HMIMBF_4$ system the hydrogen bonding between BF_4^- ion and imidazolium cation is essential [27], which causes a kind of segregation of the counterion distribution. This is demonstrated in the fact that α is almost zero in Fig. 5-9 which means almost all Br^- ions are not in the vicinity of head groups but in the diffuse layers and fully hydrated by six water molecules at any values of $\hat{Y}^{\mathrm{H}}_2$ and $\Gamma^{\mathrm{H}}_{\mathrm{DTA}}$. Such counterion distribution decreases the mixing entropy in the adsorbed film and leads the positive $\hat{g}^{\mathrm{H,E}}$ as shown in Fig. 5-5.

For the DTAB-$DTABF_4$ system, α is increased with increasing $\Gamma^{\mathrm{H}}_{\mathrm{DTA}}$ at fixed $\hat{Y}^{\mathrm{H}}_2$ as shown in Fig. 5-9(b). This trend is the same as that of the single DTAB as well as

that of the DTAB-DTAC system. However, α is decreased from the value of the ideal mixing criterion (the value of the single DTAB system as well as that of the DTAB-DTAC system as mentioned above) with increasing $\hat{Y}_2^{\mathrm{H}}$ at fixed $\Gamma_{\mathrm{DTA}}^{\mathrm{H}}$: the binding ratio of Br^- ions to DTA^+ ions is diminished by increasing the composition of BF_4^- ions even at the constant surface density $\Gamma_{\mathrm{DTA}}^{\mathrm{H}}$ as shown in Fig. 5-11. Thus it is said that the preferential binding of BF_4^- ions compared to the ideal mixing takes place in this mixed system. On the other hand, as already mentioned in Chapter 4 the surface composition of BF_4^- itself is smaller and thus that of Br^- is larger compared to the ideal mixing as shown in our previous study [26]. This means that the electrical double layer, consisting of the diffuse layer and the vicinity of the head groups, is totally enriched in Br^- ions compared to the ideal mixing but the vicinity of the head group is preferentially bound by BF_4^- ions compared to the ideal mixing. Since hydrogen bonding is not formed between DTA^+ ions and counterions, it is said that the preferential binding of BF_4^- ions to DTA^+ ions is governed by the lower dehydration free energy of BF_4^- ions compared to Br^- ions and the enrichment in Br^- ions in the electrical double layer probably comes from that a difference in size between Br^- and BF_4^- ions enhances the counterion mixing because the spaces among BF_4^- ions can be effectively shared by smaller Br^- ions which is also theoretically expected [10]. This is confirmed by the negative $\hat{g}^{\mathrm{H,E}}$ as well as the negative $\hat{a}^{\mathrm{H,E}}$.

Now let us examine closely the results of the DTAB-DTA_2SO_4 system from the viewpoints of the surface density of surfactant ions, the composition of counterion in the electrical double layer of the adsorbed film and the ratio of bound-Br. Fig. 5-9(b) shows that the α value is increased with $\Gamma_{\mathrm{DTA}}^{\mathrm{H}}$ at fixed $\hat{Y}_2^{\mathrm{H}}$ (dotted lines) similarly to other systems. The distinct difference from others is that the α value is clearly

increased with $\hat{Y}_2^{\mathrm{H}}$ from the ideal mixing criterion (the value of the single DTAB system as well as that of the DTAB-DTAC system) as demonstrated in Fig. 5-11, which is actually an opposite trend to the DTAB-$DTABF_4$ system. Therefore it is said that the preferential binding of Br^- ions to DTA^+ ions compared to the ideal mixing takes place in this system. On the other hand, the surface composition of SO_4^{2-} ions is smaller and thus that of Br^- is larger compared to the ideal mixing as demonstrated in Fig. 5-3(a) and (b), which is the same as the DTAB-$DTABF_4$ system. Therefore the electrical double layer is totally enriched in Br^- ions and also the vicinity of the head group is preferentially bound by Br^- ions to SO_4^{2-} ions compared to the ideal mixing. The preferential binding of Br^- is as expected, since the hydration free energy mainly determined by hydration enthalpy [20] is more negative for SO_4^{2-} than for Br^- and the preferential binding of Br^- is preferable from the view point of enthalpy. Also Shapovalov et al. has reported that at the higher surface charge density than 0.6 C m^{-2}, the smaller monovalent counterions are preferentially adsorbed to the solution surface to the larger hydrated multivalent ion in the Langmuir monolayers [7, 9-12]. However, this study clearly suggests that even when the surface charge density is not so high, for example, $\Gamma_{\mathrm{DTA}}^{\mathrm{H}}$ = 2.1~3.2 and thus 0.2~0.31 C m^{-2}, the vicinity of head groups of DTA^+ ion is preferentially occupied by Br^- ions.

There are other interesting points for the DTAB-DTA_2SO_4 system. The one is that although the electrical double layer is enriched in SO_4^{2-} compared to the bulk solution due to the stronger electric interaction, it abounds in Br^- compared to the ideal mixing as shown in Fig. 5-3(a) and (b). The abundance in Br^- compared to the ideal mixing results in negative $\hat{g}^{\mathrm{H,E}}$ and is due to the preferential binding of Br^- ions in the vicinity of the head groups, which lowers $\hat{g}^{\mathrm{H,E}}$ from the viewpoint of enthalpy, as well

as the effective filling the confined space among the larger SO_4^{2-} ions by the smaller Br^- ions, which lowers $\hat{g}^{H,E}$ from the viewpoint of entropy. The other is that the preferential binding becomes more prominent as the $\hat{Y}_2^H$ value becomes larger and thus the surface composition of Br^- becomes smaller as shown in Fig. 5-11. This indicates that Br^- ions are mainly released from the diffuse layer rather than the vicinity of headgroups as the surface composition of Br^- becomes smaller. This result is in contrast to that for the DTAB-$DTABF_4$ system where the ratio of bound-Br decreases as the surface composition of Br^- becomes smaller, which indicates that Br^- ions are mainly released from the vicinity of headgroups rather than the diffuse layer. However it is said for the both systems that the ratio of the number of counterions in the vicinity of surfactant head groups to those in the diffuse layer is raised for the counterions having comparatively less negative hydration free energy (BF_4 for the DTAB-$DTABF_4$, Br for the DTAB-DTA_2SO_4 system), that is, the counterions having comparatively less negative hydration energy are mainly released from the diffuse layer when their surface composition is decreased. This clearly provides one of the evidences of ion specific effect on the adsorption phenomena: the hydration free energy and thus the enthalpy contribution to the free energy of adsorption of counterions, besides the entropy contribution arising from the difference in size of them, plays very essential role for determining the distribution and miscibility of counterions in the electrical double layer.

5-7 References

1. Parsons, D. F.; Ninham, B. W. *Langmuir* **2010**, 26, 6430.
2. Besteman, K.; Zevenbergen, M. A.; Lemay, S. G. *Phys. Rev. E* **2005**, 72, 061501.
3. Alargova, R. G.; Danov, K. D.; Petkov, J. T.; Kralchevsky, P. A.; Broze, G.;

Mehreteab, A. *Langmuir* **1997**, 13, 5544.

4. Petkov, J. T.; Tucker, I. M.; Penfold, J.; Thomas, R. K.; Petsev, D. N.; Dong, C. C.; Golding, S.; Grillo I. *Langmuir* **2010**, 26, 16699.
5. Para, G.; Warszynski, P. *Colloids and Surfaces A* **2007**, 300, 346.
6. Slavchov, R. I.; Novev, J. K.; Peshkova, T. V.; Grozev, N. A. *J. Colloid and Interface Sci*. **2013**, 403, 113.
7. Shapovalov, V. L.; Brezesinski, G. *J. Phys. Chem. B* **2006**, 110, 10032.
8. Shapovalov, V. L.; Ryskin, M. E.; Konovalov, O. V.; Hermelink, A.; Brezesinski, G. *J. Phys. Chem. B* **2007**, 111, 3927.
9. Biesheuvel, P. M.; van Soestbergen, M. *J. Colloid and Interface Sci.* **2007**, 316, 490.
10. Valisko, M.; Boda, D.; Gillespie, D. *J. Phys. Chem. C* **2007**, 111, 15575.
11. Woelki, S.; Kohler, H. H. *Chem. Phys.* **2000**, 261, 421.
12. Taboada-Serrano, P.; Yiacoumi, S.; Tsouris, C. *J. Chem. Phys.* **2005**, 123, 054703.
13. Day, R. A.; Underwood, A. L. *Quantitative Analysis 4th edition*; Prentice-Hall, Inc.: New Jersey, 1980.
14. Voeks, J. F.; Tartar, H. V. *J. Phys. Chem.* **1956**, 59, 1190.
15. Kohlrausch, F. *Sitzungsberichte der Königlich Preussischen Akademie der Wissenschaften* **1900**, 2, 1002.
16. Debye, P.; Huckel, E. *Physikalische Zeitschrift* **1923**, 24, 185.
17. Onsager, L.; Fuoss, R. *J. Phys. Chem.* **1932**, 36, 2689.
18. Aratono, M.; Villeneuve, M.; Takiue, T.; Ikeda, N.; Iyota, H. *J. Colloid and Interface Sci.* **1998**, 200, 161.
19. Imai, Y.; Li, H. H.; Takumi, H.; Tanida, H.; Watanabe, I.; Takiue, T.; Matsubara, H.;

Aratono, M. *J. Colloid and Interface Sci.* **2012**, 388, 219.

20. Marcus, Y. *Biophysical Chemistry* **1994**, 51, 111.
21. Eliad, L.; Salitra, G.; Soffer, A.; Aurbach, D. *J. Phys. Chem. B* **2001**, 105, 6880.
22. Takiue, T.; Matsuo, T.; Ikeda, N.; Motomura, K.; Aratono, M. *J. Phys. Chem. B* **1998**, 102, 5840.
23. Hayami, Y.; Nomura, T.; Villeneuve, M.; Takiue, T.; Aratono, M. *Colloid Polym. Sci.* **2002**, 280, 146.
24. Shimamoto, K.; Onohara, A.; Takumi, H.; Watanabe, I.; Tanida, H.; Matsubara, H.; Takiue, T.; Aratono, M. *Langmuir* **2009**, 25, 9954.
25. Aratono, M.; Kashimoto, K.; Matsuda, T.; Muroi, S.; Takata, Y.; Ikeda, N.; Takiue, T. *Langmuir* **2005**, 21, 7398.
26. Li, H. H.; Imai, Y.; Yamanaka, M.; Hayami, Y.; Takiue, T.; Matsubara, H.; Aratono, M. *J. Colloid and Interface Sci.* **2011**, 359, 189.
27. Dong, K.; Zhang, S.; Wang, D.; Yao, X. *J. Phys. Chem. A* **2006,** 110, 9775.

Chapter 6 The Effect of the Arrangement of Hydrophilic Head Groups in Adsorbed Films on Counterion Distribution.

6-1 Introduction

In Chapter 3, it was suggested that the adsorbed film could not be homogeneous in molecular level, and the counterions distribution could be influenced by the arrangement of hydrophilic head groups in the adsorbed film and vice versa. The one of such examples was suggested by Petkov et al. that the sharing of Al^{3+} counterions by three surfactant ions due to strong electrostatic interaction could induce the formation of complicated multilayer at air/water interface [1, 2]. Kjellander et al. also insisted that ion-ion correlation could cause the inhomogeneous arrangement of adsorbed ionic species and that the effect was theoretically described with two-body correlation function [3]. In our previous thermodynamic studies of binary surfactant mixtures, a staggered arrangement of head groups, which is an example of inhomogeneous arrangement of adsorbed species, was suggested for HTAB-DTAB mixed system (see below). Therefore in this Chapter is concerned with the relation between the bromide ion distribution and the arrangement of surfactant ions using TR-XAFS method for the HTAB-DTAB system.

Fig. 6-1 displays the excess Gibbs energy of adsorption $\hat{g}^{\mathrm{H,E}}$ vs. surface composition of DTAB $\hat{X}_2^{\mathrm{H}}$ curves at two given surface tensions. Since the excess Gibbs energy of adsorption is negative and the excess molecular area is also negative, it was suggested that DTAB molecules could use effectively the space among the hydrocarbon chains of HTAB molecules and their polar head groups took a staggered arrangement at the surface [4].

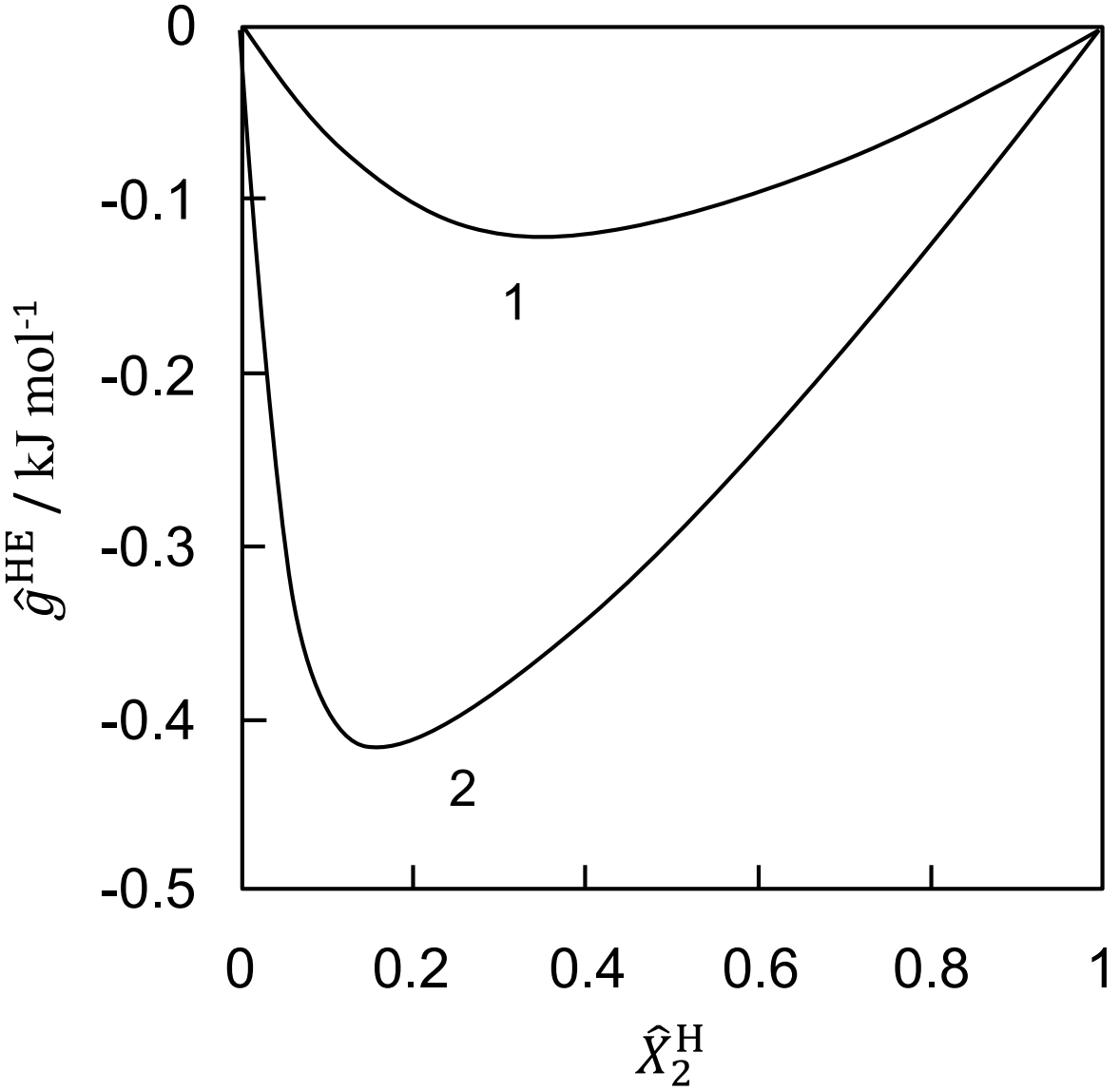

Figure 6-1. Excess Gibbs energy of adsorption vs. surface composition curves for HTAB-DTAB mixed system at (1) 60.0 and (2) 45.0 mN m^{-1}.

6-2 Counterion distribution in the HTAB –DTAB mixed system

The TR-XAFS was applied to this system and, the effect of surface charge due to the adsorbed surfactant cations on counterion distribution was explored by examining the relation of the ratio of bound-Br to surface density of surfactant ions. The TR-XAFS spectra for the HTAB- DTAB system are displayed at $\hat{X}_2^{\mathrm{H}}$ = 0.2 and γ = 60.0 and 45.0 mNm^{-1} in Fig. 6-2. From the obtained TR-XAFS spectra, the surface density of surfactant ions was evaluated by Jump value analysis as shown in Chapter 4 and is shown in Fig. 6-3, where the surface density obtained through thermodynamic analysis is drawn by solid lines. The coincidence between the surface densities obtained from both methods is generally satisfactory. The surface density has a maximum around $\hat{X}_2^{\mathrm{H}}$ = 0.2. This is in accord with the observation that around the $\hat{X}_2^{\mathrm{H}}$, the excess Gibbs energy takes a minimum and thus an effective packing is expected in the mixed system.

In order to examine the distribution of Br^- ions from the standpoint of their solvation structure, the EXAFS χ spectra was calculated from the TR-XAFS spectra in the same procedure shown in Chapter 3 and displayed in Fig. 6-4(a) and (b). The dependence of the spectrum on the surface composition was not so large but the isosbestic points were surely observed. Therefore, we evaluated α for each spectrum by the least square method using Eq. 3-3 and the reference spectra of χ_1 and χ_2 for the DTAB single surfactant system. The result is plotted against surface composition $\hat{X}_2^{\mathrm{H}}$ in Fig. 6-5.

In Fig. 3-4, the α value of DTAB and HTAB is increased linearly with increasing surface densities of surfactant cations and almost the same at the given surface density. Here it should be noted that the curves in Fig. 6-5 are drawn at given surface tensions. Since the surface density of HTA^+ ions is a little higher than that of DTA^+ ions at a

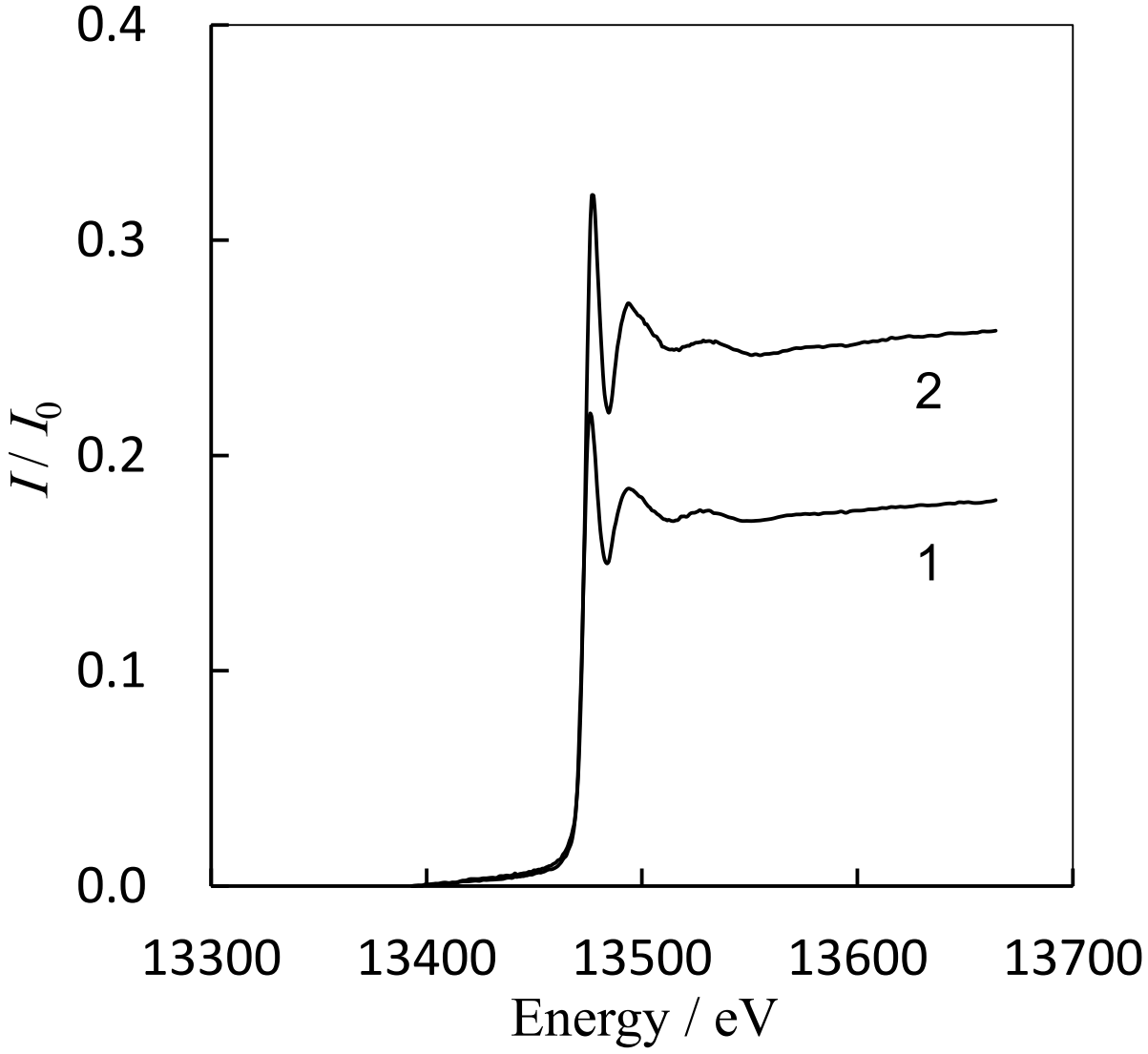

Figure 6-2. The TR-XAFS spectra for HTAB-DTAB mixed system at $\hat{X}_2^{\mathrm{H}} = 0.2$ and (1) 60.0 and (2) 45.0 mN m^{-1}.

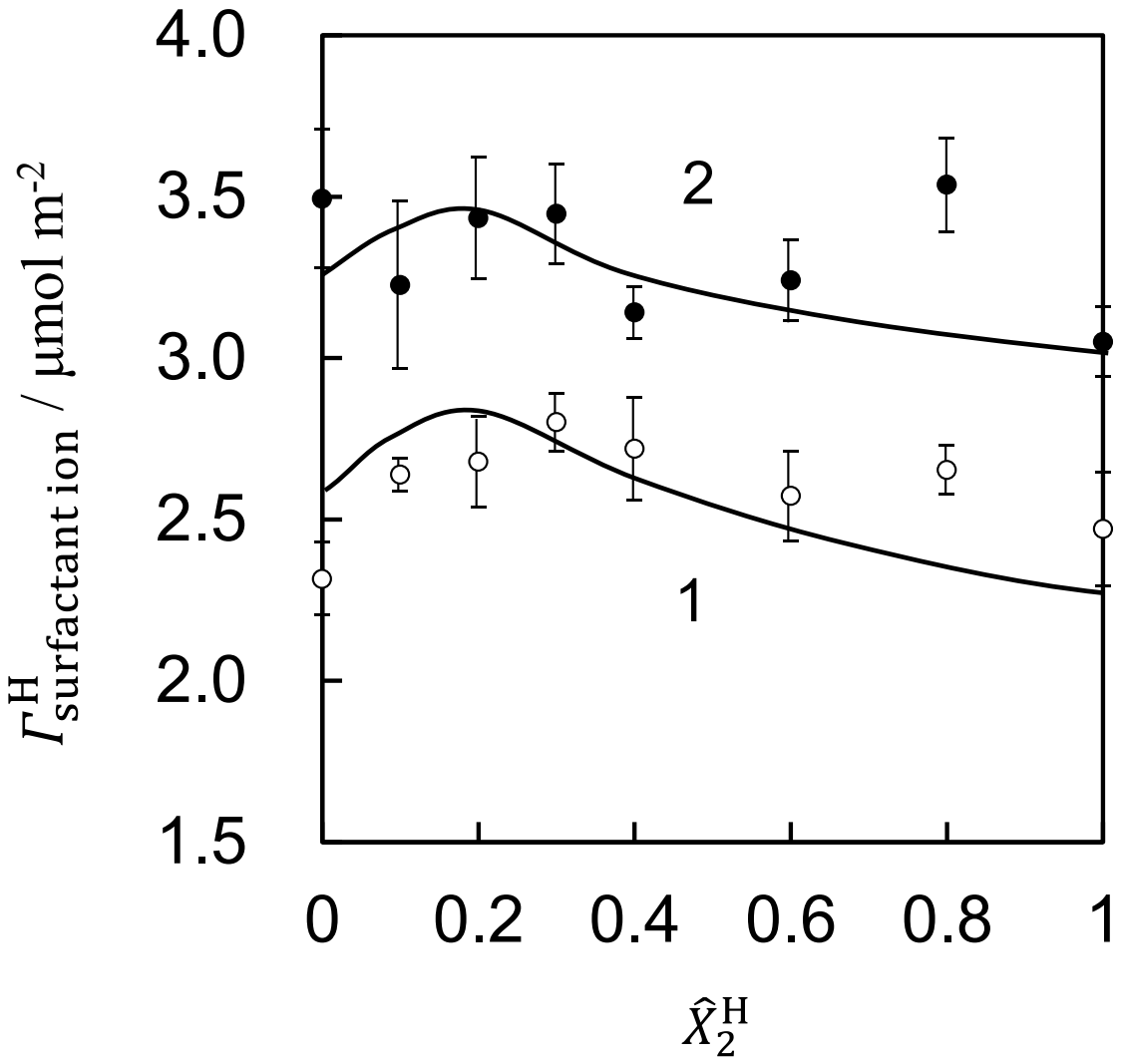

Figure 6-3. Surface density of surfactant ions vs. surface composition curves for HTAB-DTAB systems at (1) 60.0 and (2) 45.0 mN m^{-1}. Solid curves and open circles respectively represent the data from surface tensiometry and TR-XAFS.

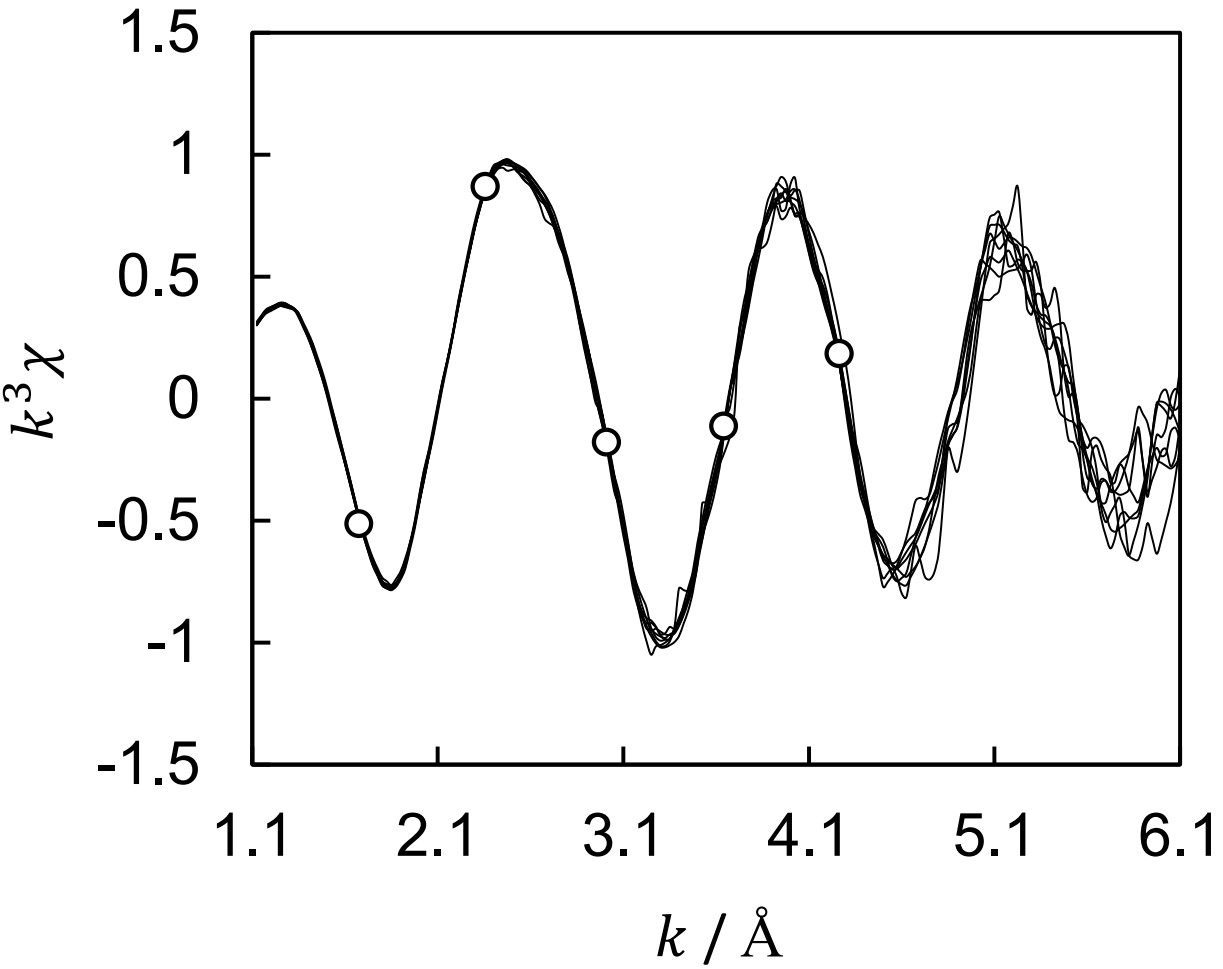

Figure 6-4(a). EXAFS $k^3\chi$ spectra of Br^- ion in the adsorbed film of HTAB-DTAB system at (a) 60.0 mN m^{-1} and, $\hat{X}_2^{\mathrm{H}} = 0$, 0.1, 0.2, 0.3, 0.4, 0.6, 0.8, 1. Open circles are the isosbestic points observed.

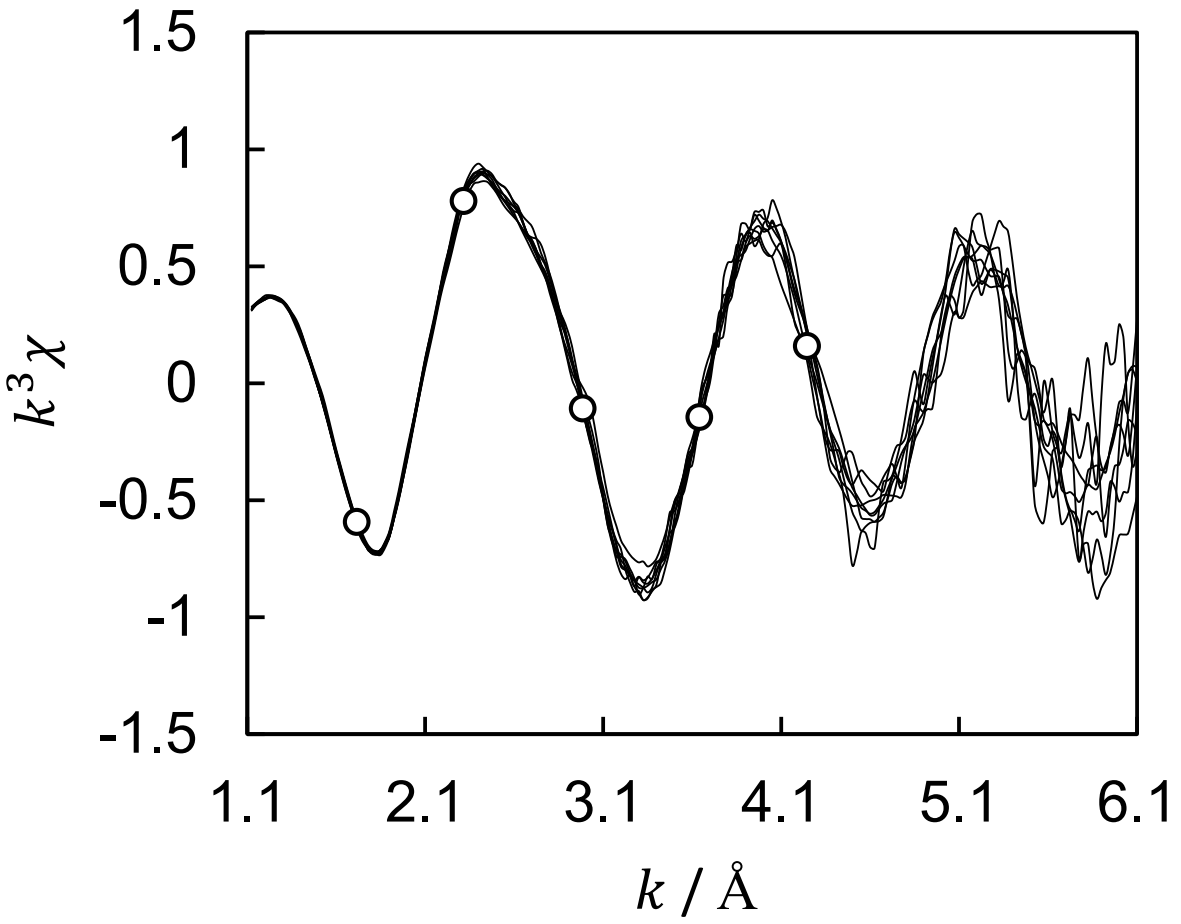

Figure 6-4(b). EXAFS $k^3\chi$ spectra of Br^- ion in the adsorbed film of HTAB-DTAB system at (a) 45.0 mN m^{-1} and, $\hat{X}_2^{\mathrm{H}} = 0, 0.1, 0.2, 0.3, 0.4, 0.6, 0.8, 1$. Open circles are the isosbestic points observed.

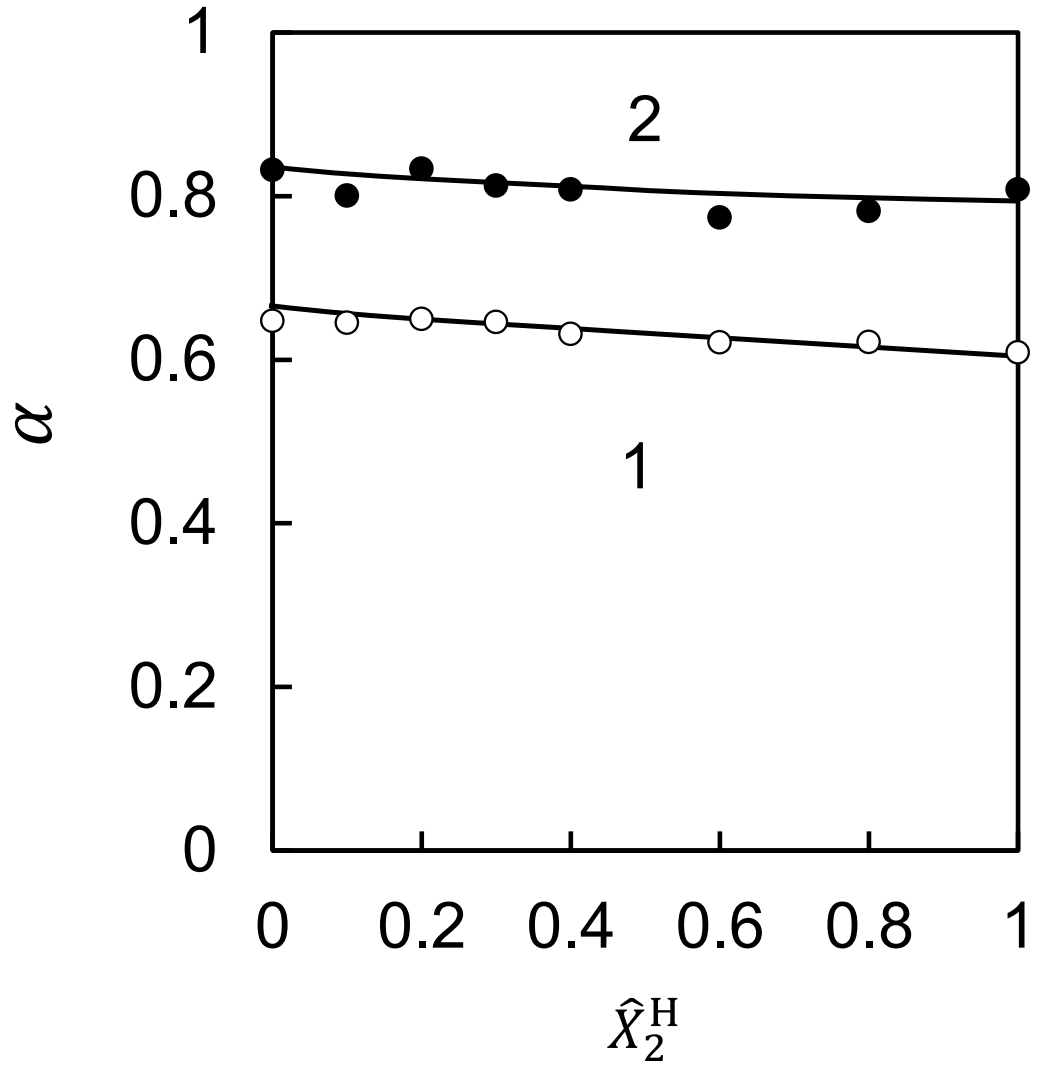

Figure 6-5. The ratio of bound-Br vs. surface composition curves for HTAB and DTAB mixed system at (1) 60.0 and (2) 45.0 mN m^{-1}.

given surface tension, the α value of pure HTAB ($\hat{X}_2^{\mathrm{H}} = 0$) is a little higher than that of pure DTAB ($\hat{X}_2^{\mathrm{H}} = 1$). Fig. 6-5 shows that the value of α is slightly decreased with increasing the surface composition of DTAB, and no maximum is observed in spite of the effective packing of surfactants in the adsorbed film. However it should be remembered from the consideration in Chapter 5 that the more important correlation to investigate the counterion distribution more closely is not the α vs. $\hat{X}_2^{\mathrm{H}}$ plots at given surface tensions but the α vs. $\Gamma^{\mathrm{H}}_{\mathrm{surfactant\,ion}}$ plots. The latter is constructed from Figs. 6-3 and 6-5 and demonstrated in Fig. 6-6, where the corresponding lines for the DTAB and HTAB single systems are the same as explained in Fig. 3-4 and is shown by a solid line.

It should be noted in Fig. 6-6 that the α value for the mixed system is lower than that for the single systems at fixed surface density. Here let us remember that for the DeMIMBr single surfactant system, the α value is also smaller than the solid line and an effective stacking packing is expected due to the plane ring structure of the head groups of $DeMIM^+$ ions. Then one of the possible situations is that the staggered arrangement of surfactant ions enhances the inhomogeneous distribution of ion species and the domain like structure (islands or clusters) is dispersed in the adsorbed film.

It should be noted here that in the theoretical fittings conducted by Kalinin et al. [5] and Warszynski et al. [6] using the surface tension and surface potential data, the expected ratio of the number of counterions in the Stern layer to those in the diffuse layer is much higher than the ratio of bound-Br in this study, although these two theory traced satisfactorily the experimental values of both surface tension and surface potential. Taking into account that TR-XAFS provides the information on counterion distribution without any model of electrical double layer, this result implies that

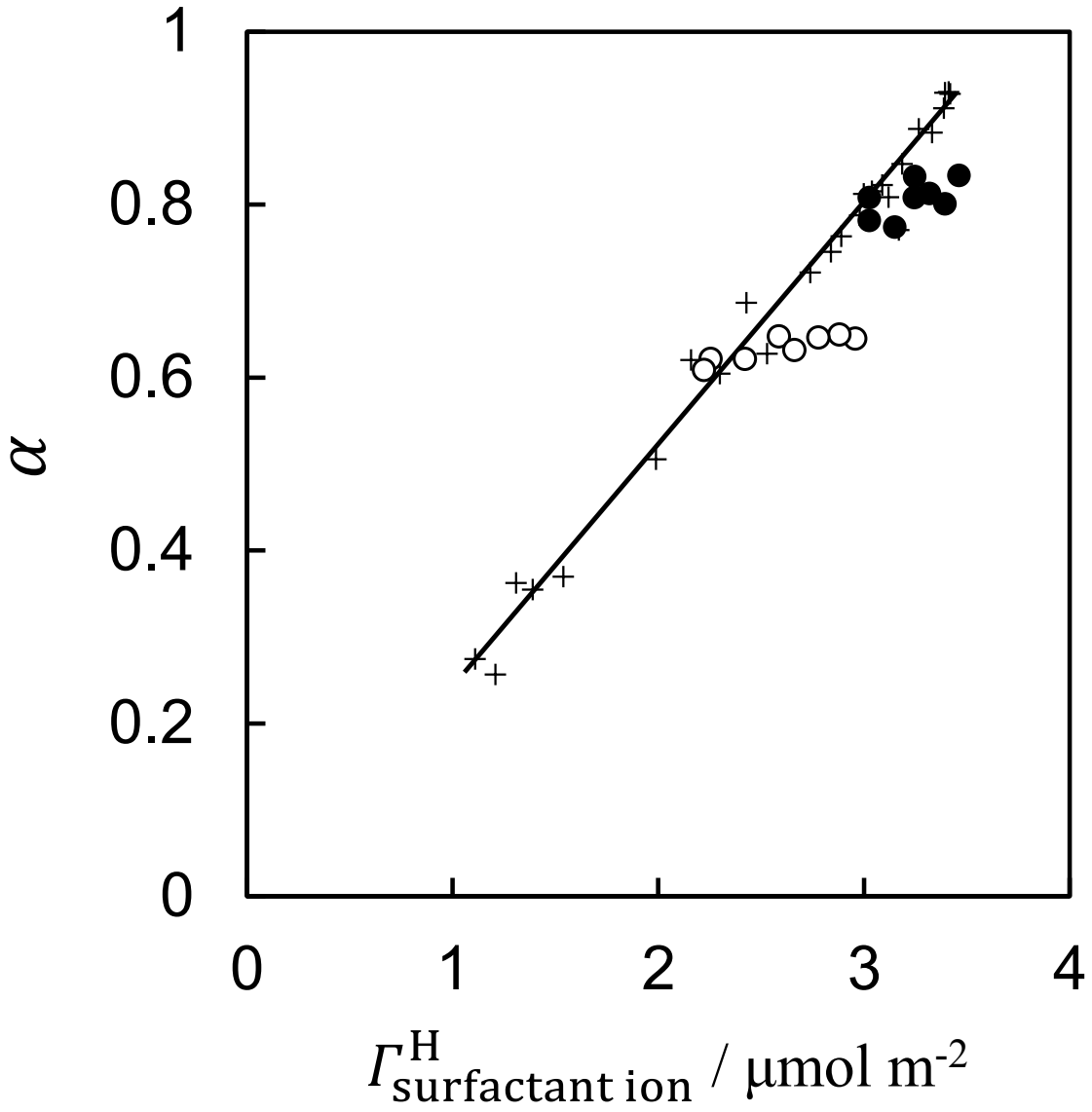

Figure 6-6. The ratio of bound-Br vs. surface density of surfactant ions for HTAB-DTAB system. Open and filled circles respectively represent the data at 60.0 and 45.0 mN m^{-1}. Cross symbols and solid line represent the data for the single systems of DTAB and HTAB.

incorporating the ratio of bound-Br in addition to surface tension and surface potential in the theoretical models describing counterion distribution could greatly facilitates the clarifying the specific ion effects on interfacial and colloidal phenomena. Especially for the systems in which the strong ion-ion correlations are induced, researches are highly required because in such systems many important phenomena, for example inhomogeneous ion distribution, multilayer formation and charge inversion, are often observed and expected. TR-XAFS technique has a great potential for clarifying the specific ion effects in such systems.

6-3 References

1. Alargova, R. G.; Danov, K. D.; Petkov, J. T.; Kralchevsky, P. A.; Broze, G.; Mehreteab, A. *Langmuir* **1997**, 13, 5544.
2. Petkov, J. T.; Tucker, I. M.; Penfold, J.; Thomas, R. K.; Petsev, D. N.; Dong, C. C.; Golding, S.; Grillo I. *Langmuir* **2010**, 26, 16699.
3. Kjellander, R.; Marcelja, S. *J. Chem. Phys.* **1985**, 82, 2122.
4. Kashimoto, K.; Matsubara, H.; Takahara, H.; Nakano, T.; Takiue, T.; Aratono, M. *Colloid. Polym. Sci.* **2004**, 283, 329.
5. Kalinin, V. V.; Radke, C. J. *Colloids and Surfaces A* **1996**, 114, 337.
6. Para, G.; Warszynski, P. *Colloids and Surfaces A* **2007**, 300, 346.

Chapter 7 Summary

In this thesis, the specific ion effect was investigated by examining the counterion distribution in the surfactant adsorbed films with the aid of the bound ratio of bromide ion evaluated from TR-XAFS measurement as well as by evaluating thermodynamic physicochemical variables through surface tensiometry followed by the analysis based on our original thermodynamic formulation.

In the single counterion systems of DTAB, HTAB, DTAB with added NaBr, DeMIMBr and HTAB-DTAB mixture, the ratio of bound-Br was increased with increasing the surface density of surfactant ions. The notable results for these systems are as follows; the values of the ratio of bound-Br for HTAB, DTAB with NaBr were rather close to that for DTAB at a fixed surface density of surfactant ions which indicated that the difference in chain length and adding electrolyte are not so much influential on counterion distribution, whereas those for DeMIMBr and HTAB-DTAB mixture were evidently smaller than that for DTAB possibly due to the effective packing of surfactant ions which provided the conceivable situation that the adsorbed molecules were definitely not homogeneously dispersed but a part of them were molecularly dispersed around the domains (islands or clusters) with the bound Br ions. From these results, it was suggested that both the density and arrangement of surface charge due to surfactant ions could influence counterion distribution in the electrical double layer.

For the binary counterion mixed systems, the distribution and miscibility in the electrical double layers of adsorbed films was investigated. The notable points are as follows; in the DTAB-DTAC system the mixing of Cl^- ions had practically no influences to the distribution of Br^- ions in the adsorbed film and ideal mixing was observed because the nature of counterions was similar. In the HMIMBr-$HMIMBF_4$ system the

hydrogen bonding between BF_4^- ion and imidazolium cation is essential, which causes a kind of segregation of the counterion distribution. In the DTAB-$DTABF_4$ and DTAB-DTA_2SO_4 systems, on the other hand, preferential binding of counterions having lower hydration and adsorption energy and a remarkable difference in size between them yielded the preferable counterion mixing in the electrical double layer. The three essential factors that cause the specific ion effect, the size, the hydration and the hydrogen bonding with surfactant ions and counterions was suggested.

Our methods contribute to clarifying the Hofmeister specific counterion effect in colloidal and interfacial systems. Especially, TR-XAFS provides the information on counterion distribution without any model of electrical double layer, therefore, this technique has a great potential for facilitating the development of fundamental theoretical models of that.

Acknowledgments

I wish to express my great gratitude to Professor Makoto Aratono for his introduction to profound and fascinating world of interfacial science and his kind and helpful suggestions and discussions throughout this work. I am also thankful to Professor Takanori Takiue for his great encouragements, and Associate Professor Michio Yamanaka for his thoughtful discussions, and Assistant Professor Hiroki Matsubara for his specially witted suggestions.

Then, I also wish to appreciate Professor Iwao Watanabe of Ritsumeikan University and Associate Professor Hajime Tanida of Kyoto University, for technical advices for their XAFS measurements. I express my special thanks to Yuhei Tokiwa and Shusaku Ueno for their kind helping in XAFS measurements.

Moreover, I wish to express special thanks to all my colleagues who have good time with me and always encourage me. Finally, I express my great thanks to my family and Haruka Horiuchi for supporting me when things are tough.

This work was supported by the Research Fellowships for Young Scientists (No. 24 3699) from the Japan Society for the Promotion of Science (JSPS). This work has been performed under the approval of the Photon Factory Advisory Committee (proposal no. 2012 G518), which is greatly appreciated.